ENHANCING ROBOTIC COMMUNICATIONS VIA MOBILITY DIVERSITY ALGORITHMS

Daniel Bonilla Licea

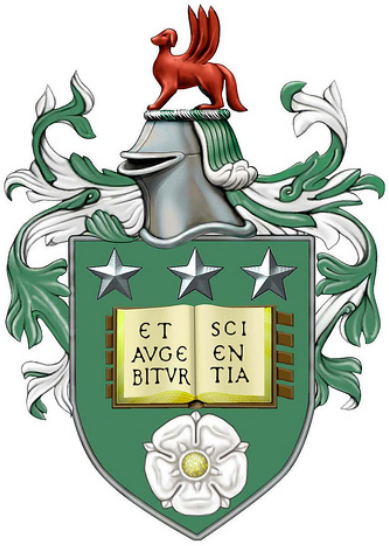

Submitted in accordance with the requirements for the degree of
Doctor of Philosophy

School of Electronic & Electrical Engineering,
University of Leeds.

August 2016

Declaration

The candidate confirms that the work submitted is his/her own, except where work which has formed part of jointly authored publications has been included. The contribution of the candidate and the other authors to this work has been explicitly indicated below. The candidate confirms that appropriate credit has been given within the thesis where reference has been made to the work of others. It is to assert that the candidate has contributed solely to the technical part of the joint publication under the guidance of his academic supervisors. Detailed breakdown of the publications is presented in the first chapter of this thesis.

Acknowledgements

First of all I would like to thank Dr. McLernon who was my academic supervisor during my doctoral studies. His guidance from my first conference paper until this thesis has been invaluable.

I am grateful to Prof. Mounir Ghogho for his suggestions and support during the development of my doctoral studies.

I would like to acknowledge CONACYT (the Mexican National Council for Science and Technology) for awarding me the scholarship that allowed me to complete my studies. I am also thankful for the complementary financial aid provided to me by the Secretariat of Public Education of Mexico.

I am also grateful for the support of my parents Moisés and Martha as well as my brothers Samuel and Moïse.

Finally, I would also like to thank my friends and colleagues for all their support.

Abstract

Nowadays wireless communications is an important aspect of mobile robotics. It is common that mobile robots need to establish wireless links to exchange information with other robots, base stations or sensor nodes. And, as in traditional mobile communications small-scale wireless channel fading also occurs in these scenarios. This phenomenon means that the channel gain will vary significantly over small-distances and in a random manner. This degrades both the communication ability of the robots and as a consequence, their overall performance in executing certain tasks. There is therefore a clear need to compensate for this small-scale fading.

We could of course compensate small-scale fading in robotic communications using classical diversity techniques. But these diversity techniques were designed for transceivers that either cannot move, or can move but have no control over their position. In the context of robotic communications we can think of mobile robots as transceivers who know their own position and can also control it. This allows us to create a new form of diversity called *mobility diversity* whose principle is as follows. If the mobile robot experiences a poor channel gain due to a deep fading then it can alter its location by a small amount in order to find a new point with a higher channel gain (note that a low channel gain requires more transmitter energy to achieve the same SNR at the receiver as a high channel gain). Now, the more points the robot explores then the higher is the probability of obtaining a high channel gain but the consumption of mechanical energy also increases. Thus efficient mobility diversity algorithms (MDAs) must be able to deliver high channel gains while simultaneously using a small amount of mechanical energy.

In this thesis, we start by simultaneously considering the theoretical aspects of both wireless communications and robotics that underpin this interdisciplinary problem. We then develop intelligent algorithms (MDAs) to solve the maximise channel gain/ minimise mechanical energy challenge while looking at various modifications that can occur–i.e., predetermined and adaptive stopping points; MDAs for robots as wireless relays; MDAs that incorporate energy harvesting; and finally optimisation over a continuous search space.

In summary, mobility diversity is a relatively new research area in an early stage of development. In this thesis we have developed a comprehensive theory for MDAs that will form the basis for future applications as outlined in chapter 7.

Publications

- D. Bonilla Licea, D. McLernon, M. Ghogho and S. A. Raza Zaidi, "An energy saving robot mobility diversity algorithm for wireless communications", 21st European Signal Processing Conference (EUSIPCO 2013), Marrakech, 2013.
- D. Bonilla Licea, D. McLernon and M. Ghogho, "A Robotic Mobility Diversity Algorithm with Markovian Trajectory Planners", Proc. of IEEE Workshop on Machine Learning and Signal Processing, Southampton, 2013.
- D. Bonilla Licea, D. McLernon and M. Ghogho, "Designing Optimal Trajectory Planners for Robotic Communications", Proc. of IET Intelligent Signal Processing (ISP'13) Conference, London, 2013.
- D. Bonilla Licea, D. McLernon, M. Ghogho, "Optimal trajectory design for a DTOA based multi-robot angle of arrival estimation system for rescue operations", IEEE International Conference on Acoustics, Speech and Signal Processing (ICASSP), 2014, pp. 6800-6804.
- D. Bonilla Licea, M. Ghogho, D. McLernon and S. A. Raza Zaidi, "Mobility Diversity-Assisted Wireless Communication for Mobile Robots", IEEE Transactions on Robotics, vol. 32, no. 1, 2016, pp. 214-229.
- D. Bonilla Licea, S. A. Raza Zaidi, D. McLernon and M. Ghogho, "Improving Radio Energy Harvesting in Robots Using Mobility Diversity", IEEE Transactions on Signal Processing, vol. 64, no. 8, 2016, pp. 2065-2077.
- D. Bonilla Licea, D. McLernon and M. Ghogho, "Path Planners with Memory for Mobility Diversity Algorithms", conditionally accepted for publication in IEEE Transactions on Robotics.
- D. Bonilla Licea, D. McLernon, M. Ghogho, "Continuous Searching Space Mobility Diversity Algorithm", to be submitted.
- D. Bonilla Licea, D. McLernon and M. Ghogho, "Multiple-link MDMTA for Robotic Networks", to be submitted.

Contents

List of Figures

List of Tables

Acronyms

- BER: Bit error rate.
- BS: Base station.
- CMDA: Continuous mobility diversity algorithm.
- DDR: Differential drive robot.
- IPPF-1: Iterative path planner function with memory order one.
- IPPF-2: Iterative path planner function with memory order two.
- MDA: Mobility diversity algorithm.
- MDMTA: Mobility diversity with multi-threshold algorithm.
- MR: Mobile robot.
- RBPPM-2: Rule based path planner with memory order two.
- RF: Radio frequency.
- RR: Robotic relay.
- SA: Simulated annealing.
- SNR: Signal to noise ratio.
- TOMR: Three-wheeled omnidirectional mobile robot.
- UCA: Uniform circular array.

Chapter 1

Introduction

Wireless communications is nowadays an important aspect of mobile robots and is a unique research field within the general mobile communications research area. Its uniqueness comes from the fact that for general mobile communications the position of the transceiver is seen as a random and uncontrollable process. But in wireless communications for mobile robots the position of the transceiver is a controllable parameter due to the nature of the mobile robot. Therefore in wireless communications for mobile robots we can control the position of the transceiver in addition to all the other aspects of the classical communications systems (e.g. transmission frequency, transmission power, modulation scheme, etc.). This opens up the possibility to use new communications techniques.

Within this research field we find different problems that are being studied. For example in [1] the authors consider the problem of keeping a certain transmission rate in an optical wireless link between a drone and a ground robot that is exploring some area. In this problem the ground robot is equipped with a fixed optical receiver (composed of either a PIN photodiode or an avalanche photodiode) pointing upwards while the the drone is equipped with an adjustable optical transmitter (composed of either a light-emitting diode or a laser diode) pointing to the ground robot's optical receiver. The transmission rate of such a link depends on the relative position of the drone with respect to the optical receiver of the ground robot. So the authors design a control law that makes the drone maintain a certain relative position with the ground robot at all times. This allows the drone to follow the ground robot while maintaining a certain transmission rate.

Collaborative systems are also being studied. In [2] the authors consider the problem of a team of robots with sensing and mapping capabilities trying to escape from a maze. It is assumed at the beginning that the robots know nothing about the maze and so they have to sense it to start constructing a map and then find a way out. If each robot shares the information that they have gathered about the maze with the other robots it can accelerate (for all the robots) the process of escaping from the maze. So the authors design a communications algorithm that has as its ultimate goal to allow all the robots to escape from the maze as fast as possible.

This involves designing how each robot must explore the maze and how they should share the map with the other robots.

In [3] the authors consider a mobile robotic network that is tasked with constructing a map of occluded structures using RF wireless channel measurements. The wireless channel is affected by the mechanisms [4] which are path loss, shadowing (or large-scale fading) and multipath-fading (or small-scale fading). The occluded structure to be mapped is located in between two mobile robots which establish a wireless link between them and then estimate the wireless channel. They use a high gain antenna to reduce the effects of small-scale fading and since they know the distance between them they can estimate the path loss term. In consequence from the wireless channel estimate they isolate the effect of the shadowing which gives information about the occluded structure located in the middle of the wireless link. So after both robots take various RF wireless channel measurements at different positions around the occluded structure they combine them to construct an estimated map of that structure.

Connectivity in robotic networks is also a problem that is being studied within this research area. In [5] the authors consider a robotic network which must maintain an end-to-end communications channel between a base station and the leader of the robotic team while the team leader has to move around to some pre-specified locations in order to perform some pre-assigned tasks. So the authors design a distributed control law for all the robotic team so that the team leader can explore the pre-assigned locations while the rest of the robots adapt their locations in order to ensure a certain predefined quality in the end-to-end communications channel.

In [8] and [9] the authors consider a team of autonomous robots in which a leader must perform a certain task while the other robots must optimize their position in order to maintain a certain quality in the wireless end-to-end communications link from the leader to an access point; in [7] and [10] the authors consider a similar problem in which which an autonomous robotic network must attain a desired configuration of the robots positions while maintaining a certain communications quality; then in [6] the authors maximize the coverage area of a mobile sensor network while ensuring wireless communications between its members; in [11] the authors consider a cooperative mobile sensor network and then design control laws so that at each iteration the sensor nodes gather a maximum amount of information.

As the reader see there are a large variety of problems being studied in the area of robotics communications. In this thesis we will focus on one particular problem within this area. The problem we are referring to is the compensation of small-scale fading using the robot's mobility. Small-scale fading [12] is a common phenomenon in RF wireless communications that affects the gain of the wireless channel. It occurs when, mainly due to reflection, various copies of the transmitted signal arrive at the receiver's antenna and depending on their phases they combine in a constructive or destructive way. This produces random variations in the wireless channel gain over very small distances (fractions of the wavelength used in the transmission). These

variations can degrade significantly the signal to noise ratio and in some cases even impede any communication at all. Therefore it must be compensated.

The effects of small-scale fading can be reduced by using high gain (directional) antennae as in [3]. This class of antenna can be bulky because they need a reflector in order to obtain their high gain and a mechanism to point the antenna in the desired direction. Thus this solution would require adding more hardware to the mobile robot and thus increase cost and weight which in turn will increase also its energy consumption. Another solution is the use of classical diversity techniques [12]. The idea behind diversity is that due to small-scale fading the channel gain varies randomly across different positions, times and/or frequencies and so the probability that all channels exhibit simultaneously poor gain is lower than the probability that a single channel exhibits poor gain. Diversity techniques construct a new 'artificial channel' by combining multiple channels. In consequence, this 'artificial channel' has a low probability of experiencing a poor gain. Diversity techniques have been extensively studied and developed in the wireless communications literature for more than 50 years and they have been devised for transceivers that are either stationary (e.g., a base station) or whose movement is random and uncontrolled (e.g., a user of a cellular network). But as mentioned above, robotics communications are unique due to the fact that the position of the transceiver is controllable and taking into account that small-scale fading varies significantly over small distances this opens up the possibility of developing a new class of diversity that compensates small-scale fading using the robot's mobility.

The main idea behind this diversity technique is as follows. The gain of RF wireless channels exhibiting small-scale fading varies significantly over very small distances. Therefore if the robot is communicating through an RF wireless channel and the channel gain is poor (due to a deep fade) then the robot can move slightly to find a location where the channel gain is higher.

In the next section we present brief review of the papers that have used this kind of (mobility) diversity in order to present to the reader the state of the art of this technique at the moment in which we started doing research on.

1.1 Related Work

The amount of literature dealing with the topic of compensating small-scale fading by controlling the position of the transceiver is relatively scarce when compared with other research topics in communications. But in this section we briefly present the most important papers addressing this problem.

To the author's knowledge the first work in which mobility was controlled in order to compensate small-scale fading is [13]. In that paper the authors consider an RF wireless link experiencing small-scale fading and they showed experimentally that: (i) when the channel gain is bad due to the small-scale fading individuals can move in the surroundings to alter the physical configuration of the scatterers and therefore to

alter the small-scale fading in order to try to obtain high channel gains in the wireless channel; (ii) it is possible to move the transmitter very small distances in order to find a position in which the channel gain is high. In other words the authors showed that we can take advantage of the small-scale fading by either altering the physical configuration of the surroundings or by altering the position of the transmitter. In that paper, the authors provided mobility to a transmitter node by placing it on a motorized turntable and so the transmitter moves in a circular path. The channel is then measured at various points along that circular path and the node stops at a position when the channel gain is high. This technique was used by the same authors in [14] to compensate small-scale fading in a wireless sensor network.

In [15] the authors consider the problem of moving a robot to compensate small-scale fading but without deviating too much from its initial position. The authors suggest making the robot explore a finite number of points and then make it return to the point that exhibits the best channel gain. Regarding the physical configurations of the points explored by the robot the authors propose two configurations: (i) points arranged in a circular path; (ii) points arranged in an hexagonal lattice contained in a circle. The size of both configurations are calculated in order to obtain independent wireless channels.

In [16] the authors refer to the mobility diversity principle as RF mobility gain. In that article the authors mention that one of the key elements of this technique is how the mobile robot (MR) samples the RF map– i.e., the shape of what we refer to (in this thesis) as the search space. This is due to the fact that as the frequency decreases the distance that the MR needs to move in order to observe higher variations on the channel gain increases and so using mobility to compensate small-scale fading becomes more costly. In addition, the authors test experimentally the concept of mobility diversity with a MR. The test was done in an office building with an RF carrier frequency of 1.254 GHz and under non-line of sight conditions. The small-scale fading observed in this experiment was Rayleigh. The authors tested four different search spaces: (i) a random path, a linear path, a circular path and a helical path. The results of these experiments show that this technique can significantly improve the channel gain by making the MR move just small distances. They [16] also commented that this technique can increase the received signal power and improve the packet reception more than any coding scheme could achieve.

In [17] the authors propose to compensate small-scale fading by exploring N points randomly distributed in a small circle centered around the robot's initial position and then making the robot go to the point with the highest channel gain. In that paper the number of points and the size of the circle are design parameters which are arbitrarily determined.

In [18] the authors consider a mobile wireless robotic network where wireless links are affected by multipath, small-scale fading. The authors propose to use coordinated micro-motions to compensate for the small-scale fading and improve the overall performance of the network. In this algorithm each mobile robot can ex-

plore N positions in its near vicinity. A distributed algorithm is used to coordinate the movement of the robots so that collectively they find their optimum position to improve the performance of the network according to some predefined metric. Specifically the authors consider the case of $N = 2$, where both positions are separated a distance of $\lambda/2$, and the case of $N = 5$ where the positions form a uniform circular array of radius $\lambda/2$ with a central element. This is done in order to obtain independent channels at each position. In that article the authors show experimentally that these micro-movements can indeed increase significantly the throughput of the robotic network.

As can be observed from the previous summary in [13]-[18] the authors propose different configurations for the points explored by the robot in order to compensate for small-scale fading but another variant to this problem is considered in [19]-[23] where the authors consider that the mobile robot must follow a predefined path while communicating with a base station through an RF wireless channel experiencing small-scale fading. In this case, as opposed to [13]-[18], in order to compensate the small-scale fading the authors do not focus on determining the location of the points where the robot transmits but rather on determining its velocity profile. The solution in those articles is roughly based on the idea of following the predetermined path but spending more time at points (in the predefined path) with high channel gain (due to constructive interference generated by the small-scale fading) and less time at points (in the predefined path) with poor channel gain (due to destructive interference generated by the small-scale fading). Note that this approach works due to the fact that in the presence of small-scale fading then the channel gain varies significantly over small distances.

In this thesis we focus on the first variant of the problem –i.e., the design of the physical configuration of the points explored by the robot in order to compensate the small-scale fading. As we can see from [13]-[18] it is clear that the fact that we can compensate small-scale fading by moving the transceiver has already been proved experimentally. We also observe that in those works the authors understand that the points where the robot measures the wireless channel gain must be selected so that the wireless channel gains are independent. Nevertheless, we also note that there is no formal method to calculate the location of those points. This is the state of the art from which we start our research on the problem of compensating small-scale fading in robotics communications by controlling the robot's mobility.

1.2 Mobility Diversity Algorithms

We will refer to the diversity technique that uses the robot's mobility to compensate small-scale fading as mobility diversity and thus any algorithm implementing this technique will be referred to as a mobility diversity algorithm (MDA). In this section we will give a general overview of the structure and classification of MDAs.

In order to present an overview of MDAs consider first a mobile robot (MR)

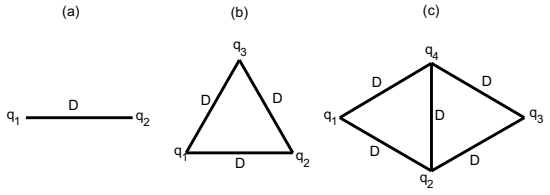

Figure 1.1: Search spaces for : (a) 2 stopping points, (b) 3 stopping points and (c) 4 stopping points (see later in thesis).

equipped with a single antenna communicating with a static node, which remains temporally stationary during the execution of the MDA, through a time-invariant wireless channel exhibiting small-scale flat fading. Due to the small-scale fading the wireless channel gain varies significantly over small distances with respect to the wavelength of the RF carrier used in the transmission. Therefore if the MR is experiencing poor channel gain due to the small-scale fading it can explore a search space in order to find a point with higher channel gain. Note that the greater the search space then the higher the number of points explored and the higher is the probability for the MR to find a point with a high channel gain. But the distance the MR travels also increases and so also the amount of energy spent in locomotion. So with this drawback the location of the points to be explored (as well as the number) must be optimized in order to allow the MR to obtain a high channel gain while expending low amounts of energy in the process.

The main component of the MDA is the search space. The search space is the spatial region that the MR is allowed to explore in order to find a point with a high channel gain. It can be discrete and so consists of a series of points as in Fig. 1.1 (to be described later in the thesis). In this case the MR moves from point to point stopping at each one to measure the channel gain and so we refer to these points as stopping points. This allows the MR to collect as many (noisy) samples from the receiver in order to obtain a channel estimate as accurate as needed. The discrete search space is characterized by the number of stopping points (its cardinality) and their geometry (its physical distribution).

Alternatively the search space can be continuous –i.e., it consists of a continuous path. In Fig. 1.2 (see later in the thesis) we observe some examples of continuous exploration paths. In this case the MR moves along the continuous path while collecting wireless channel samples and stops only at the end of the path. Since the MR stops only once at the end of the continuous search space (and not multiple times as in the discrete search space) then it can benefit from its inertia to use less energy during the exploration of the search space. Also note that for the continuous search space the number of explored points is determined by the MR receiver's spatial sampling rate and not by the size of the search space. For the discrete search space the number of explored points depends on its size (cardinality). The continuous search space is characterized by its length and its shape.

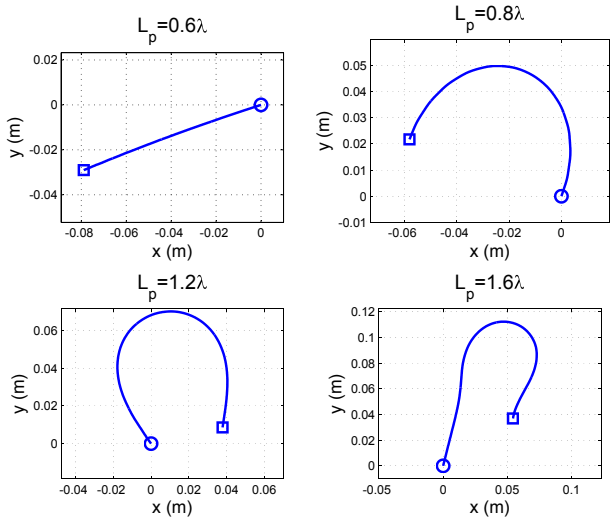

Figure 1.2: Optimized continuous path $\mathcal{P}$ for $N = 25$ and different values of L_p. $\mathbf{d}_1$ and $\mathbf{d}_N$ are represented with a circle and with a square respectively (see later in thesis).

The search space can also be either predetermined or adaptive. A predetermined search space means that it has already been fully defined (number of stopping points and physical configuration or length and shape) prior to the MDA execution. The advantage of predetermined spaces is that they can be designed off-line and then loaded into the MR's memory thus making this approach suitable for MRs with low computational capacity. The search spaces in Figs. 1.1 and 1.2 are examples of predetermined search spaces. Note that a predetermined space can also be either random or deterministic.

An adaptive search space is a search space that is being calculated (in real time) during the MDA execution according to the channel measurements that are being obtained. This type of search space requires more computation by the MR but it can perform better than the predetermined one because it adapts to each particular scenario. In Fig. 1.3 we observe four realizations of an adaptive discrete search space with eight stopping points. Theoretically speaking we could also have adaptive continuous search spaces but we have not yet found how to generate them.

Once the class of search space is selected we also need to define the way in which the MR is going to explore it. This means we need to define the order in which the MR is going to explore and also to decide what to do if it encounter a point with a high channel gain during the exploration. Now, once the MR finishes exploring the search space we need to determine the best action. Should it stay at that point and establish communications from it? Should it go to the best point in the search space? What does 'best point' means in this context?

We also need to determine the execution time of the MDA. If the execution time

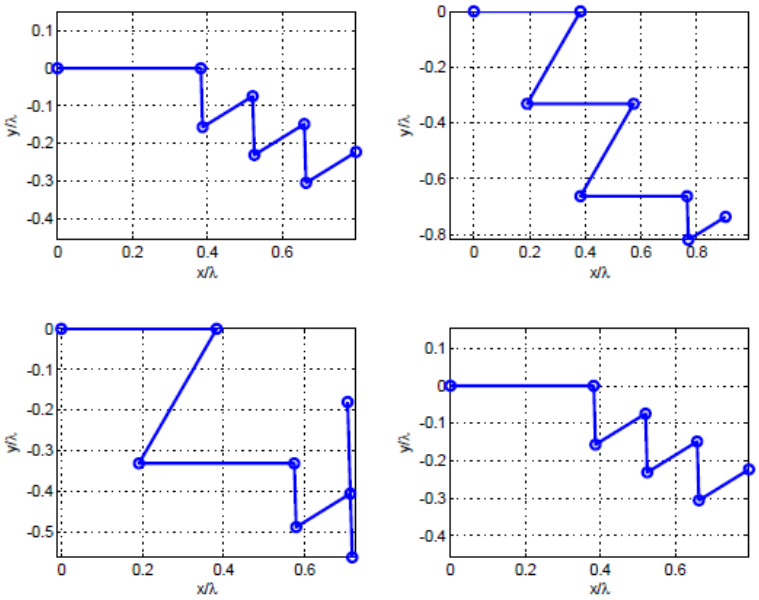

Figure 1.3: Different realizations of an adaptive path with eight stopping points.

is short the MR has to move fast and so the consumption of mechanical energy will be high. On the other hand if the execution time is long then the MR can move slowly and so the mechanical energy consumption will be lower but then the MR will have to wait longer between the start of the MDA execution and the establishment of the wireless link with its intended destination. Once this has been settled we need to design the control signals to move the MR during the MDA execution. These will determine the energy consumption and so they have to be optimized to minimize this consumption.

This concludes with the general overview of the MDA. In the next subsection we will present the organization of the chapters and their contribution.

1.3 Thesis Organization and Contribution

In the past, when analog televisions had bad reception and did not allow the spectator to watch their tv shows the users used to move the antenna to different positions until the reception was improved. This can be seen as an early and manual implementation of mobility diversity. The same technique is sometimes applied by cell-phone users. Therefore, strictly speaking the concept of mobility diversity by itself is not completely new but what is new is its automatization, optimization and implementation within autonomous agents (i.e., MRs).

In this thesis we start our study of MDAs from the state of the art presented in section 1.1 and we will examine all aspects of MDAs mentioned in section 1.2, but we will mainly focus on the design of the search space. Now we present the content

of each chapter and briefly mention the main contributions of each chapter.

In chapter 2 we consider the problem of MDAs with predetermined discrete search spaces. The main contributions of this chapter are as follows. We define what an optimum stopping point geometry means and we show that the definition is not unique. This leads to the development of two different techniques to optimize the geometry of the stopping points. We also develop the concept of adaptive diversity order which indicates how to optimize the number of stopping points. Finally, in chapter 2 we also propose the MDMTA approach which is a general MDA for discrete search spaces. The work presented in that chapter is taken from our journal paper:

- D. Bonilla Licea, M. Ghogho, D. McLernon and S. A. Raza Zaidi, "Mobility Diversity-Assisted Wireless Communication for Mobile Robots", IEEE Transactions on Robotics, vol. 32, no. 1, 2016, pp. 214-229.

which in turn is an extension of our earlier conference paper:

- D. Bonilla Licea, D. McLernon, M. Ghogho and S. A. Raza Zaidi, "An energy saving robot mobility diversity algorithm for wireless communications", 21st European Signal Processing Conference (EUSIPCO 2013), Marrakech, 2013.

In chapter 3 we consider the problem of MDAs with adaptive discrete search spaces, which is a continuation of chapter 2. In this case we solve the problem of how to design path planners to determine adaptively the optimum location of the stopping points. The main contributions of this chapter are first of all to show that contrary to classic diversity techniques, in the case of MDAs the channel correlation can be beneficial. We also demonstrate that by controlling the channel correlation we can obtain a higher channel gain than when all the channels are independent. We consider this a major breakthrough in the communications research area. We also design various optimum path planners with any memory order and show that MDAs using path planners with memory can outperform MDAs using predetermined stopping point geometries in both the channel gain obtained and the amount of mechanical energy spent. The path planners with memory order one and two presented in this chapter were first proposed in the conference paper:

- D. Bonilla Licea, D. McLernon and M. Ghogho, "A Robotic Mobility Diversity Algorithm with Markovian Trajectory Planners", Proc. of IEEE Workshop on Machine Learning and Signal Processing, Southampton, 2013.

Then the inspiration for the path planners with arbitrary memory order was taken from the conference paper:

- D. Bonilla Licea, D. McLernon and M. Ghogho, "Designing Optimal Trajectory Planners for Robotic Communications", Proc. of IET Intelligent Signal Processing (ISP'13) Conference, London, 2013.

Nevertheless, we later developed much more efficient and theoretically solid path planners with arbitrary memory order which perform much better in all aspects. Therefore we decided to leave out from this thesis the path planners presented in the IET conference paper above. Finally, we refined and extended all of our work regarding path planners with memory for MDAs in the following journal paper:

- D. Bonilla Licea, D. McLernon and M. Ghogho, "Path Planners with Memory for Mobility Diversity Algorithms", conditionally accepted for publication in IEEE Transactions on Robotics.

In chapters 2 and 3 we studied the MDAs with discrete search spaces considering SISO channels. In chapter 4 we extend even further that work to consider MDAs that compensate small-scale fading at various links simultaneously. Particularly we focus on the development of double-link path planners for MDAs that can be used in robotic relays in the context of robotic wireless networks. The contributions of this chapter is the development of path planners that can improve small-scale fading at various links simultaneously. The content of the chapter is taken from:

- D. Bonilla Licea, D. McLernon and M. Ghogho, "Multiple-link MDMTA for Robotic Networks", to be submitted.

The first part of the thesis, composed by chapters 2 to 4, consists of a rigorous treatment of various aspects of MDAs with discrete search spaces. The second part of the thesis, composed by chapters 5 and 6, treats the problem of MDAs with continuous search space.

In chapter 5 we show how an MDA with a continuous search space can be used to improve an RF energy harvesting system for a MR. In this chapter we restrict the shape of the continuous search space to be a straight line but we show how to optimize its length and all the other parameters involved. The main contribution of this chapter is to show that optimized MDAs can enhance RF energy harvesting and also the optimization of the continuous search space length. The content of this chapter was published in the following journal paper:

- D. Bonilla Licea, S. A. Raza Zaidi, D. McLernon and M. Ghogho, "Improving Radio Energy Harvesting in Robots Using Mobility Diversity", IEEE Transactions on Signal Processing, vol. 64, no. 8, 2016, pp. 2065-2077.

In chapter 5 we started to study MDAs with continuous search spaces but we restricted the shape of the search space to a straight line and we only optimized its length. In chapter 6 we continue with the study of MDAs with a continuous search space but in this chapter we show how we can derive the optimum shape of the continuous search space. The main contribution of this chapter is a general method to obtain the shape of the continuous path that forms the continuous search space (given a desired overall length). The content of this chapter is taken from:

- D. Bonilla Licea, D. McLernon, M. Ghogho, "Continuous Searching Space Mobility Diversity Algorithm", to be submitted.

Finally, we have to mention that part of the technique used to derive the shape of the continuous path was inspired by our work on an alternative topic on robotics communications presented in the following conference paper:

- D. Bonilla Licea, D. McLernon, M. Ghogho, "Optimal trajectory design for a DTOA based multi-robot angle of arrival estimation system for rescue operations", IEEE International Conference on Acoustics, Speech and Signal Processing (ICASSP), 2014, pp. 6800-6804.

Chapter 2

MDA with Predetermined Stopping Points

As mentioned in chapter 1 the search space for MDAs can be either predetermined or adaptive as well as discrete or continuous. In this chapter we start our treatment of MDAs with the simplest class of the search space which corresponds to the predetermined discrete search space. This type of search space is composed of N stopping points whose geometry is stored in the MR's memory prior to the MDA execution. Hence the predetermined use of the word.

In order to study MDAs in a systematic way we now introduce a general MDA and explicitly identify each one of its components and how they interact with each other. This general MDA is the mobility diversity with multi-threshold algorithm (MDMTA). Due to its generality, other different MDAs can be seen as particular cases of the MDMTA and so by studying it we can gain insight about other MDAs.

The physical distribution of the stopping points, which we will also refer to as the stopping points geometry, play an important role in the MDMTA performance. If the stopping points are far from each other then the wireless channel at those points will be approximately independent and thus the expected value of the maximum channel gain will be maximized[1]. This implies that the MDA using that geometry, depending on its internal parameters, will obtain a high channel gain. Therefore, in a first instance we could simply randomly locate the stopping points, as was proposed in [17], while ensuring that the minimum distance between them is at least on the order of half wavelength in order to obtain independent wireless channels. Nevertheless, this approach does not consider the distances that the robot has to travel during the MDMTA execution. So the distance traveled by the MR and the energy used in locomotion may be large. Therefore this approach is not efficient from an energy point of view.

A more efficient and intelligent approach to the design of the stopping points

[1] This is when we consider only predetermined geometries. In the next chapter we shall see that when we consider adaptive geometries this is not true anymore.

geometry requires both consideration of the correlation of the wireless channels at the stopping points and the amount of mechanical energy used by the MR to explore the stopping points. So in this chapter we will consider realistic probabilistic models for the wireless channels as well as realistic dynamical models for the MR. This will allow us to optimize the stopping points geometry (and the other internal parameters of the MDMTA) in order to obtain high channel gains while using as little energy as possible in exploration of the stopping points.

The main contribution of this chapter is the solution to the problem of how to optimise the stopping points geometry for any number of stopping points. In addition, we demonstrate that the interpretation of optimum stopping points geometry is not unique. To illustrate this we derive two different methods to optimise these geometries according to different criteria. Another contribution of this chapter is the concept of adaptive diversity order which allows us to adapt the number of stopping points (diversity order) of the MDMTA to select the optimum number for each particular case just prior to the algorithm execution. The MDMTA is also another contribution. But, a more important contribution than the MDMTA itself is the formalization and the identification of its components. This formalization and identification of its components facilitates the study MDAs.

We start this chapter in section 2.1 by introducing the wireless channel model as well as the dynamical model for the MR. Then in section 2.2 we present in detail the MDMTA (with each one of its components) and explain how they interact with each other. We then present the core element of this chapter (and one of the most important parts of this thesis) in subsection 2.3.1. Here we derive different optimum stopping point geometries and also optimise their exploration order. In subsection 2.3.2 we show how to optimise the rest of the MDMTA parameters and in subsection 2.3.3 we introduce the concept of adaptive diversity order that allows us to optimise the number of stopping points. In section 2.4 we analyse some properties of the MDMTA and finally in sections 2.5 and in 2.6 we discuss some results regarding the behaviour of the MDMTA and present some conclusions for the MDA with a predetermined discrete search space.

2.1 System Model

2.1.1 MR Model

In this chapter, we consider an omnidirectional MR, i.e., a MR that can move in any direction at any time. In particular we select a three-wheel omnidirectional mobile robot[2] (TOMR) [24]. A TOMR is a MR with three omnidirectional wheels [25], where each wheel is driven by its own motor. The distance from the center of the robot to each wheel is denoted by L. The TOMR model described in this subsection

[2]Although we select this particular MR the results presented in this chapter can be applied to any other type of omnidirectional MR.

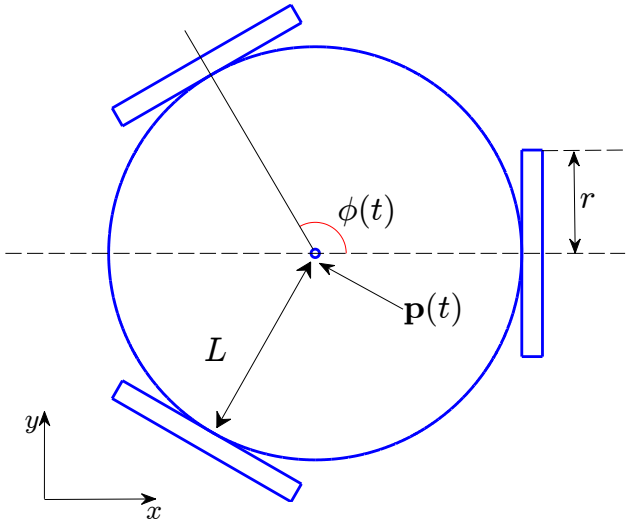

Figure 2.1: Three-wheeled omnidirectional mobile robot at position $\mathbf{p}(t) = [x_g(t) \;\; y_g(t)]^T$, orientation $\phi(t)$ and with an antenna at its centre.

is a version of the model presented in [26]. The robot is equipped with an antenna installed at the geometrical center of the robot (see Fig. 2.1).

The TOMR position at time t in the global coordinate frame is $\mathbf{p}(t)$ and its pose is $\mathbf{p_o}(t) = [\mathbf{p}^T(t) \;\; \phi(t)]^T$, where $\phi(t)$ is its orientation. The TOMR pose is related to the control inputs as follows [26]:

$$\dot{\mathbf{z}}(t) \;\; = \;\; \begin{bmatrix} \mathbf{O}_{3\times3} & \mathbf{I}_{3\times3} \\ \mathbf{O}_{3\times3} & \mathbf{R}(t)\dot{\mathbf{R}}^T(t) - \mathbf{A}^{-1}\mathbf{C} \end{bmatrix} \mathbf{z}(t) + \begin{bmatrix} \mathbf{O}_{3\times3} \\ \mathbf{A}^{-1}\mathbf{R}(t)\mathbf{D} \end{bmatrix} \mathbf{u}(t), \tag{2.1}$$

where $\mathbf{z}(t) = [\mathbf{p_o^T}(t) \;\; \dot{\mathbf{p}}_\mathbf{o}^\mathbf{T}(t)]^T$, $\mathbf{u}(t) = [u_1(t) \;\; u_2(t) \;\; u_3(t)]^T$, $u_i(t)$ is the control input to the ith motor, $\mathbf{O}_{3\times3}$ is a 3×3 zero matrix and $\mathbf{I}_{3\times3}$ is a 3×3 identity matrix. Matrix $\mathbf{A}$ is given by

$$\mathbf{A} = \begin{bmatrix} m + \frac{3J_w}{2r^2} & 0 & 0 \\ 0 & m + \frac{3J_w}{2r^2} & 0 \\ 0 & 0 & J_c + \frac{3J_wL^2}{r^2} \end{bmatrix}, \tag{2.2}$$

where m is the total mass of the robot, r is the radius of the wheels, L is the distance from the geometric center of the robot to each wheel and J_c and J_w represent the inertia for the robot rotation and for each wheel respectively. We also have:

$$\mathbf{C} = k_1 \begin{bmatrix} 1 & 0 & 0 \\ 0 & 1 & 0 \\ 0 & 0 & 2L^2 \end{bmatrix}, \tag{2.3}$$

with k_1 being a robot-specific parameter, and the matrix $\mathbf{D}$ is:

$$\mathbf{D} = k_2 \begin{bmatrix} 0 & -\sin(\pi/3) & \sin(\pi/3) \\ 1 & -\cos(\pi/3) & -\cos(\pi/3) \\ L & L & L \end{bmatrix}, \tag{2.4}$$

where k_2 is another robot-specific parameter. Finally, the rotation matrix $\mathbf{R}(t)$ is given by:

$$\mathbf{R}(t) = \begin{bmatrix} \cos(\phi(t)) & -\sin(\phi(t)) & 0 \\ \sin(\phi(t)) & \cos(\phi(t)) & 0 \\ 0 & 0 & 1 \end{bmatrix}. \tag{2.5}$$

Now, the energy drawn from the battery by the MR's motion from time t_k to t_{k+1} is [26]:

$$E_{mech}(t_k, t_{k+1}, \mathbf{u}(t)) = \int_{t_k}^{t_{k+1}} \left(k_3 \mathbf{u}^T(t)\mathbf{u}(t) - k_4 \dot{\mathbf{p}}_{\mathbf{o}}^T(t)\mathbf{R}(t)\mathbf{D}\mathbf{u}(t) \right) dt, \tag{2.6}$$

where k_3 and k_4 are robot-specific parameters. All four parameters (k_1, k_2, k_3 and k_4) depend on various electromechanical parameters of the MR's motors but to avoid introducing more parameters and keep the notation as simple as possible we do not present any more detail. The interested reader can find more detailed expressions for k_1, k_2, k_3 and k_4 by comparing the model presented in [26] to our version.

2.1.2 Wireless Channel Model

In this and subsequent chapters we consider a MR communicating with a stationary node through a wireless channel in a static environment. The stationarity of both the node and the environment have to hold during the MDA execution and the transmission. So the static node can be another MR which remains still during that period of time. This implies that for the MDA analysis and design we can consider the wireless channel to be time invariant.

Note that if the environment or the position of one node changes during the transmission then the wireless channel may be degraded and so the MDA has to be executed again before resuming the transmission.

We assume that the MR is surrounded by various scatterers and thus the electromagnetic waves radiated by the stationary node's antenna will arrive to the MR's antenna through multiple paths each with different angles of incidence and different phases. As a consequence, these copies will combine at the MR's antenna randomly producing either constructive or destructive interference depending on the MR's location. Thus the wireless channel exhibits small-scale fading (also called multi-path fading) [27].

Furthermore we assume that the signals used for communication are narrowband, meaning that their bandwidth is small compared to RF carrier used for transmission

and so the wireless channel model is frequency independent. In consequence the small-scale fading is flat.

We also assume that there is neither line of sight between the stationary node and the MR nor a predominant wave arriving at the MR's antenna as a consequence the angle of incidence of the waves arriving at the MR's antenna is uniformly distributed on $[0, 2\pi)$ while the average power of all the incident waves at the moment of the arrival to the MR's antenna is considered the same. Thus we have Rayleigh fading [27].

Taking all the above assumptions into account we have a time invariant wireless channel exhibiting Rayleigh flat fading and so the signal received by the MR when located at point $\mathbf{p}(t)$ is:

$$y(t) = s(\mathbf{p}(t))h(\mathbf{p}(t))x(t) + n_r(t) \tag{2.7}$$

where $x(t)$ is the narrowband signal transmitted by the stationary node and $n_r(t) \sim \mathcal{CN}(0, \sigma^2)$ is[3] the additive white Gaussian noise generated at the MR's receiver. Then $s(\mathbf{p}(t))$ and $h(\mathbf{p}(t))$ are the shadowing (also known as large-scale fading) [27] and small scale fading terms respectively (both depending on the MR's position, $\mathbf{p}(t)$). Note that $h(\mathbf{p}(t)) \sim \mathcal{CN}(0, 1)$ and $|h(\mathbf{p}(t))|$ is Rayleigh distributed.

We also assume that the wireless channel is reciprocal and so the signal received by the stationary node when the MR is located at $\mathbf{p}(t)$ is given by (2.7), simply by exchanging $n_r(t)$ by the noise generated at the stationary node's receiver and $x(t)$ by the signal transmitted by the MR.

The spatial normalized covariance of $h(\mathbf{p}(t))$ is given by [28]:

$$\begin{aligned} \mathbb{E}\left[h(\mathbf{p})h^*(\mathbf{q})\right] &= J_0\left(2\pi\|\mathbf{p}-\mathbf{q}\|_2/\lambda\right) \\ &= r(\mathbf{p}, \mathbf{q}), \end{aligned} \tag{2.8}$$

while its channel gain has the following normalized spatial covariance function:

$$\frac{\mathbb{E}\left[(|h(\mathbf{p})| - \mathbb{E}[|h(\mathbf{p})|])(|h(\mathbf{q})| - \mathbb{E}[|h(\mathbf{q})|])\right]}{\mathrm{var}(|h(\mathbf{p})|)} = r^2(\mathbf{p}, \mathbf{q}). \tag{2.9}$$

where $J_0(\cdot)$ is the Bessel function of the first kind and zeroth order, $\mathrm{var}(|h(\mathbf{p})|)$ is the variance of $|h(\mathbf{p})|$ (which is the same as the variance of $|h(\mathbf{q})|$, λ is the wavelength used in the RF transmission by the stationary node and $\mathbf{p}, \mathbf{q} \in \mathbb{R}^2$ are any two points on the space.

Finally, during the execution of the MDMTA the MR moves in a small area and so we can assume that the shadowing term is constant for all the stopping points, i.e., $s(\mathbf{p}(t)) \approx s$.

[3]Note that $\mathcal{CN}(0, \sigma^2)$ means a complex normal random variable with zero mean and variance σ^2, whose real and imaginary parts are independent and identically distributed.

2.2 Mobility Diversity with Multi-Threshold Algorithm

The MDMTA is a general mobility diversity algorithm for MRs that uses a discrete search space composed of stopping points. This algorithm requires that one end of the wireless link remains fixed during its execution. We will refer to this end of the link as the stationary node. In order to implement the MDMTA the stationary node uses time division duplex transmission[4]. During the transmission time the fixed node sends a training signal so that the MR can estimate the channel gain at each stopping point. During the receiving time it waits for a response from the MR to start communicating. This occurs once the MDMTA terminates and the MR finds an optimum stopping point.

Now, the MDMTA is divided into two phases: a searching phase and a selection phase, respectively over the periods $t_1 \leq t < t_N$ and $t_N \leq t \leq t_{N+1}$. During the *searching phase* the MR stops and estimates the channel gain at N different points called stopping points. By definition the initial position of the MR is the first stopping point $\mathbf{q}_1$, i.e., $\mathbf{p}(t_1) = \mathbf{q}_1$. If at time instant t_k the estimation of the kth channel gain is greater than the threshold η_k the MDMTA terminates prematurely and the MR then transmits (at $\mathbf{q}_k$) its data to the stationary node. In this case we will say, for notational convenience, that the optimum stopping point $\mathbf{q}_{opt}$ is $\mathbf{q}_k$. If the kth channel gain is less than η_k, then the MR moves to $\mathbf{q}_{k+1}$ in $t_{k+1} - t_k$ seconds and repeats the process. If it reaches the Nth stopping point then the searching phase terminates and the selection phase initiates. During the *selection phase* the MR uses a selection rule ($\mathcal{R}_s$) to determine the optimum stopping point $\mathbf{q}_{opt}$ from which to transmit (the optimum position is not always the one with the highest channel gain as we shall later see). Then the MR moves from the stopping point $\mathbf{q}_N$ to $\mathbf{q}_{opt}$ in $t_{N+1} - t_N$ seconds.

The MDMTA requires: N, the number of stopping points to be explored; a matrix $\mathbf{Q}_N = [\mathbf{q}_1,\ \mathbf{q}_2, \cdots, \mathbf{q}_N]^T$ containing the positions of the N stopping points to be explored; an $N+1$ dimensional temporal vector $\mathbf{t} = [t_1\ \ t_2 \cdots t_{N+1}]^T$; an $N-1$ dimensional vector $\boldsymbol{\eta} = [\eta_1,\ \eta_2, \cdots,\ \eta_{N-1}]^T$ of thresholds; a selection rule $\mathcal{R}_s$ (to be explained later in this section) and (optionally) an estimate of the shadowing term s denoted by $\hat{s}$. The pseudocode of the MDMTA is summarized below in Algorithm 1 where $\mathbf{p}$ represents the position of the MR. Note that the $\hat{s}$ is in brackets in the list of input parameters for the MDMTA in Algorithm 1. This means that this parameter is optional. Later, as we shall see, we can run the MDMTA without this parameter but in this case we will not be able to use the thresholds.

The thresholds in the MDMTA are used to terminate prematurely the algorithm when the MR finds a stopping point with a high channel gain. This is in order to avoid spending more energy by exploring the rest of the stopping points. If

[4]This means that the fixed node alternates periodically its behaviour acting either as a receiver or a transmitter.

Algorithm 1 $MDMTA(N, \mathbf{Q}_N, \mathbf{t}, \boldsymbol{\eta}, \mathcal{R}_s, (\hat{s}))$

1: $\mathbf{p} \leftarrow \mathbf{q}_1$
2: **for** $k = 1$ to $N - 1$ **do**
3: $\hat{s}|\hat{h}(\mathbf{q}_k)| \leftarrow$ Estimate$[s|h(\mathbf{p})|]$ {Channel gain estimation .}
4: **if** $|\hat{h}(\mathbf{q}_k)| \geq \eta_k$ **then**
5: $\mathbf{q}_{opt} \leftarrow \mathbf{q}_k$
6: Terminate Algorithm
7: **end if**
8: $\mathbf{p} \leftarrow \mathbf{q}_{k+1}$ {The MR moves to the next stopping point in $t_{k+1} - t_k$ seconds.}
9: **end for**
10: $\hat{s}|\hat{h}(\mathbf{q}_N)| \leftarrow$ Estimate$[s|h(\mathbf{p})|]$
11: $\mathbf{q}_{opt} \leftarrow \mathcal{R}_s$ {A 'selection rule' is used to determine the optimum position.}
12: $\mathbf{p} \leftarrow \mathbf{q}_{opt}$ {The MR moves to the optimum stopping point in $t_{N+1} - t_N$ seconds.}
13: Terminate Algorithm

the thresholds are too low the probability that $|\hat{h}(\mathbf{q}_1)| \geq \eta_1$ occurs is high and so the MR will stop most of the time at the first stopping point. This implies that the probability of finding a stopping point exhibiting a high channel gain will be low. On the other hand, if the thresholds are too high then the probability that any channel gain is superior to its corresponding threshold will be considerably low and then the MDMTA will almost never be prematurely terminated, so making the thresholds useless.

Now, as mentioned above, during the execution of the MDMTA the stationary node sends a training signal to the MR. This training signal allows the MR to estimate $s|h(\mathbf{q}_k)|$ (see lines 3 and 9 of Algorithm 1) but the thresholds need to be compared with $|h(\mathbf{q}_k)|$ and not with $s|h(\mathbf{q}_k)|$ (see lines 4 to 6 of Algorithm 1). So the estimation $(\hat{s})$ of the shadowing term[5] is used to isolate $|\hat{h}(\mathbf{q}_k)|$ from the estimation of $s|h(\mathbf{q}_k)|$ for the thresholding (lines 4 to 6 of Algorithm 1).

The reason why, in general, we compare the thresholds η_k with $|h(\mathbf{q}_k)|$ instead of comparing them with the total gain $s|h(\mathbf{q}_k)|$ is as follows. If we select the thresholds η_k, without knowing s nor $|h(\mathbf{q}_k)|$ separately, and we compare them with the total gain $s|h(\mathbf{q}_k)|$ then it may happen with a non-negligible probability that η would correspond to a total gain value $s|h(\mathbf{q}_k)|$ obtained by a low value of $|h(\mathbf{q}_k)|$, i.e. a locally small value of $s|h(\mathbf{q}_k)|$. This implies that if η was selected slighlty higher then the MR could find a much better total channel gain $s|h(\mathbf{q}_k)|$ without investing significantly more mechanical energy. In other words, such procedure would not be taking full advantage of the benefits that the MDMTA can provide. So, if the designer wants to obtain a locally high total channel gain $s|h(\mathbf{q}_k)|$ it should compare it directly to $|h(\mathbf{q}_k)|$. On the other hand, depending on the application, the designer

[5]The MR can estimate the shadowing term prior to the MDMTA execution with a technique like the one stated in [29] (implemented by this robot or by a robotic network).

may just want to satisfy a certain total channel gain $s|h(\mathbf{q}_k)|$, regardless if it is locally low or high. In that case the designer can simply compare the thresholdsit directly to the total channel gain.

As mentioned above, in case the designer wants to obtain a locally high channel gain $s|h(\mathbf{q}_k)|$ then he should compare the thresholds directly with $|h(\mathbf{q}_k)|$. If the MR does not have an estimate of s and wants to compare η_k directly with $s|h(\mathbf{q}_k)|$, it would be equivalent to comparing $|h(\mathbf{q}_k)|$ with η_k/s. Since in this case s is unknown, this action would be equivalent to using random thresholds which can be too low or too high (and so having the consequences as were previously explained). Therefore, if the MR wants to execute the MDMTA but does not know $\hat{s}$, then it would be better to set $\eta_k = +\infty$ to avoid choosing the thresholds too low which would significantly reduce the probability of obtaining a high channel gain. This is why $\hat{s}$ is an optional input parameter for the MDMTA.

The selection rule selects the optimum point ($\mathbf{q}_{opt}$) based on estimates of the product $s|h(\mathbf{q}_k)|$ and so, as opposed to the thresholding issues, it is not necessary to estimate s and $|h(\mathbf{q}_k)|$ separately to implement the selection rule. Nevertheless, for the remainder of this chapter we will assume that the MR knows $\hat{s}$.

The simplest selection rule $\mathcal{R}_s$ is the *Maximum Channel Gain Rule* which selects the stopping point with the highest estimated channel gain. This selection rule was used in [17] and also in our original MDMTA [30].

Assume that the MR uses the *Maximum Channel Gain Rule*. Then, consider the particular case in which the stopping point with maximum channel gain is not $\mathbf{q}_N$ (i.e., $\mathbf{q}_{opt} \neq \mathbf{q}_N$) and also that the maximum channel gain is just slightly higher than the channel gain observed at $\mathbf{q}_N$. So, in this particular case the following events can occur. Due to the estimation errors and the slightly difference between $|h(\mathbf{q}_N)|$ and $|h(\mathbf{q}_{opt})|$ then it may happen that $\hat{s}|\hat{h}(\mathbf{q}_{opt})| > \hat{s}|\hat{h}(\mathbf{q}_N)|$, when in fact we have $s|h(\mathbf{q}_{opt})| < s|h(\mathbf{q}_N)|$. Which means that the MR would expend energy by moving from $\mathbf{q}_N$ to a stopping point with a lower channel gain ($\mathbf{q}_{opt}$). Now, another event that can occur is that $\hat{s}|\hat{h}(\mathbf{q}_{opt})| > \hat{s}|\hat{h}(\mathbf{q}_N)|$ and we have indeed $s|h(\mathbf{q}_{opt})| > s|\hat{h}(\mathbf{q}_N)|$. But the difference between the channel gains is really small. So the MR would expend energy by moving from a $\mathbf{q}_N$ to a stopping point with a marginally higher channel gain ($\mathbf{q}_{opt}$).

In order to solve these problems with the *Maximum Channel Gain Rule* we propose a new selection rule: the *Minimum Effort Rule* (see Algorithm 2). The key idea of this new selection rule is to avoid wasting mechanical energy in movement that does not provide a good improvement in the channel gain. So, the MR now moves from $\mathbf{q}_N$ to the point with the highest estimated channel gain only if the difference $((\hat{s}|\hat{h}(\mathbf{q}_{k_{max}})| - \hat{s}|\hat{h}(\mathbf{q}_N)|)$–see Algorithm 2) is significant, in other words, larger than some threshold μ, see Algorithm 2. Note that if $\mu = 0$ then this selection rule becomes the *Maximum Channel Gain Rule*. For the rest of the chapter we will assume that the MDMTA uses the *Minimum Effort Rule*.

Now that we have explained in detail the behavior and the components of the

Algorithm 2 $\mathbf{q}_{opt} \leftarrow \mathcal{R}_s(\mu)$ Minimum Effort Rule

1: $k_{max} \leftarrow \arg \max_{k=1,2,\cdots,N-1} \left\{ \hat{s}|\hat{h}(\mathbf{q}_k)| \right\}$
2: **if** $\hat{s}|\hat{h}(\mathbf{q}_{k_{max}})| - \hat{s}|\hat{h}(\mathbf{q}_N)| > \mu$ **then**
3: $\quad \mathbf{q}_{opt} \leftarrow \mathbf{q}_{k_{max}}$
4: **else**
5: $\quad \mathbf{q}_{opt} \leftarrow \mathbf{q}_N$
6: **end if**
7: return $\mathbf{q}_{opt}$

MDMTA we will proceed to explain how to optimize this algorithm in the next section.

2.3 MDMTA Optimization

In this section we will deal with the optimisation of the MDMTA which is in effect the optimisation of its parameters, the stopping points geometry and the number of stopping points. Before optimising the MDMTA we need to establish how a good MDA should behave so that we know what cost function to optimise. The objective of an MDA is to obtain high channel gain and it achieves this by moving the MR but this 'costs' mechanical energy. Thus an efficient MDA can obtain high channel gains by 'investing' low amounts of mechanical energy. So, given the number of stopping points N, the MDMTA can be optimized by maximizing a cost function that takes into account the maximum channel gain obtained and also the mechanical energy invested during the MDMTA execution. So, the general MDMTA optimization problem to be solved is:

$$\begin{aligned} &\min_{\boldsymbol{\eta},\boldsymbol{t},\mu,\mathbf{Q}_N,\mathbf{u}(t)} f\left(|h(\mathbf{q}_{opt})|, E_{mech}\left(t_1, t_{N+1}, \mathbf{u}(t)\right)\right) \\ &\text{s.t.} \\ &\mathbf{q}_k \in \mathcal{X}, \quad k = 1, 2, \cdots, N \\ &t_{N+1} - t_1 - T_{max}(N) = 0 \end{aligned} \tag{2.10}$$

where $\boldsymbol{\eta}$ is the threshold vector, $\mathbf{t}$ is the temporal vector, μ is the *Minimum Effort Rule* input parameter, $\mathbf{Q}_N$ is the matrix describing the geometry of the ordered stopping points (i.e., the order in which they must be visited), $\mathcal{X}$ is the exploration area (which must be 'small' to validate the assumption made in section 2.1.2 about the constant shadowing term the for all the stopping points) in which the stopping points are allowed to lie, $T_{max}(N)$ is a design parameters that determines the maximum execution time of the MDMTA and $f\left(|h(\mathbf{q}_{opt})|, E_{mech}\left(t_1, t_{N+1}, \mathbf{u}(t)\right)\right)$ is a general cost function depending on the optimum channel gain $|h(\mathbf{q}_{opt})|$ and the mechanical energy spent during the MDMTA execution $E_{mech}\left(t_1, t_{N+1}, \mathbf{u}(t)\right)$. This cost function should

have low values when the MDMTA is efficient (as defined above) and high values when it is inefficient. To construct this function we need to translate the previous qualitative description into mathematical language and as we shall see later there is not a unique way to do this.

This optimization problem is extremely complicated because it is non-linear, non-convex and it involves the simultaneous optimization of the MDMTA parameters jointly with the geometry of the stopping points (including the order in which they must be visited) and the control law for the MR. A suboptimal but much manageable approach is to partially decouple the optimization of the MDMTA parameters from the optimization of the stopping points geometry.

2.3.1 Stopping Points Optimization

The stopping points have a major influence on the performance of the MDMTA. They determine the maximum channel gain obtainable and also have a large influence on the amount of mechanical energy used by the MDMTA. This section, which constitutes one of the most important parts of this thesis, tackles the problem of its optimisation for any number of stopping points.

To optimise the stopping points we need first to optimise its spatial distribution. This determines the maximum channel gain obtainable. Once the geometry of the stopping points is optimised the MR needs to know in which order explore them. From a communications perspective the exploration order is irrelevant since, as mentioned above, the maximum channel gain obtainable is only determined by the stopping points geometry. Nevertheless the exploration order needs to be optimized to make the MR travel the minimum distance possible in order to minimise the amount of mechanical energy. In this section, we will first discuss the optimisation of the stopping points geometry and then the optimisation of the exploration order.

The reason why we decided to consider an omnidirectional MR is because it significantly simplifies the optimisation of the stopping points. An omnidirectional MR can traverse any geometry of stopping points in any order always moving in straight line from point to point but other types of MR may have difficulties in traversing certain geometries due to their kinematic constraints [25]. Thus, the omnidirectionality of the MR allows us to freely design the geometry without having to take into account any kinematic constraints.

We present two different approaches for the optimisation of the stopping points geometry. In the first approach the points are restricted to a predefined exploration area and then we arrange them in such a way that the expected value of the maximum of the channel gain at all the points is maximised. Mathematically this can be stated as follows:

$$\max_{\mathbf{Q}_N^u} \qquad \mathbb{E}[\max_j |h(\mathbf{q}_j^u)|] \tag{2.11}$$

$$\text{s.t.}$$

$$\mathbf{q}_k^u \in \mathcal{X}_e(\rho), \quad k = 1, 2, \cdots, N \tag{2.12}$$

with:

$$\mathcal{X}_e(\rho) = \{[x \;\; y]^T \mid x^2 + y^2 \leq \rho^2\}. \tag{2.13}$$

where $\mathcal{X}_e(\rho)$ represents the exploration area, $\mathbf{Q}_N^u = [\mathbf{q}_1^u,\ \mathbf{q}_2^u, \cdots, \mathbf{q}_N^u]^T$ is the matrix of unordered stopping points (i.e., this matrix describes the stopping points geometry but it does not indicate the order in which they must be explored). By contrast, $\mathbf{Q}_N$ has the stopping points arranged in the exact order that they must be visited. Later in this section we will explain how to derive $\mathbf{Q}_N$ from $\mathbf{Q}_N^u$.

Note that in the optimization problem (2.11) we are not explicitly considering mechanical energy. But by selecting properly the size of the exploration area $\mathcal{X}_e(\rho)$ and by optimizing the exploration order of the stopping points (see later in this chapter) we can reduce the amount of mechanical energy used.

The solution of this optimization problem depends on the particular shape of the exploration area $\mathcal{X}_e(\rho)$ which for simplicity we choose to be circular with radius ρ. Other choices are also possible (e.g., a rectangular, elliptic or even a non-convex shape) but we will not consider them in this thesis.

Although in general there is no analytical expression for the cost function in (2.11), in theory we could obtain an estimate by evaluating it via Monte Carlo simulations and then using an heuristic optimization algorithm to optimize it. Then the problem is that if the variance of the estimation error is not small enough the optimization algorithm could have trouble converging or delivering a reliable solution. But to achieve a variance small enough we need to perform a high number of Monte Carlo simulations to estimate the true value of the cost function thus making the optimization process computationally too costly and slow. Therefore, even if in theory (2.11) can be solved in practice this can be problematic in particular as the number of stopping points N increases.

So we need a more tractable approach. To do this we can use the common knowledge from the communications literature regarding the fact that the expected value of the maximum channel gain of various channels is maximized when all the channels are independent, (see chapter 9 of [12]). We shall illustrate this in section 2.4.1 for the reader unfamiliar with this result. Thus instead of directly optimising $\mathbb{E}[\max_j |h(\mathbf{q}_j^u)|]$ (for which there is not an analytical expression) an alternative and simpler approach is to minimise the Frobenius norm of the spatial covariance matrix $\mathbf{C}_N^u$ of the channel gains with the entry of the ith row and jth column given by $\mathbf{C}_N^u(i,j) = J_0^2\left(2\pi\|\mathbf{q}_i^u - \mathbf{q}_j^u\|_2/\lambda\right)$. The resulting modified optimization problem is now:

$$\min_{\mathbf{Q}_N^u} \qquad \|\mathbf{C}_N^u\|_F^2 \tag{2.14}$$

s.t.

$$\mathbf{q}_k^u \in \mathcal{X}_e(\rho), \quad k = 1, 2, \cdots, N \tag{2.15}$$

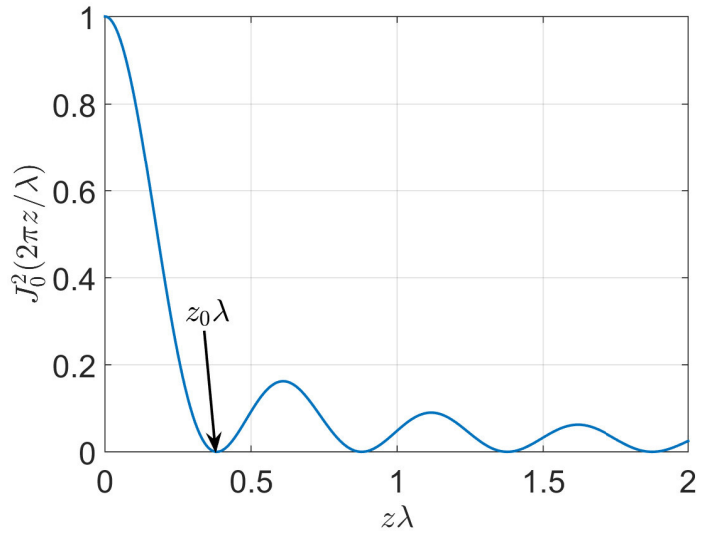

Figure 2.2: Definition of z_0 as the smallest value of z that produces a zero covariance.

where $\|\cdot\|_F$ is the Frobenius norm. Before we continue let us define z_0 as the smallest value of z that satisfies $J_0^2(2\pi z/\lambda) = 0$. For illustration purposes we show z_0 in Fig. 2.2

This optimization problem is non-linear, non-convex, with multiple local minima and is $2N$-dimensional (2 variables per stopping point) but at least the search space is constrained and we have an analytical expression for the cost function. Antenna array geometry optimization problems [31] have been solved before using the *simulated annealing* (SA) algorithm [32] which is a heuristic searching method. Mathematically, the stopping points geometry problem is similar in the sense that both problems have to determine an optimum distribution of points in the space (although the cost functions may differ). Therefore we will also use SA to solve (2.14). In Figs. 2.3 to 2.6 we observe the geometries obtained by solving (2.14) with the SA algorithm for $N = 3, 4, \cdots, 8$ and with different radii of the circular exploration area. The SA algorithm aims to find the global solution of the optimization problem through a well designed random search. This implies that generally in our problem the geometries obtained by the SA will be very close to the optimum depending on how long we run the SA algorithm and also on the values the parameters used to run it. For example in Fig. 2.3 for $N = 8$ we observe that the geometry is quite close to a uniform circular array (UCA) and so we may reasonably deduce that the actual optimum geometry is the UCA. This deduction is confirmed by comparing the cost function evaluated with the geometry obtained by the SA with the one evaluated with the UCA geometry.

It is interesting to note that for small exploration areas ($\rho \leq z_0/2$) the optimum geometries (at least for $N \leq 8$) are points on a UCA. But as ρ grows the shape of the optimum geometries changes. The case of $N = 4$ is particularly interesting

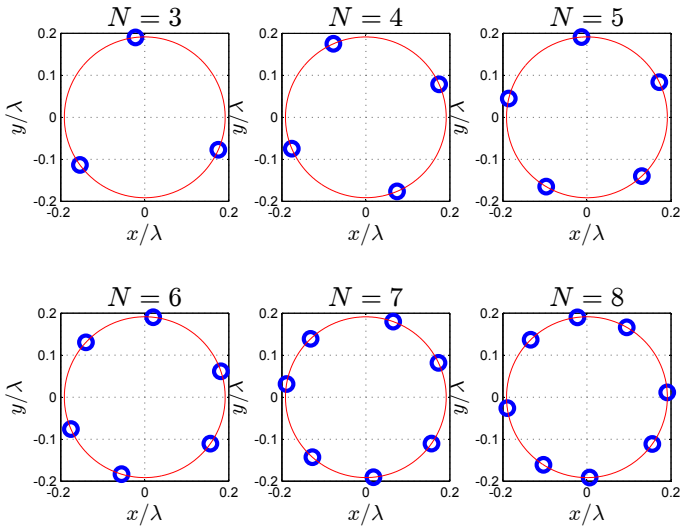

Figure 2.3: Geometries obtained by solving (2.14) with $\mathcal{X}_e(0.5z_0)$ using SA for $N = 3, 4, \cdots, 8$ stopping points.

because the geometry transforms gradually from a perfect square, for small ρ, to a rhombus, for higher values of ρ. This shows that, in general, the shape of the optimum geometries depends on the size of the exploration area. In addition, these results are obtained using a circular exploration area and so if we change the shape of the exploration area (e.g., elliptic or rectangular) the shapes of the optimum geometries may also differ. Now, if we observe Fig. 2.6 we note that the geometries obtained are no longer regular and look more random and spread out. This is because for $\rho \geq z_0$ and a low number of stopping points the number of local minima increases considerably as the exploration area increases. Many of these local minima will have a high value of $\mathbb{E}[\max_j |h(\mathbf{q}_j)|]$ but they will also have the stopping points more separated from each other and so it will demand the MR to travels over longer distances and consequently use more mechanical energy.

Now, the second approach for optimizing the stopping points geometries consists in arranging the points in such a manner that they provide us with a high channel gain while making the points lie as close as possible so that the MR has to move as little as possible. Mathematically this problem can be stated as follows:

$$\min_{\mathbf{Q}_N^u} \quad (1-\theta)\|\mathbf{C}_N^u\|_F^2 + \theta \sum_{j=1}^{N} \left(\mathbf{q}_j^u - \frac{1}{N} \sum_{i=1}^{N} \mathbf{q}_i^u \right)^2 \tag{2.16}$$

where θ is a design parameter. The cost function minimized in (2.16) is a convex combination of both the correlation among the channels and the actual spatial spread of the stopping points. Therefore, this cost function will allow us to obtain geometries with channels that have low correlation (and thus large $\mathbb{E}[\max_j |h(\mathbf{q}_j)|]$), with points

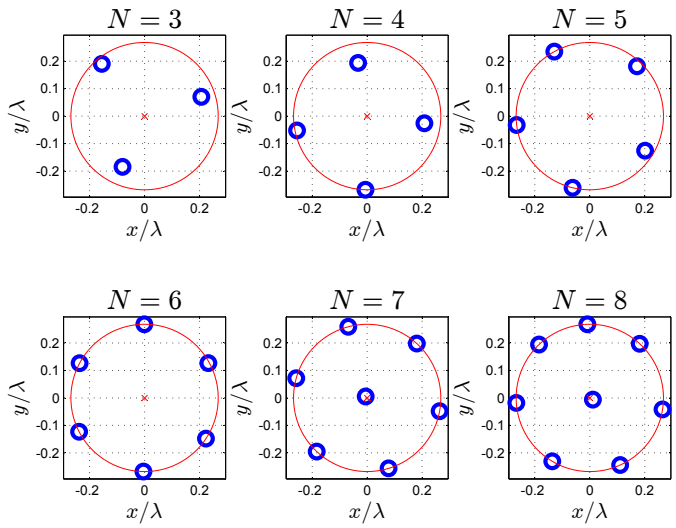

Figure 2.4: Geometries obtained by solving (2.14) with $\mathcal{X}_e(0.7z_0)$ using SA for $N = 3, 4, \cdots, 8$ stopping points.

that are close together (and so will require a small amount of mechanical energy from the MR while traversing this geometry).

Note that θ in (2.16 has the same role as ρ in (2.14. These parameters are used to control how far from each other will be the stopping points. The further (closer) the stopping points are the lower (higher) the correlation between their channels and so the maximum channel gain obtainable increases (decreases) but the amount of mechanical energy required to explore such geometry also increases (decreases).

In Figs. 2.7 to 2.10 we can see the geometries obtained by solving (2.16) with the SA algorithm for $N = 3, 4, \cdots, 8$ and different values of θ. For high values of θ (see Fig. 2.7) and $N > 3$ we can observe a curious phenomenon: the optimum geometries have two points overlapping on the center while the remaining $N - 2$ points form a UCA. It seems to happen for $N = 8$ and $\theta = 0.9$ (see Fig. 2.8).

This phenomenon occurs when the second term (i.e., point spatial spread) in (2.16) takes much larger values than the first term (i.e., spatial correlation). When this happens the optimum solution to (2.16) has stopping points overlapped at the center of the configuration in order to reduce the spatial spread even while the spatial correlation is significantly increased. Note that in the limit when the second term is much more important than the first term the solution to (2.16) will tend to a single point (i.e., all the points overlapped). Therefore when choosing (2.16) to obtain the optimum geometries we need to be careful not to select high values of θ and/or N that could produce such undesired behaviour.

We should emphasise that if θ is not large enough then the optimum geometries for $N = 3$ and $N = 4$ are the equilateral triangle (as in (2.14)) and the rhombus geometry (as in (2.14) for $\rho > 0.5z_0$). Finally, we should mention that as the number

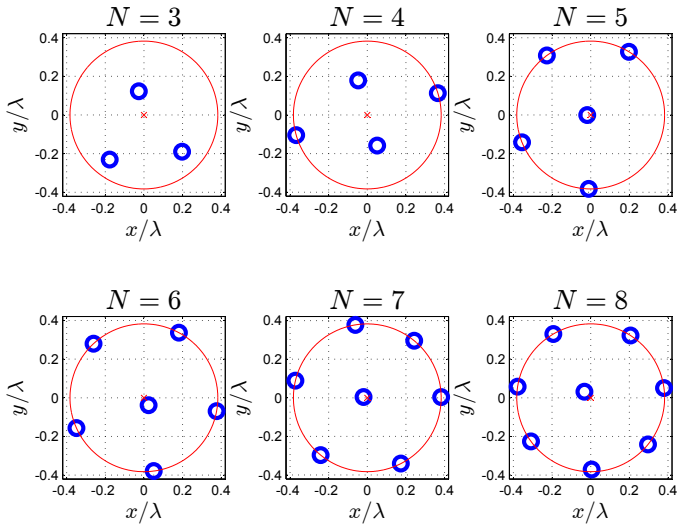

Figure 2.5: Geometries obtained by solving (2.14) with $\mathcal{X}_e(z_0)$ using SA for $N = 3, 4, \cdots, 8$ stopping points.

of stopping points N increases and/or the parameter θ decreases it becomes more difficult to solve (2.16) using the SA algorithm.

It is important to highlight that the geometries shown in Figs. 2.3 to 2.10, which are typical cases, can easily be contained into a square of side 2λ. So, given these small dimensions, then along with experimental results relating to the spatial autocorrelation function of the shadowing term (s) presented in [33], our assumption that s is approximately constant for all stopping points is clearly justified.

We have also to point out that in the design of the geometries only the relative position of the stopping points is important. This is because the relative position of the stopping points determine channel correlation between all the channels which in turn determines the maximum channel gain that can be obtained such geometry. This can be corroborated by analysing (2.14)-(2.16).

It is interesting to note that although the geometries obtained by solving (2.16) and (2.14) are optimal they are also different. This shows that there is not a unique way to define an optimum stopping points geometry.

Once we have the optimum matrix[6] $\mathbf{Q}_N^u$ of unordered points we have to establish the optimum exploration order for the stopping points (i.e., the matrix $\mathbf{Q}_N$). We remind the reader that by definition $\mathbf{q}_1$ will be the initial position of the MR. A matrix $\mathbf{Q}_N$ is optimum[7] if it minimizes the following cost function:

$$J\left(\mathbf{Q}_N\right) = \sum_{k=1}^{N-1} \|\mathbf{q}_{k+1} - \mathbf{q}_k\|_2 + \frac{1}{N} \sum_{j=1}^{N-1} \|\mathbf{q}_j - \mathbf{q}_N\|_2. \tag{2.17}$$

[6] Obtained by solving either (2.14) or (2.16).

[7] Because of the symmetry of the geometries there may be many equivalent optimum orders.

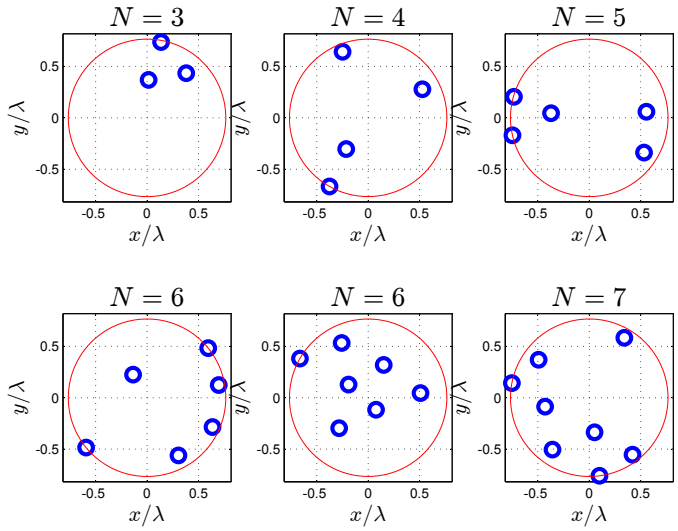

Figure 2.6: Geometries obtained by solving (2.14) with $\mathcal{X}_e(2z_0)$ using SA for $N = 3, 4, \cdots, 8$ stopping points.

The first summation on the right hand side of (2.17) is the distance travelled by the MR while traversing the whole geometry starting at $\mathbf{q}_1$ and finishing at $\mathbf{q}_N$; the second summation is the average distance that the MR needs to travel (after exploring the whole geometry) from $\mathbf{q}_N$ to the point with the highest channel gain. So, the optimum ordering problem can be stated as:

$$\min_{\mathbf{Q}_N} \quad J\left(\mathbf{Q}_N\right) \tag{2.18}$$

s.t.

$$\mathbf{Q}_N = \mathbf{P}\mathbf{Q}_N^u \tag{2.19}$$

where $\mathbf{P}$ is a permutation matrix and (2.18) is a combinatorial optimization problem. This problem can be solved using "branch and bound"[8] [34] as follows: we first create a tree, where the jth level (the root node is considered the zeroth level) of the tree represents the possible values for $\mathbf{q}_{N+1-j}$ (which are included in $\mathbf{Q}_N^u$). Then we set a bound $\mathcal{B} = +\infty$ (a required parameter for the algorithm) and we explore the leftmost path in the tree until reaching the leaf. Once we reach the leaf we update the value of $\mathcal{B}$ with (2.17) evaluated along the path explored in the tree. After this, we proceed to explore the next path to the right in the tree. At the jth level of that path we evaluate the partial cost function:

$$J_{BB}\left(j\right) = \sum_{k=N+1-j}^{N-1} \|\mathbf{q}_{k+1} - \mathbf{q}_k\|_2 + \frac{1}{N} \sum_{k=N+1-j}^{N-1} \|\mathbf{q}_k - \mathbf{q}_N\|_2. \tag{2.20}$$

[8]This algorithm is also used to solve the classical travelling salesman problem which is similar to the problem (2.18).

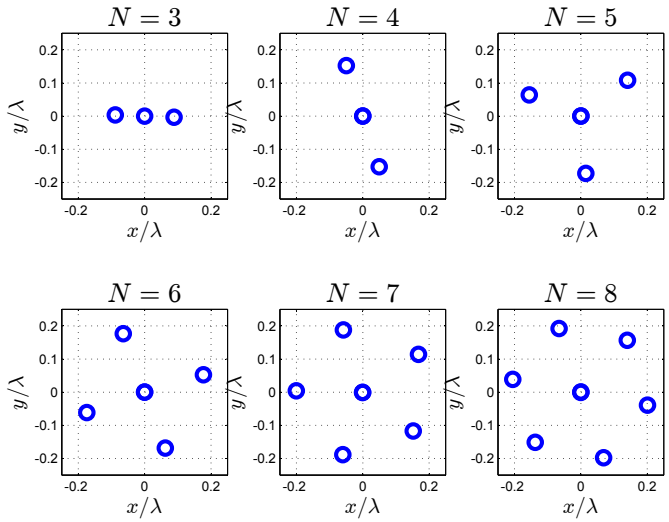

Figure 2.7: Geometries obtained by solving (2.16) with $\theta = 0.95$ using SA for $N = 3, 4, \cdots, 8$ stopping points. For $N > 3$ the central circle represents two overlapping points.

If $J_{BB}(j) \geq \mathcal{B}$ we prune the corresponding subtree and proceed to explore the next path in the tree. If we reach a leaf (i.e., $j = N$) then we update the bound $\mathcal{B} = J_{BB}(N)$ again and explore the next path in the tree. Once we reach the rightmost path the algorithm is terminated and we take as solution the rightmost path that reached a leaf. This method is not necessarily the most efficient way to solve (2.18) but finding the most efficient algorithm to solve it is outside the scope of this thesis.

We should mention that (2.18) is slightly different from the classical travelling salesman problem in that we are not looking to optimize a tour that starts at $\mathbf{q}_1$, passes through all the stopping points and finishes at $\mathbf{q}_1$ but rather to optimize a path that starts at $\mathbf{q}_1$, passes through all the stopping points until $\mathbf{q}_N$ and then whose finishing position is a random variable uniformly distributed among all the stopping points; the cost function (2.17) to be minimized is the expected value of the distance travelled during this path.

In Fig. 2.11 we observe an optimum unordered set of points taken from the optimum matrix $\mathbf{Q}_N^u$ obtained by solving (2.14) with the SA for $\mathcal{X}_e(z_0)$ and also we observe the ordered set of stopping points taken from the optimum matrix $\mathbf{Q}_N$. If we do not optimize the permutation matrix and we simply select $\mathbf{P} = \mathbf{I}$ then the MR, when using the MDMTA without thresholds and using *Maximum Channel Gain Rule*, will travel an average distance of $\approx 5.88 z_0$. On the other hand if we optimize $\mathbf{P}$ then the MR, under the same conditions, will travel an average distance of $\approx 4.8 z_0$. By optimizing the exploration order of the stopping points the MDMTA will require the MR to travel smaller distances and so it will be more energy efficient.

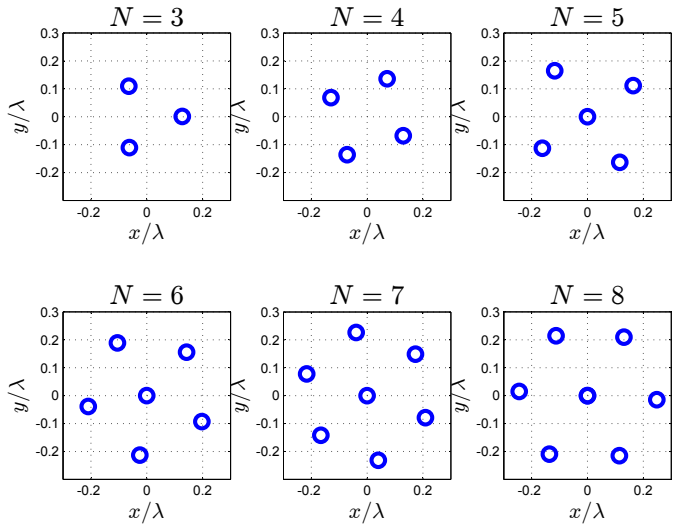

Figure 2.8: Geometries obtained by solving (2.16) with $\theta = 0.9$ using SA for $N = 3, 4, \cdots, 8$ stopping points. For $N = 8$ the central circle represents two overlapping points.

Finally, the partial decoupling of the geometry optimization (together with the optimum ordering) from the optimization of the MDMTA parameters allows us to create an 'optimum geometry dictionary'. This 'optimum geometry dictionary' is indexed by[9] N, ζ and contains at each entry the optimum ordered geometry for those particular parameters. As we will show in the next section, the use of this 'optimum geometry dictionary' can help us to reduce the complexity of the MDMTA optimization.

2.3.2 Optimization of the MDMTA Parameters

In the preceding subsection we showed different methods to optimize the stopping points geometry. Now, in this section we show how to optimize the rest of the MDMTA parameters given that we have already chosen an optimum geometry (including its optimum exploration order). For simplicity, in the rest of the chapter each geometry will be referred to by the pair of parameters (N,ζ) where N is the number of stopping points and $\zeta = \rho$ if we obtained the geometry by solving (2.14) or $\zeta = \theta$ if we obtained it by solving (2.16).

The approach used for optimizing the MDMTA parameters may be adapted according to the particular application of the MDMTA. To illustrate this consider the following two applications:

1. The MR has to transmit a finite amount of data (e.g., a set of pictures, video or

[9] Whether $\zeta = \rho$ or $\zeta = \theta$ depends upon whether we chose (2.14) or (2.16) for the geometry optimization.

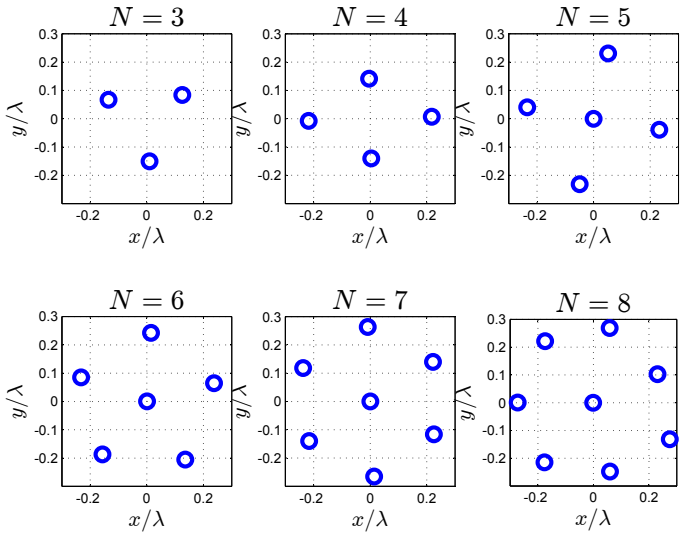

Figure 2.9: Geometries obtained by solving (2.16) with $\theta = 0.8$ using SA for $N = 3, 4, \cdots, 8$ stopping points.

sensor measurements) consisting of M bits to the stationary node and the bit duration is T_b. The MR uses power control to ensure a reference receive power P_{ref} at the stationary node. In addition the MR cannot radiate more power than P_{max} and if it cannot satisfy P_{ref} at the receiver then it does not transmit at all. In this application the MR can use the MDMTA to minimize the amount of energy. So, in this case, the MDMTA must be optimized to minimize the total amount of energy expended (i.e., the energy used for transmission plus energy used for motion during the MDMTA execution).

2. The MR has to establish a wireless link with the stationary node to exchange an undetermined amount of data. This can occur if the MR, equipped with a camera, is performing a surveillance task and continuously transmits the images recorded to the stationary node. In this application the MDMTA can be used by the MR prior to the establishment of the wireless link to maximize its signal to noise ratio (SNR) in order to obtain a high transmission rate. So, in this application the MDMTA should be optimized to obtain a high SNR while using as little as possible mechanical energy in the process.

In the first application we want to minimize the total amount of energy. If we take into account P_{max} and the outage probability then the statement of the problem becomes more complicated. A simpler approach is to assume $P_{max} = +\infty$ for this

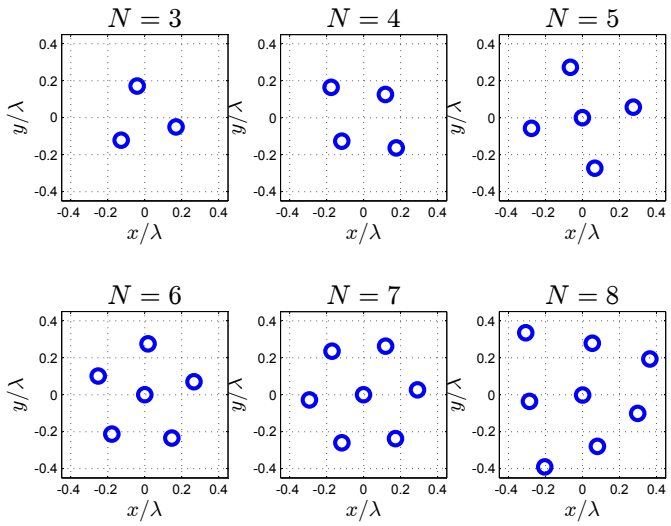

Figure 2.10: Geometries obtained by solving (2.16) with $\theta = 0.5$ using SA for $N = 3, 4, \cdots, 8$ stopping points.

optimization. The resulting optimization problem is now:

$$\begin{aligned} &\min_{\boldsymbol{\eta},\boldsymbol{t},\mu,\zeta,\mathbf{u}(t)} \mathbb{E}\left[\frac{\frac{\alpha}{|h(\mathbf{q}_{opt})|^2} + E_{mech}\left(t_1, t_{N+1}, \mathbf{u}(t)\right)}{\frac{\alpha}{|h(\mathbf{q}_1)|^2}}\right] \\ &\text{s.t.} \\ &t_{N+1} - t_1 - T_{max}(N) = 0 \end{aligned} \tag{2.21}$$

where $\alpha = \frac{MT_bP_{ref}}{s^2}$, $\boldsymbol{\eta}$ is the threshold vector, $\mathbf{t}$ is the temporal vector, μ is the input parameter for the *Minimum Effort Rule* and ζ is the design parameter for the geometry optimization (i.e., $\zeta = \rho$ if we optimize (2.14) and $\zeta = \theta$ if we optimize (2.16)). Inside the expected value of the cost function we have, in the numerator, the total amount of energy that the MR will use if it adopts the MDMTA and, in the denominator, the total amount of energy that the MR will use if it transmits from its initial position and does not use the MDMTA. So, this cost function tells us (on average) how much the energy consumption is decreased by the use of the MDMTA.

Now, in the second application the optimization problem can be seen as an investment problem: we want to maximize the revenue (the SNR) while minimizing the investment (the mechanical energy). Therefore, the optimization problem for

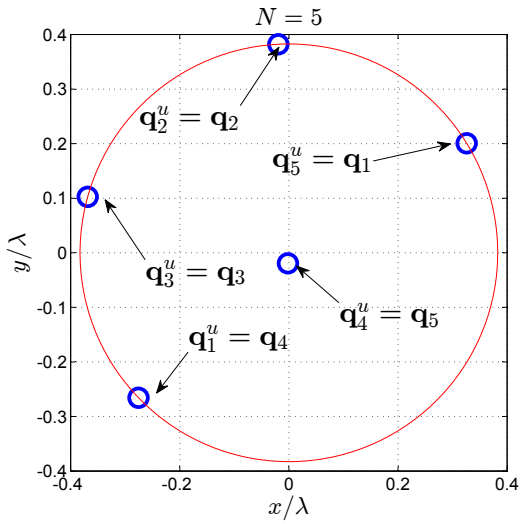

Figure 2.11: Geometry obtained using SA with $\mathcal{X}_e(z_0)$ for $N = 5$ stopping points.

this application can be mathematically stated[10] as:

$$\min_{\boldsymbol{\eta},\boldsymbol{t},\mu,\zeta,\mathbf{u}(t)} (\beta - 1)\mathbb{E}\left[|h(\mathbf{q}_{opt})|^2\right] + \beta\mathbb{E}\left[E_{mech}\left(t_1, t_{N+1}, \mathbf{u}(t)\right)\right] \tag{2.22}$$

s.t.

$$t_{N+1} - t_1 - T_{max}(N) = 0$$

where $\boldsymbol{\eta}$ is the threshold vector, $\mathbf{t}$ is the temporal vector, μ is the input parameter for the selection rule, ζ is the input parameter for the geometry optimization ($\zeta = \rho$ if we optimize (2.14) and $\zeta = \theta$ if we optimize (2.16)) and $\beta \in [0, 1]$ is a design parameter. The cost function is a convex combination of $-\mathbb{E}\left[|h(\mathbf{q}_{opt})|^2\right]$ with $\mathbb{E}\left[E_{mech}\left(t_1, t_{N+1}, \mathbf{u}(t)\right)\right]$. Therefore, decreasing β means that the improvement in the SNR becomes more important and so the MR is allowed to use more mechanical energy to achieve this goal.

Now, regarding the choices of the input parameters for the optimization problems (2.21) and (2.22) will depend on the particular application and the objective of the designer. If the MR has to send a finite (and known) number of bits then the designer should choose optimization problem (2.21) and choose $\alpha = \frac{MT_bP_{ref}}{s^2}$, $\boldsymbol{\eta}$ (as mentioned before) in order to minimize the total amount of energy used.

On the other hand if for the particular MR that is considered the energy used for transmission is negligible with respect to the mechanical energy then could select optimization problem (2.22) in order to obtain a high channel gain but avoiding to spend too much mechanical energy in the process. As mentioned before, this

[10] We modelled our problem as an investment problem but we multiplied the optimization target by -1 to re-state it as a minimization problem so that all the MDMTA parameter optimization problems in this chapter are minimization problems.

compromise is controlled by the parameter β. If the number of bits to be sent is too high or if the bit error rate required is too low then we should select β low in order to prioritize the obtention of a high channel gain over the saving of mechanical energy. Nevertheless, for the same MR, if the energy in the battery is low then the designer could give more importance to saving energy and so he could select a medium or high (close to 1) value of β depending on the battery level, the importance of the transmission at that moment as well as the size of the payload.

We have to mention that the cost functions of the optimization problems (2.21) and (2.22) are two different forms of the cost function for the more general optimization problem (2.10).

Now, the first step in the optimization of (2.21) and (2.22) is the optimization of the control law used by MR to move. In both cases it is intuitive that the optimum control law used by the MR must allow it to move from one stopping point to the next one in a finite time $t_{k+1} - t_k$ while using minimum energy. Therefore the optimum control law $\mathbf{u}(t)$ for $t \in [t_k, t_{k+1}]$ for the TOMR considered in this chapter is obtained as follows[11]:

$$\begin{aligned} &\min_{\mathbf{u}(t)} E_{mech}\left(t_k, t_{k+1}, \mathbf{u}(t)\right) \\ &\text{s.t.} \\ &\mathbf{A}\ddot{\mathbf{p}}_o(t) + \mathbf{C}\dot{\mathbf{p}}_o(t) = \mathbf{D}\mathbf{u}(t) \\ &\mathbf{p}_o(t_k) = [\mathbf{q}_d^T(k) \quad 0]^T,\ \mathbf{p}_o(t_{k+1}) = [\mathbf{q}_a^T(k) \quad 0]^T \\ &\dot{\mathbf{p}}_o(t_k) = \mathbf{0}, \quad \dot{\mathbf{p}}_o(t_{k+1}) = \mathbf{0} \end{aligned} \tag{2.23}$$

where $k = 1, 2, \cdots, N$, $t_1 = 0$ and $\mathbf{q}_d(k)$ and $\mathbf{q}_a(k)$ are the departure and arrival points at the kth iteration[12]. The cost function corresponds to the mechanical energy consumed by the TOMR, see (2.6). The first restriction describes the TOMR's dynamical model (as described in section 2.1.1) and the remaining restrictions ensure that the TOMR is motionless at both the departure point $\mathbf{q}_d(k)$ and at the arrival point $\mathbf{q}_a(k)$ while completing the movement in $t_{k+1} - t_k$ seconds.

This is a classical optimum control problem that can be solved analytically using calculus of variations. Specifically we can solve the Euler-Lagrange equation [35] to optimize the functional in (2.23) to derive the optimum control law. The resulting control law for $t \in [t_k, t_{k+1}]$, is given by

$$\mathbf{u}_k^*(t) = \frac{\mathbf{A}_{1,1}\dot{v}_k^*(t) + k_1 v_k^*(t)}{k_2} \begin{bmatrix} \frac{2\sin(\psi_{a,b}(k))}{3} \\ -\frac{\sin(\psi_{a,b}(k))}{3} - \frac{\cos(\psi_{a,b}(k))}{\sqrt{3}} \\ -\frac{\sin(\psi_{a,b}(k))}{3} + \frac{\cos(\psi_{a,b}(k))}{\sqrt{3}} \end{bmatrix} \tag{2.24}$$

where[13] $\psi_{a,b}(k) = \measuredangle(\mathbf{q}_a(k) - \mathbf{q}_d(k))$ and $v_k^*(t)$ is the optimum translational velocity

[11] In order to be able to simplify the problem and obtain an analytical expression for the optimum control law we restricted the MR orientation to remain constant during the whole movement, i.e., $\dot{\phi}(t) = 0$ and without loss of generality we also set $\phi(t) = 0$ (see Fig. 2.1).

[12] At the kth iteration $\mathbf{q}_d(k) = \mathbf{q}_k$, $\mathbf{q}_a(k) = \mathbf{q}_{k+1}$ for $k = 1, 2, \cdots, N-1$, $\mathbf{q}_d(N) = \mathbf{q}_N$ and $\mathbf{q}_a(N) = \mathbf{q}_{opt}$, where $\mathbf{q}_{opt}$ is the optimum point chosen by the selection rule.

[13] $\measuredangle(\mathbf{q}_a(k) - \mathbf{q}_d(k))$ represents the angle of the vector $\mathbf{q}_a(k) - \mathbf{q}_d(k)$.

for $t \in [t_k, t_{k+1}]$ and is given by:

$$v_k^*(t) = \|\mathbf{q}_a(k) - \mathbf{q}_d(k)\|_2 \cdot (K_{v1}(\Delta_k)e^{\frac{-t}{\sqrt{\tau}}} + K_{v2}(\Delta_k)e^{\frac{t}{\sqrt{\tau}}} + K_{v3}(\Delta_k)) \tag{2.25}$$

with $\Delta_k = t_{k+1} - t_k$ and:

$$\tau = \frac{2\mathbf{A}_{1,1}^2 k_3}{2k_1^2 k_3 - 3k_1 k_2^2 k_4}, \tag{2.26}$$

$$K_{v_1}(\Delta_k) = \frac{1-e^{\frac{\Delta_k}{\sqrt{\tau}}}}{4\sqrt{\tau}\left(1-\cosh\left(\frac{\Delta_k}{\sqrt{\tau}}\right)\right)+2\Delta_k \sinh\left(\frac{\Delta_k}{\sqrt{\tau}}\right)},$$

$$K_{v_2}(\Delta_k) = \frac{e^{\frac{-\Delta_k}{\sqrt{\tau}}}-1}{4\sqrt{\tau}\left(1-\cosh\left(\frac{\Delta_k}{\sqrt{\tau}}\right)\right)+2\Delta_k \sinh\left(\frac{\Delta_k}{\sqrt{\tau}}\right)}, \tag{2.27}$$

$$K_{v_3}(\Delta_k) = \frac{2\sinh\left(\frac{\Delta_k}{\sqrt{\tau}}\right)}{4\sqrt{\tau}\left(1-\cosh\left(\frac{\Delta_k}{\sqrt{\tau}}\right)\right)+2\Delta_k \sinh\left(\frac{\Delta_k}{\sqrt{\tau}}\right)}.$$

Therefore, when the optimum control law $\mathbf{u}_k^*(t)$ is used for moving during the kth iteration the mechanical energy consumed over that movement is:

$$E_{mech}\left(t_k, t_{k+1}, \mathbf{u}_k^*(t)\right) = \mathcal{K}(\Delta_k)\|\mathbf{q}_a(k) - \mathbf{q}_d(k)\|_2^2 \tag{2.28}$$

where $\mathcal{K}(\Delta_k)$ is given by (2.29).

$$\begin{aligned}
\mathcal{K}(\Delta_k) &= \left(\frac{2k_3\mathbf{A}_{1,1}^2 - \sqrt{\tau}\mathbf{A}_{1,1}(4k_1k_3 - 3k_2^2k_4) + \tau k_1(2k_1k_3 - 3k_2^2k_4)}{6\sqrt{\tau}k_2^2}\right) \\
&\times \left(1 - e^{\frac{-2\Delta_k}{\sqrt{\tau}}}\right) K_{v_1}^2(\Delta_k) \\
&+ \left(\frac{\mathbf{A}_{1,1}(3k_2^2k_4 - 4k_1k_3) + 2k_1\sqrt{\tau}(2k_1k_3 - 3k_2^2k_4)}{3k_2^2}\right) \\
&\times \left(1 - e^{\frac{-\Delta_k}{\sqrt{\tau}}}\right) K_{v_1}(\Delta_k)K_{v_3}(\Delta_k) \\
&+ \left(\frac{k_1(2k_1k_3 - 3k_2^2k_4)}{3k_2^2}\right)\left(2K_{v_1}(\Delta_k)K_{v_2}(\Delta_k) + K_{v_3}^2(\Delta_k)\right)\Delta_k \\
&- \left(\frac{4k_3\mathbf{A}_{1,1}^2}{3k_2^2\tau}\right) K_{v_1}(\Delta_k)K_{v_2}(\Delta_k)\Delta_k \\
&+ \left(\frac{\mathbf{A}_{1,1}(4k_1k_3 - 3k_2^2k_4) + 2k_1\sqrt{\tau}(2k_1k_3 - 3k_2^2k_4)}{3k_2^2}\right) \\
&\times \left(e^{\frac{\Delta_k}{\sqrt{\tau}}} - 1\right) K_{v_2}(\Delta_k)K_{v_3}(\Delta_k) \\
&+ \left(\frac{2k_3\mathbf{A}_{1,1}^2 + \sqrt{\tau}\mathbf{A}_{1,1}(4k_1k_3 - 3k_2^2k_4) + \tau k_1(2k_1k_3 - 3k_2^2k_4)}{6\sqrt{\tau}k_2^2}\right) \\
&\times \left(e^{\frac{2\Delta_k}{\sqrt{\tau}}} - 1\right) K_{v_2}^2(\Delta_k).
\end{aligned} \tag{2.29}$$

Once we have the optimum control law ($\mathbf{u}^*(t)$) and having access to an 'optimum geometry dictionary' (see subsection 2.3.1) calculated a-priori, then the searching space of (2.21) and (2.22) is reduced to $2N$ variables: $\eta_1, \eta_2, \cdots \eta_{N-1}$, $t_2, t_3 \cdots, t_N$, ζ and μ. If we do not use an 'optimum geometry dictionary' then we would have to embed the geometry optimization problem into the optimization of the MDMTA parameters which would increase considerably the amount of calculations needed.

Now, if the designer does not have a dynamic model for the MR then a suboptimal approach is to replace the mechanical energy term in the cost functions of (2.10), (2.21) and (2.22) with the distance travelled by the MR.

Note that if we want to implement the MDMTA with a non-omnidirectional MR (e.g., a differential drive mobile robot) then the design of the stopping points geometry would have to take into account its kinematic restrictions. In general the MR could not directly move in straight line from stopping point to stopping point and probably a joint design of both the optimum stopping points geometry and the minimum energy control law would be necessary. These considerations are beyond the scope of this thesis but the material already presented in this chapter could be used as a departure point to develop such techniques.

Finally, we should mention that in general there is no analytical expression for the cost functions of (2.10), (2.21) and (2.22) and so they must be evaluated by simulations. When calculating the value of the cost function by simulations we will obtain the true value plus a random error (which will be small if we use a large enough number of iterations to calculate it). This makes it more complicated to exactly solve these optimization problems. In this chapter (see simulation section) we use the SA algorithm but this does not guarantee us an optimum solution but rather a good or a near optimum solution if we let the SA run for a significant amount of time and we also obtain a small enough error in the cost function by using a large enough number of simulations to evaluate it.

This is because the SA algorithm uses a random search mechanism to determine the testing points where it evaluates the optimisation target. When the SA is used in an optimisation problem whose optimisation space is bounded and discrete then the probability that it reaches the global optimum tends to 1 as it runs for long enough time. But when the search space is continuous, due to the random search component, we can only guarantee that we will reach a point close to the global optimum. In addition, we have to mention that the random mechanism in the SA helps to get out of local optima [32] but sometimes it may fail to do that and so we may end near a local optima rather than near the global optima. One way to compensate for this is to run the SA various times with different initial conditions. Note that in our case this problem is accentuated as we increase the number of stopping points and also as the area in which the stopping points are allowed to lie increases. This is because all these actions increase the number of local optima and therefore it becomes more difficult for the SA to avoid them. Nevertheless, despite all these inconvinients the SA algorithm can produce good results as long as the number of stopping points is

not too high.

2.3.3 Adaptive Diversity Order

We have already shown how to optimise the geometry of the stopping points, the visiting order of the points and all the parameters of the MDMTA, except for the actual number of stopping points N. In this subsection we address this last optimisation problem.

The optimisation of N prior to each invoking of the MDMTA is called *Adaptive Diversity Order* [30]. This is due to the fact that the diversity order of the MDMTA (and of any MDA with discrete search space) is given by the number of stopping points N. The *Adaptive Diversity Order* is one of the elements that differentiates the MDMTA from other diversity techniques in which the diversity order is fixed once the system is deployed (e.g., multi-antenna diversity techniques). Now, assuming that the MR has in memory a list of various optimal geometries with the respective to MDMTA optimum parameter values then N can be optimized as follows:

$$\begin{aligned} &\min_{N} f^*(N, \xi, T_{max}(N)) \\ &\text{s.t.} \\ &T_{max}(N) \leq T_M \\ &N \leq N_{max} \end{aligned} \tag{2.30}$$

where $\xi = \alpha$ ($\xi = \beta$) if we chose the (2.21) ((2.22)) to optimize the parameters of the MDMTA, $f^*(N, \xi, T_{max}(N))$ denotes the minimum value of the cost function of the optimization problem selected ((2.21) or (2.22)), N_{max} is a predefined maximum value that N may take[14], and $T_{max}(N)$ is the maximum execution time allowed[15] for N stopping points while T_M is the maximum execution time allowed for any number of stopping points.

There are many possible choices for $T_{max}(N)$ but we will only mention two. One option is to set the same duration independently of the number of stopping points $T_{max}(N) = T_M$ and another option is to set the duration proportional to the number of stopping points $T_{max}(N) = \frac{T_M N}{N_{max}}$. The mechanical energy is a decreasing function of $T_{max}(N)$ and since $T_M \geq \frac{T_M N}{N_{max}}$, in general the first option uses less energy while the second option results in a lower MDMTA execution time. So, depending on the particular design requirements we can choose one option or the other.

Now, the minimum value of $T_{max}(N)$ depends on the maximum velocity of the MR, the number of stopping points and the distance between adjacent stopping points. To give a rough idea of typical values of $T_{max}(N)$ for the MDMTA we develop a loose upper bound for its minimum value. As mentioned previously, in typical scenarios the optimum geometries obtained by solving (2.14) or (2.16), the

[14] A reasonable value for N_{max} can be around 10 or less.

[15] The actual execution time is a random variable that at most takes the value of $T_{max}(N)$.

distance between adjacent stopping points is in general less than a wavelength λ, see Figs. 2.3 to 2.10. If the carrier frequency used is higher than 1GHz then the wavelength is smaller than 30cm and according to the experimental results in [26], the article from which we extracted the TOMR model for this chapter, this particular MR can at least travel 50cm in one second. Therefore the MR can now move from stopping point to stopping point in less than one second. Now, the time taken for the MR to estimate the channel at each stopping point will depend on the amount of data utilized for this process but in general the time required for this task could easily be assumed less than one second[16]. Considering all this information we can say that the minimum value for $T_{max}(N)$, for this particular robot, is loosely bounded by $2N$ seconds: $N-1$ seconds to traverse all the N stopping points, N seconds to measure the channel at all the stopping points and around one second to go from $\mathbf{q}_N$ to $\mathbf{q}_{opt}$.

With the introduction of the adaptive diversity order concept we have completed the discussion about the design and optimization of the MDMTA.

2.4 MDMTA Analysis

A general analysis of the MDMTA is extremely complicated and in most cases it is not possible to obtain analytical results. Nevertheless there is one particular case of interest in which we can obtain exact analytical expressions for the c.d.f. (cumulative distribution function) of $|h(\mathbf{q}_{opt})|$ and the p.m.f. (probability mass function) of E_{mech}. This is the case for the MDMTA with two stopping points, using the *Maximum Channel Gain Rule* and assuming perfect channel estimation. Although we have neglected the localization error up to now, we will analyze its effects on the MDMTA in this section.

2.4.1 Two Stopping Points and Perfect Channel Gain Estimation

In this subsection we derive the c.d.f. of $|h(\mathbf{q}_{opt})|$ and the p.m.f. of E_{mech} for the MDMTA when using the *Maximum Channel Gain Rule* as the selection rule and assuming perfect channel estimation (i.e., the MR measures the channel gain without error). From the MDMTA description we can derive the following expression for the channel gain at $\mathbf{q}_{opt}$:

$$\begin{aligned} \Pr(|h(\mathbf{q}_{opt})| < x) &= \Pr(|h(\mathbf{q}_1)| < x, |h(\mathbf{q}_1)| \geq \eta_1) \\ &+ \Pr(\max(|h(\mathbf{q}_1)|, |h(\mathbf{q}_2)|) < x, |h(\mathbf{q}_1)| < \eta_1), \end{aligned} \quad (2.31)$$

where the first probability of the right hand side represents the case where the channel gain at the first stopping point is higher than the threshold η_1 and so $\mathbf{q}_{opt} = \mathbf{q}_1$. The

[16] In this chapter for simplicity we are not considering this time but it should be considered when the MDMTA is implemented.

second term represents the case where the MR reaches $\mathbf{q}_2$ and uses the *Maximum Channel Gain Rule* to determine $\mathbf{q}_{opt}$. Performing some probability calculations on (2.31) we obtain:

$$\begin{aligned}\Pr(|h(\mathbf{q}_{opt})| < x) &= \Pr(\eta_1 \leq |h(\mathbf{q}_1)| < x) \\ &+ \Pr(|h(\mathbf{q}_2)| < |h(\mathbf{q}_1)| < x, |h(\mathbf{q}_1)| < \eta_1) \\ &+ \Pr(|h(\mathbf{q}_1)| < |h(\mathbf{q}_2)| < x, |h(\mathbf{q}_1)| < \eta_1). \end{aligned} \tag{2.32}$$

In order to simplify we first analyze the c.d.f. for $x < \eta_1$ and then for $x \geq \eta_1$. For $x < \eta_1$ we have:

$$\Pr(|h(\mathbf{q}_{opt})| < x) = \Pr(|h(\mathbf{q}_2)| < |h(\mathbf{q}_1)| < x) + \Pr(|h(\mathbf{q}_1)| < |h(\mathbf{q}_2)| < x), \tag{2.33}$$

and $\Pr(|h(\mathbf{q}_2)| < |h(\mathbf{q}_1)| < x) = \Pr(|h(\mathbf{q}_1)| < |h(\mathbf{q}_2)| < x)$ due to the fact that the channel at both stopping points is identically distributed so we have:

$$\Pr(|h(\mathbf{q}_{opt})| < x) = 2\Pr(|h(\mathbf{q}_1)| < |h(\mathbf{q}_2)| < x). \tag{2.34}$$

and using the total probability theorem we can write:

$$\Pr(|h(\mathbf{q}_{opt})| < x) = 2\int_0^x \Pr(|h(\mathbf{q}_2)| < y \mid |h(\mathbf{q}_1)| = y) f_{|h(\mathbf{q}_1)|}(y)\mathrm{d}y. \tag{2.35}$$

where $f_{|h(\mathbf{q}_1)|}(y)$ is the unconditional (probability density function) p.d.f. of $|h(\mathbf{q}_1)|$ which is Rayleigh distributed with $\mathbb{E}[|h(\mathbf{q}_1)|^2] = 1$ and so we have:

$$\Pr(|h(\mathbf{q}_{opt})| < x) = 4\int_0^x \Pr(|h(\mathbf{q}_2)| < y \mid |h(\mathbf{q}_1)| = y) y e^{-y^2}\mathrm{d}y. \tag{2.36}$$

Since $h(\mathbf{q}_2)$ is a zero-mean complex Gaussian random variable then when we condition the random variable $|h(\mathbf{q}_2)|$ on the realisation of $|h(\mathbf{q}_1)| = y$ it becomes a Rician random variable with the following distribution:

$$f_{|h(\mathbf{q}_2)| \mid |h(\mathbf{q}_1)|=y}(z) = \frac{2z}{1-\gamma^2} e^{\frac{-(z^2+\gamma^2 y^2)}{1-\gamma^2}} I_0\left(\frac{2\gamma z y}{1-\gamma^2}\right) \tag{2.37}$$

where $I_0(\cdot)$ is modified Bessel function of the first kind and zero order and $\gamma = r(\mathbf{q}_1, \mathbf{q}_2)$, see (2.9). From the Rician distribution (2.37) we have then:

$$\int_0^x \Pr(|h(\mathbf{q}_2)| < y \mid |h(\mathbf{q}_1)| = y) = \int_0^y f_{|h(\mathbf{q}_2)| \mid |h(\mathbf{q}_1)|=y}(z)\mathrm{d}z \tag{2.38}$$

$$\int_0^x \Pr(|h(\mathbf{q}_2)| < y \mid |h(\mathbf{q}_1)| = y) = 1 - Q_1\left(\frac{\sqrt{2}y\gamma}{\sqrt{1-\gamma^2}}, \frac{\sqrt{2}y}{\sqrt{1-\gamma^2}}\right) \tag{2.39}$$

where $Q_1(\cdot,\cdot)$ is the modified Marcum Q-function. Now, substituting (2.39) in (2.36) gives us:

$$\Pr(|h(\mathbf{q}_{opt})| < x) = 4\int_0^x \left(1 - Q_1\left(\frac{\sqrt{2}y\gamma}{\sqrt{1-\gamma^2}}, \frac{\sqrt{2}y}{\sqrt{1-\gamma^2}}\right)\right) ye^{-y^2}\mathrm{d}y. \tag{2.40}$$

$$\begin{aligned}\Pr(|h(\mathbf{q}_{opt})| < x) &= 2(1-e^{-x^2}) \\ &- 4\int_0^x Q_1\left(\frac{\sqrt{2}y\gamma}{\sqrt{1-\gamma^2}}, \frac{\sqrt{2}y}{\sqrt{1-\gamma^2}}\right) ye^{-y^2}\mathrm{d}y.\end{aligned} \tag{2.41}$$

Now, in[36] we find the following integral:

$$\begin{aligned}\int_0^c e^{\frac{-p^2x^2}{2}} Q_1(ax,bx)\mathrm{d}x &= \frac{1}{2p^2}\left(1+\frac{t}{r}\right)\left[1+e^{\frac{-sc^2}{2}}I_0(abc^2)\right] \\ &- e^{\frac{-p^2c^2}{2}}Q_1(ac,bc) - \frac{t}{r}Q_1\left(c\sqrt{\frac{s-r}{2}}, c\sqrt{\frac{s+r}{2}}\right)\end{aligned} \tag{2.42}$$

with $s = p^2+a^2+b^2$, $t = p^2+a^2-b^2$ and $r = \sqrt{s^2-4a^2b^2}$. So, using this integral into (2.41) and simplifying terms we obtain:

$$\Pr(|h(\mathbf{q}_{opt})| < x) = 1 - e^{\frac{-2x^2}{1-\gamma^2}}I_0\left(\frac{2\gamma x^2}{1-\gamma^2}\right) - 2e^{-x^2}\left(1 - Q_1\left(\frac{\gamma\sqrt{2}x}{\sqrt{1-\gamma^2}}, \frac{\sqrt{2}x}{\sqrt{1-\gamma^2}}\right)\right) \tag{2.43}$$

And for $x \geq \eta_1$ we have:

$$P(|h(\mathbf{q}_{opt})| < x) = P(\eta_1 \leq |h(\mathbf{q}_1)| < x) + P(|h(\mathbf{q}_2)| < x, |h(\mathbf{q}_1)| < \eta_1) \tag{2.44}$$

where again using the integrals from [36] the c.d.f. of $|h(\mathbf{q}_{opt})|$ reduces to:

$$\begin{aligned}\Pr(|h(\mathbf{q}_{opt})| < x) &= e^{-x^2}Q_1\left(\frac{\sqrt{2}x\gamma}{\sqrt{1-\gamma^2}}, \frac{\sqrt{2}\eta_1}{\sqrt{1-\gamma^2}}\right) \\ &- e^{-\eta_1^2}Q_1\left(\frac{\sqrt{2}x}{\sqrt{1-\gamma^2}}, \frac{\sqrt{2}\gamma\eta_1}{\sqrt{1-\gamma^2}}\right) \\ &+ 1 - 2e^{-x^2} + e^{-\eta_1^2}.\end{aligned} \tag{2.45}$$

Now, using a similar approach the p.m.f. of the mechanical energy consumed by the TOMR when using the optimum control law (2.24) becomes:

$$\Pr(E_{mech} = 0) = e^{-\eta_1^2}, \tag{2.46}$$

$$\begin{aligned}\Pr(E_{mech} = \mathcal{K}(T_1)\|\mathbf{q}_1 - \mathbf{q}_2\|_2^2) &= \frac{1}{2}\left(1 + e^{\frac{-2\eta_1^2}{1-\gamma^2}} I_0\left(\frac{2\gamma\eta_1^2}{1-\gamma^2}\right)\right) \\ &- e^{-\eta_1^2} Q_1\left(\frac{\gamma\sqrt{2}\eta_1}{\sqrt{1-\gamma^2}}, \frac{\sqrt{2}\eta_1}{\sqrt{1-\gamma^2}}\right), \quad (2.47)\end{aligned}$$

$$\begin{aligned}\Pr(E_{mech} = (\mathcal{K}(T_1) + \mathcal{K}(T_2))\,\|\mathbf{q}_1 - \mathbf{q}_2\|_2^2) &= \frac{1}{2}\left(1 - e^{\frac{-2\eta_1^2}{1-\gamma^2}} I_0\left(\frac{2\gamma\eta_1^2}{1-\gamma^2}\right)\right) \\ &+ e^{-\eta_1^2} Q_1\left(\frac{\gamma\sqrt{2}\eta_1}{\sqrt{1-\gamma^2}}, \frac{\sqrt{2}\eta_1}{\sqrt{1-\gamma^2}}\right) \\ &- e^{-\eta_1^2}. \quad (2.48)\end{aligned}$$

Note that $\Pr(E_{mech} = 0)$ is equivalent to the probability that the first channel gain is superior to η_1 and since $|h(\mathbf{q}_1)|$ follows. Now, $\Pr(E_{mech} = (\mathcal{K}(T_1) + \mathcal{K}(T_2))\,\|\mathbf{q}_1 - \mathbf{q}_2\|_2^2)$ is equivalent to the probability to the case in which the MR reaches $\mathbf{q}_2$ (and so $|h(\mathbf{q}_1)| < \eta_1$) and has to return to $\mathbf{q}_1$ because $|h(\mathbf{q}_1)| > |h(\mathbf{q}_2)|$. In other words, $\Pr(E_{mech} = (\mathcal{K}(T_1) + \mathcal{K}(T_2))\,\|\mathbf{q}_1 - \mathbf{q}_2\|_2^2)$ is equivalent to the probability that $\Pr(|h(\mathbf{q}_2)| < |h(\mathbf{q}_1)| < x, |h(\mathbf{q}_1)| < \eta_1)$ which in turn is equivalent to $\frac{1}{2}\Pr(|h(\mathbf{q}_{opt})| < x)$ when $x < \eta_1$ (see (2.32) − (2.43)) and so (2.48) results. Finally, the remaining possibility for E_{mech} is to take the value of $\mathcal{K}(T_1)\|\mathbf{q}_1 - \mathbf{q}_2\|_2^2$ and so we have $\Pr(E_{mech} = \mathcal{K}(T_1)\|\mathbf{q}_1 - \mathbf{q}_2\|_2^2) = 1 - \Pr(E_{mech} = (\mathcal{K}(T_1) + \mathcal{K}(T_2))\,\|\mathbf{q}_1 - \mathbf{q}_2\|_2^2) - \Pr(E_{mech} = 0)$. As consequence (2.47) follows.

In Fig. 2.12 we observe the normalized versions[17] of $\mathbb{E}[|h(\mathbf{q}_{opt})|]$ and $\mathbb{E}[E_{mech}]$ (calculated from equations (2.43), (2.45) and (2.46)-(2.48)) as functions of η_1. We observe that as η_1 decreases then $\mathbb{E}[E_{mech}]$ reduces faster than $\mathbb{E}[|h(\mathbf{q}_{opt})|]$. This is why we can use the thresholds to slightly reduce $\mathbb{E}[|h(\mathbf{q}_{opt})|]$ while significantly reducing the mechanical energy consumption. For example, from Fig. 2.12, we observe that if $\eta_1 = 1.5$ then $\mathbb{E}[|h(\mathbf{q}_{opt})|]$ is practically unaffected but $\mathbb{E}[E_{mech}]$ is reduced by more than 10%.

2.4.2 Localization Error Impact

In this subsection we briefly discuss the impact of the localization error on the MDMTA. By definition the initial position of the MR is $\mathbf{q}_1$. We assume that the MR uses "dead reckoning [25]" to estimate its relative location to $\mathbf{q}_1$. Then as the MR starts to move from stopping point to stopping point, during the exploration phase the localization error starts to accumulate and so the actual geometry of the stopping points deviates more from the intended geometry as the number of stopping points increases. This is the first effect. Now, during the selection phase, if the jth stopping point was selected as the optimum stopping point then the MR will move

[17] The normalization is made with respect to the parameter values when $\eta_1 = +\infty$.

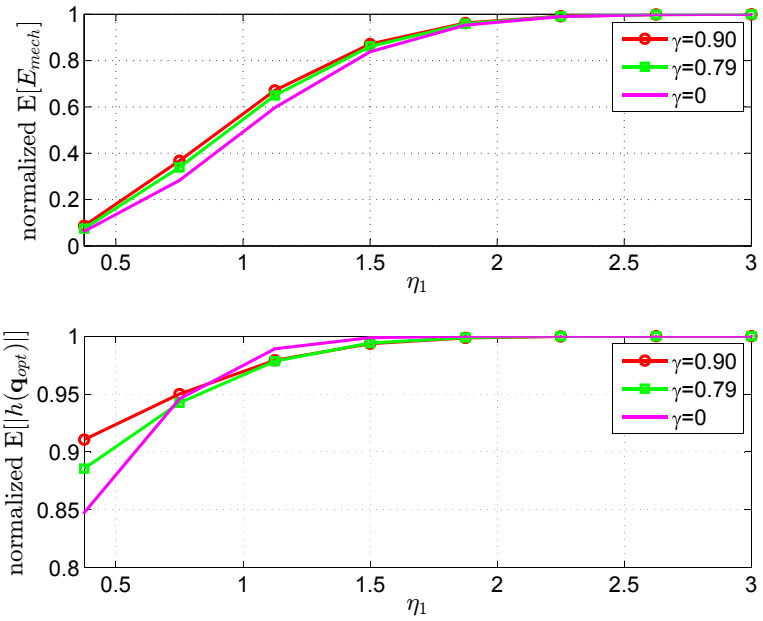

Figure 2.12: Normalized values for $\mathbb{E}[|h(\mathbf{q}_{opt})|]$ and $\mathbb{E}[E_{mech}]$ as a function of the threshold η_1 for different γ values and $T_1 = T_2$.

believing that it is moving from $\mathbf{q}_N$ to $\mathbf{q}_j$ while in reality it will be moving from $\mathbf{p}(t_N)(\neq \mathbf{q}_N$ due to localization error) to a random point centered at $\mathbf{p}(t_j)$ $(\neq \mathbf{q}_j$ also due to the localization error). Note that $\mathbf{p}(t_N)$ is a random variable (centered at $\mathbf{q}_N$) whose variance depends on both the accuracy of the MR motion and the number of stopping points in the explored geometry. In other words $|h(\mathbf{p}(t_{N+1}))| \neq |h(\mathbf{p}(t_j))|$, and this is the second effect. If the localization error is small then $\mathbf{p}(t_{N+1})$ and $\mathbf{p}(t_j)$ will be close enough, and their channels will be highly correlated and so that $|h(\mathbf{p}(t_{N+1}))| \approx |h(\mathbf{p}(t_j))|$.

Finally we have to mention that as the effects of the localization error accumulate more with the number of stopping points then localization error is one of the elements that in practice limits the maximum number (N_{max}) of stopping points that the MR can explore during the MDMTA.

2.5 Simulations

In the simulations, we selected the robot parameters to fit the TOMR used in [26] which describes a real robot. These corresponding parameters are shown in table 2.1. In addition, we will assume throughout this section that the error term in the channel gain estimation has a variance $\sigma_n^2 = 0.05$ which corresponds to a low estimation error.

We first compare three different types of geometries:

Table 2.1: TOMR parameters.

$m = 1.989\text{kg}$	$J_c = 0.020691\text{kg} \cdot \text{m}^2$	$J_w = 0.060\text{g} \cdot \text{m}^2$
$r = 3\text{cm}$	$L = 12.55\text{cm}$	$k_1 = 35.0330\text{N/m}$
$k_2 = 38.7342\text{N}$	$k_3 = 72.9114\text{W}$	$k_4 = 1$

Table 2.2: MDMTA results for the geometry $\mathcal{G}_{z_0}(N)$.

N	2	3	4	5
$\mathbb{E}[E_{mech}]$	0.1432	0.2521	0.4221	0.5305
$\mathbb{E}[\lvert h(\mathbf{q}_{opt})\rvert^2]$	1.4775	1.7944	2.0143	2.1774

1. The linear geometry $\mathcal{L}_{z_0}(N)$: In this geometry there are N linear points arranged uniformly spaced at a distance z_0. These points are ordered from left to right.

2. The random geometries $\mathcal{R}_{z_0}(N)$ and $\mathcal{R}_{1.5z_0}(N)$: In these geometries the points are arranged randomly inside a circle of radius z_0 and $1.5z_0$ respectively. The points are not optimally ordered. The random geometries inside a circle to combat fading was suggested in [17].

3. The optimized geometry $\mathcal{G}_{z_0}(N)$: This is obtained by solving (2.14) for a circular area of radius $\rho = z_0$. The points are optimally ordered according to (2.18).

In order to compare the geometries we use the MDMTA without thresholds and with the *Maximum Channel Gain Rule*. We assume a wavelength $\lambda = 30\text{cm}$ and $t_{k+1} - t_k = 1\text{s}$ for $k = 1, 2, \cdots, N$.

In tables 2.2 to 2.5 we observe, for different number of stopping points, the expected value of the mechanical energy used by the MDMTA for each geometry as well as the power of the optimum channel obtained. We first observe that with the geometry $\mathcal{G}_{z_0}(N)$ we obtain a channel gain with the same characteristics as with $\mathcal{L}_{z_0}(N)$, but using less mechanical energy. The random geometry $\mathcal{R}_{z_0}(N)$ has the same exploration area as $\mathcal{G}_{z_0}(N)$ but provides a poorer channel gain than when using the MDMTA. If the TOMR adopts the random geometry $\mathcal{R}_{1.5z_0}(N)$ then it will use more mechanical energy while still obtaining poorer channel gains. Therefore, incorporating an optimum geometry into the MDMTA will allow the MR to obtain good channel gains while using less mechanical energy.

Now, we optimise all the parameters of the MDMTA by solving (2.22) with $\beta = 0.6$, $T_{max}(N) = N$ and optimizing it assuming the estimation error for the channel gain mentioned at the beginning of this section. The selection rule chosen

Table 2.3: MDMTA results for the geometry $\mathcal{L}_{z_0}(N)$.

N	2	3	4	5
$\mathbb{E}[E_{mech}]$	0.1432	0.3496	0.6186	0.9529
$\mathbb{E}[\lvert h(\mathbf{q}_{opt})\rvert^2]$	1.4780	1.7812	2.0034	2.1779

Table 2.4: MDMTA results for the geometry $\mathcal{R}_{z_0}(N)$.

N	2	3	4	5
$\mathbb{E}[E_{mech}]$	0.0952	0.1706	0.2404	0.3087
$\mathbb{E}[\lvert h(\mathbf{q}_{opt})\rvert^2]$	1.3658	1.5818	1.7279	1.8364

was the *Minimum Effort Rule*. The results for this optimized algorithm are shown in table 2.6. Now, if we compare tables 2.2 and 2.6 we observe that the power of the optimum channel gain obtained with the optimized algorithm is around 97% to 92% of the one for the non optimized version. But the mechanical energy used by the optimized algorithm is around 50% (and in some cases even 31%) of the one for the non optimized version. Therefore, by choosing the parameter β appropriately we can sacrifice channel gain a little but at the same time significantly reduce the mechanical energy consumption thus making the MDMTA more energy efficient.

Now, we consider the case in which the TOMR must transmit a file of $M =$ 100MB to a stationary node. The duration of each bit is $T_b = 500$ns. The MR must satisfy a minimum power of $P_{ref} = 100\mu$W at the stationary node receiver and it cannot transmit more than $P_{max} = 40$mW. We assume that the shadowing term $s = 0.5$ is known. The wavelength used for this transmission is $\lambda = 15$cm. We optimize the MDMTA with the *Minimum Effort Rule* according to (2.21) for $N = 2$ and $T_{max}(2) = 5$s. By using this optimized MDMTA the outage probability decreases from 10^{-2} to 10^{-3}. In addition, when the communication is successful the energy reduction factor reaches 78%. In other words, when the communication is successful the MR saves 22% of the energy that it would use if it did not employ the MDMTA at all and if $P_{max} = +\infty$. These results show that the MDMTA reduces the outage probability and in the successful communication cases can also reduce considerably the amount of total energy expended (energy used in transmission plus energy used in motion).

Finally, we illustrate a possible implementation of the MDMTA in a practical scenario. Consider a robotic wireless network that needs to communicate with a MR in order to connect it to the robotic network. To do this a node (another MR) from the robotic network that remains temporally stationary starts to operate in a time division duplex mode. During the transmission period it transmits a training signal to the MR and during the receiving period it waits for an "answer' from the MR. Now, the MR receives this signal but due to small scale fading the received signal has a poor SNR and so it decides to implement the MDMTA to improve the quality of the wireless link before answering the stationary node. To avoid making the stationary

Table 2.5: MDMTA results for the geometry $\mathcal{R}_{1.5z_0}(N)$.

N	2	3	4	5
$\mathbb{E}[E_{mech}]$	0.2147	0.3829	0.5393	0.6915
$\mathbb{E}[\lvert h(\mathbf{q}_{opt})\rvert^2]$	1.4093	1.6598	1.8369	1.9647

Table 2.6: MDMTA optimised according to (2.22) results.

N	2	3	4	5
$\mathbb{E}[E_{mech}]$	0.0774	0.1274	0.1602	0.1651
$\mathbb{E}[\lvert h(\mathbf{q}_{opt})\rvert^2]$	1.4470	1.7321	1.9038	2.0055

node wait too long the designer sets in the MR's program the time limit $T_M = 5$ seconds. The MR has in memory a number of geometries of different sizes and different number of stopping points (up to $N = 5$) optimized according to (2.14) and (2.18). The MR also has in memory two preloaded tables containing the optimum parameters of the MDMTA according to (2.22). It will also have the corresponding value of the cost function for up to $N = 5$ stopping points and for different values of the parameter β. The first preloaded table has the optimum parameters of the algorithm using the thresholds $\eta_k = +\infty$, while the second preloaded table gives the optimum value of all the parameters including the thresholds. If the MR's battery is almost full, and establishing communication with the robotic network is very important, it will select β small to prioritize finding a large channel gain (as opposed to expenditure of mechanical energy, see (2.22)). Now, in order to apply the adaptive diversity mechanism it first realizes that in this particular case it does not have an estimate of the shadowing term (s) and so it explores all the entries of the first table (i.e., the table containing the optimized parameters when $\eta_k = +\infty$) having small β and then selects the row with the lowest cost function value. Then the MR reads that row, picks the values for all its parameters (including the number and the ordered geometry for the stopping points) and executes the MDMTA according to Algorithm 1. Finally, when it reaches $\mathbf{q}_{opt}$ it answers to the stationary node.

2.6 Conclusions

In this chapter we have developed the MDMTA which is a general MDA for discrete search spaces and we have clearly identified and formalized each one of its components. This makes it easier to analyze MDAs with discrete search spaces and as we shall see in the next chapters this will also allow us to create new MDAs by modifying the MDMTA components and/or adding more components.

We solved the problem of obtaining optimum predetermined geometries for any number of stopping points. We also showed that the meaning of optimum geometry can have various interpretations and so the solution to the optimisation of predeter-

mined geometries for a given number of stopping points has not a unique solution. We provided two different solutions, each one derived from a different interpretation of this optimality.

We also showed that by using optimum geometries in the MDMTA we can make it more efficient by obtaining higher channel gains while using less mechanical energy. So in summary, we have developed a basic theory for MDAs with discrete search spaces, proposed a general MDA (for discrete search spaces) and verified its advantages via simulation and analytical results.

In the next chapter we continue developing the theory for MDAs with discrete search spaces. To do this we now explore how to improve the location of the stopping points by calculating their position adaptively during the MDA execution rather than using predetermined geometries.

Chapter 3

MDA with Adaptive Stopping Points

In chapter 2 we studied in detail the case of the MDA with a predetermined discrete search space and solved the problem of optimising the predetermined geometry of the stopping points. We showed as well the benefits of such optimisation. Now, our next step in the study of MDAs is to consider adaptive locations for the stopping points. This will be achieved by using path planners with memory which will now be developed in this chapter.

As shown in the last chapter the design of predetermined geometries is based on the principle that the expected value of the maximum gain of N channels is maximized[1] when all the channels are independent. But the design of path planners with memory to adaptively calculate the location of the stopping points is based on a different principle. If the MR measures the channel at its current location and wants to improve the average channel gain at its next location then it must choose the next location so that the channel (at the next location) is uncorrelated to the channel at the current location if its gain is poor and correlated if the channel at the current location is high. In other words, by controlling the channel correlation rather than try to select always uncorrelated channels. We will formally derive this result in this chapter. Then we will extend it to construct various path planners with memory to adaptively determine the location of the stopping points.

The main contribution of this chapter is the development of optimum path planners with memory for MDAs with discrete search spaces, which as will be demonstrated can outperform the MDAs with predetermined discrete search spaces both in terms of the channel gain obtained and the energy used in motion. In the context of diversity techniques channel correlation has always being considered as something negative that degrades the performance of the diversity techniques [12]. But in this chapter we demonstrate that in the context of MDAs it is possible to harness channel correlation to improve the performance of MDAs with respect to the case in which all the channels are independent. This constitutes one of the major contribution of this thesis.

[1] This holds only under the restriction that the stopping points geometry is predetermined.

This chapter is organized as follows. First we introduce the general form of a path planner with memory and show how it fits into the theory of the MDMTA presented in the previous chapter. Then in section 3.2 we derive the optimum path planner with memory order one. In 3.3 we analyse it and demonstrate the new properties of the wireless channel that are introduced by use of path planners with memory. Then we continue with the development of a path planner with memory order two in section 3.4 and we generalise them to derive path planners with arbitrary memory order in section 3.5.

The models used in this chapter for the wireless channel gain and for the mobile robot will be the same as in the previous chapter but for convenience we re-write the channel model:

$$y(t) = sh(\mathbf{p}(t))x(t) + n_r(t) \tag{3.1}$$

where $x(t)$ and $y(t)$ are the transmitted and received signals while $n_r(t)$ is the additive white Gaussian noise at the receiver, $h(\mathbf{p}(t))$ is the small-scale fading term and s is the shadowing term which is considered to be constant for all the stopping points. In addition we will assume that s is known for this chapter.

3.1 Path Planners with Memory for MDAs

In this chapter the location of the next stopping point is calculated as a function of the channel at the current and previous stopping points as well as their locations. So, in general when the MR is located at the stopping point $\mathbf{q}_k$ at time instant t_k it can calculate the next stopping point $\mathbf{q}_{k+1}$ using a path planner with memory order $M(k)$ as follows:

$$\mathbf{q}_{k+1} = \mathbf{f}_{M(k)}\left(\mathbf{Q}_{M(k)}(k), \hat{\mathbf{H}}_{M(k)}(k), k\right) \tag{3.2}$$

where $\mathbf{Q}_{M(k)}(k) = [\mathbf{q}_{k-M(k)+1},\ \mathbf{q}_{k-M(k)+2}, \cdots, \mathbf{q}_k]^T$ is a matrix containing the current location of the MR and the $M(k)$ previous stopping points; $\hat{\mathbf{H}}_{M(k)}(k) = [\hat{h}\left(\mathbf{q}_{k-M(k)+1}\right),$ $\hat{h}\left(\mathbf{q}_{k-M(k)+2}\right) \cdots, \hat{h}\left(\mathbf{q}_k\right)]^T$, $\hat{h}(\mathbf{q_k})$ is the estimation for $h(\mathbf{q_k})$ with estimation errors $\hat{h}(\mathbf{q_k}) - h(\mathbf{q_k}) \sim \mathcal{CN}(0, \sigma_e^2)$ and $\mathbf{f}_{M(k)}(\cdot,\cdot,\cdot)$ is a general iterative path planner function with memory order $M(k)$ (IPPF-$M(k)$) to be developed and analysed throughout this chapter.

Note that in the previous chapter we didn't mention explicitly the path planner when we presented the components of the MDMTA but we indeed used a memoryless one (i.e., $M(k) = 0$) which can be described mathematically as follows:

$$f_0(\mathbf{Q}_N, -, k) = \mathbf{I}_N(k+1)\mathbf{Q}_N \tag{3.3}$$

where $\mathbf{I}_N(k+1)$ is the $k+1$th row of an $N \times N$ identity matrix, $\mathbf{Q}_N$ is given in (2.19) and the hyphen in the second input argument of (3.3) means that in this case the second input to the planner function is not used. Now, in order to further clarify the interaction of the path planner within the MDMTA we rewrite the pseudocode

of the MDMTA in 3 just with minor modifications in the presentation and the list of input parameters.

Algorithm 3 $MDMTA(N, M(k), \mathbf{f}_{M(k)}, \mathbf{t}, \boldsymbol{\eta}, \mathcal{R}_s, (\hat{s}))$

1: $\mathbf{p} \leftarrow \mathbf{q}_1$
2: **for** $k = 1$ to $N-1$ **do**
3: $\hat{sh}(\mathbf{q}_k) \leftarrow$ Estimate$[sh(\mathbf{p})]$ {Channel gain estimation .}
4: **if** $|\hat{h}(\mathbf{q}_k)| \geq \eta_k$ **then**
5: $\mathbf{q}_{opt} \leftarrow \mathbf{q}_k$
6: Terminate Algorithm
7: **end if**
8: $\mathbf{q}_{k+1} = \mathbf{f}_{M(k)}\left(\mathbf{Q}_{M(k)}(k), \hat{\mathbf{H}}_{M(k)}(k), k\right)$ {The path planner is used to calculate the next stopping point.}
9: $\mathbf{p} \leftarrow \mathbf{q}_{k+1}$ {The MR moves to the next stopping point in $t_{k+1} - t_k$ seconds.}
10: **end for**
11: $\hat{sh}(\mathbf{q}_N) \leftarrow$ Estimate$[sh(\mathbf{p})]$
12: $\mathbf{q}_{opt} \leftarrow \mathcal{R}_s$ {A 'selection rule' is used to determine the optimum position.}
13: $\mathbf{p} \leftarrow \mathbf{q}_{opt}$ {The MR moves to the optimum stopping point in $t_{N+1} - t_N$ seconds.}
14: Terminate Algorithm

Note also that the memory order is in general a function of time and does not necessarily have to be a constant. The reason behind this will become evident when we present the path planners with arbitrary memory order in section 3.5.

In this chapter we will consider again an omnidirectional MR and so the MR will move in straight line from stopping point to stopping point. Also, for simplicity and to strictly focus on the spatial dimension (i.e., the location of the stopping points) and not on the temporal aspects, we will restrict $t_{k+1} - t_k = T$. In chapter 5 we will discuss more about the temporal aspects of MDAs. In addition we will use the same model for the wireless channel as in the previous chapter.

During the *searching phase* of the MDMTA, at time instant t_k the MR knows $\{\hat{h}(\mathbf{q}_j)\}_{j=1}^{k}$ but the IPPF-$M(k)$ has only access to $\{\hat{h}(\mathbf{q}_j)\}_{j=k-M(k)+1}^{k}$ because it has memory order $M(k) \leq k$.

Claim: The IPPF-$M(k)$'s predictor model for the wireless channel $h(\mathbf{q}_{k+1})$ at time instant t_k when the IPPF-$M(k)$ has knowledge of $\{\hat{h}(\mathbf{q}_j)\}_{j=k-M(k)+1}^{k}$ and $\{\mathbf{q}_j\}_{j=k-M(k)+1}^{k}$ is given by:

$$\tilde{h}_{M(k)}(\mathbf{q}_{k+1}) \;=\; \mathbf{p}(k+1, M(k)+1) \begin{bmatrix} \mathbf{P}^{-1}(k, M(k)) \hat{\mathbf{H}}_{M(k)}(k) \\ \nu_{k+1} \end{bmatrix} \tag{3.4}$$

where ν_{k+1} is zero-mean complex Gaussian random variable with unit variance and and also ν_j and ν_k are independent if $k \neq j$; the matrix $\mathbf{P}(k, M(k))$ is a lower triangular matrix with $\mathbf{C}(k, M(k)) = \mathbf{P}(k, M(k))\mathbf{P}^T(k, M(k))$ and $\mathbf{p}(k+1, M(k)+1)$ is the

last row of the matrix $\mathbf{P}(k+1, M(k)+1)$. In addition, $\mathbf{C}(k, M(k))$ is an $M(k)\times M(k)$ correlation matrix with entries $\mathbf{C}_{mn}(k, M(k)) = r(\mathbf{q}_{k-M(k)+m}, \mathbf{q}_{k-M(k)+n})$, where $r(\cdot,\cdot)$ is the channel correlation given by (2.8).

Proof: The set of channels $\{h(\mathbf{q}_j)\}_{j=k-M(k)+1}^{k}$ is a set of correlated zero-mean complex Gaussian random variables with unit variance whose correlation matrix is $\mathbf{C}(k, M(k))$ with entries $\mathbf{C}_{mn}(k, M(k)) = r(\mathbf{q}_{k-M(k)+m}, \mathbf{q}_{k-M(k)+n})$. Therefore an statistical model for $\{h(\mathbf{q}_j)\}_{j=k-M(k)+1}^{k}$ is given by:

$$\begin{bmatrix} h(\mathbf{q}_{k-M(k)+1}) \\ h(\mathbf{q}_{k-M(k)+2}) \\ \vdots \\ h(\mathbf{q}_k) \end{bmatrix} = \mathbf{P}(k, M(k)) \begin{bmatrix} \nu_{k-M(k)+1} \\ \nu_{k-M(k)+2} \\ \vdots \\ \nu_k \end{bmatrix} \tag{3.5}$$

where $\{\nu_j\}_{j=k-M(k)+1}^{k}$ is a set i.i.d. zero-mean complex Gaussian random variables with unit variance that serve to construct the set of correlated random variables that represent the wireless channels $\{h(\mathbf{q}_j)\}_{j=k-M(k)+1}^{k}$. We also have:

$$\begin{bmatrix} h(\mathbf{q}_{k-M(k)+1}) \\ h(\mathbf{q}_{k-M(k)+2}) \\ \vdots \\ h(\mathbf{q}_k) \\ h(\mathbf{q}_{k+1}) \end{bmatrix} = \mathbf{P}(k+1, M(k+1)) \begin{bmatrix} \nu_{k-M(k)+1} \\ \nu_{k-M(k)+2} \\ \vdots \\ \nu_k \\ \nu_{k+1} \end{bmatrix} \tag{3.6}$$

$$\begin{bmatrix} h(\mathbf{q}_{k-M(k)+1}) \\ h(\mathbf{q}_{k-M(k)+2}) \\ \vdots \\ h(\mathbf{q}_k) \\ h(\mathbf{q}_{k+1}) \end{bmatrix} = \mathbf{P}(k+1, M(k+1)) \begin{bmatrix} \mathbf{P}^{-1}(k, M(k)) \begin{bmatrix} h(\mathbf{q}_{k-M(k)+1}) \\ h(\mathbf{q}_{k-M(k)+2}) \\ \vdots \\ h(\mathbf{q}_k) \end{bmatrix} \\ \nu_{k+1} \end{bmatrix} \tag{3.7}$$

Note that the last row of (3.7) is a statiscal model that relates the channel $h(\mathbf{q}_{k+1})$ to the set of the channels $\{h(\mathbf{q}_j)\}_{j=k-M(k)+1}^{k}$. So, if we neglect the channel estimation error and take the last row of (3.7) we obtain the IPPF-$M(k)$'s predictor model for $h(\mathbf{q}_{k+1})$ given by (3.4). ■

For mathematical simplicity we will assume during the development of this chapter that the channel estimation error is negligible and so $\hat{h}(\mathbf{q_k}) = h(\mathbf{q_k})$ but in the simulation section we will take the error into account to observe its effects on the performance of the path planners.

Note that for this kind of path planner the MR needs to know the small scale fading term in (3.1). To do this the MR first needs to perform a channel estimation which will produce an estimate of the product of the small-scale fading and the shadowing term. Then it needs to isolate the small-scale fading term and to do this

the MR needs to have access to an estimate of the shadowing term s. Therefore for all the path planners with memory in this chapter we will consider that the MR has an estimate of s.

3.2 Path Planners with Memory Order One

In this section we develop the iterative path planner in (3.2) with memory order one, i.e., with $M(k) = 1$. We will refer to this path planner as IPPF-1 and its general form is:

$$\begin{aligned} \mathbf{f}_1(\mathbf{q}_k, h(\mathbf{q}_k), k) &= d_1(h(\mathbf{q}_k))\mathbf{v}(k) + \mathbf{q}_k, \\ \mathbf{v}(k) &= [\cos(\psi(k)) \quad \sin(\psi(k))]^T \end{aligned} \tag{3.8}$$

where $d_1(h(\mathbf{q}_k))$ is a distance function that determines the distance between the kth and the $k+1$th stopping points (i.e., $\|\mathbf{q}_{k+1} - \mathbf{q}_k\|_2$) and $\psi(k)$ is the direction in which the MR has to move to arrive at $\mathbf{q}_{k+1}$ by departing from $\mathbf{q}_k$.

As mentioned in the previous chapter an efficient MDA should obtain a high channel gain while using little mechanical energy. So one way to optimise the IPPF-1 in (3.8) is as follows:

$$\begin{aligned} &\max_{d_1(h(\mathbf{q}_k)),\psi(k)} \theta\mathbb{E}\left[|h(\mathbf{q}_{opt})|\right] - (1-\theta)\mathbb{E}\left[\sum_{k=1}^{N} E_m\left(t_k, t_{k+1}, \mathbf{u}_k^*(t)\right)\right] \\ &\text{s.t.} \\ &\mathbf{q}_{k+1} = d_1(h(\mathbf{q}_k))\mathbf{v}(k) + \mathbf{q}_k \quad k = 1, 2, \cdots, N-1 \\ &\mathbf{q}_{N+1} = \mathbf{q}_{opt} \end{aligned} \tag{3.9}$$

where $\mathbf{u}_k^*(t)$ is the optimum control law derived in section 2.3.2 that moves the MR in straight line from $\mathbf{q}_k$ to $\mathbf{q}_{k+1}$ in $t_{k+1} - t_k$ seconds. The optimization target in this problem is a convex combination of the expected value of the channel gain at $\mathbf{q}_{opt}$ and the negative of the average mechanical energy used during the MDA execution. This optimization target has the same form as the one we used in (2.22) in chapter 2 where we casted the optimization problem as an 'investment problem'. The design parameter $\theta \in [0, 1]$ defines the importance of obtaining a high channel gain with respect to the mechanical energy consumption.

The first equality restriction in (3.9) refers to the fact that the stopping points are calculated using the IPPF-1. The second restriction is added for notational convenience to simplify the expression of the term that represents the mechanical energy used during the whole algorithm execution (i.e., from time instant t_1 until t_{N+1}) in the optimisation target in (3.9).

The optimization target of (3.9) is a functional that depends on the functions $d_1(h(\mathbf{q}_k))$ and $\psi(k)$ and so theoretically it could be solved using dynamic programming [35]. But, in general there is no an analytical expression for the optimisation

target in (3.9) (specifically for the term $\mathbb{E}\left[|h(\mathbf{q}_{opt})|\right]$) so in practice we must evaluate it by Monte Carlo simulations, thus making the optimization process computationally expensive. This problem is accentuated by the fact that the optimisation target depends on two functions rather than a single one.

This can be alleviated by first optimising $d_1(h(\mathbf{q}_k))$ assuming $\psi(k)$ constant (i.e., $\psi(k) = \psi(1)$) and then optimize $\psi(k)$ using the previously optimized $d_1(h(\mathbf{q}_k))$. This produces two optimization problems with smaller search spaces which are simpler and computationally cheaper to solve than directly trying to solve (3.9).

We can further simplify the optimization of $d_1(h(\mathbf{q}_k))$ by restricting it to be a specific parameterized function and then optimise its parameters. This is because optimising a few parameters of a function is computationally cheaper than finding the optimal form of the function itself. To achieve this we first note that for $M(k) = 1$ the predictor (3.4) can be written as:

$$\tilde{h}_1(\mathbf{q}_{k+1}) = \nu_{k+1}\sqrt{1 - r^2(\mathbf{q}_k, \mathbf{q}_{k+1})} + h(\mathbf{q}_k)r(\mathbf{q}_k, \mathbf{q}_{k+1}), \tag{3.10}$$

with power:

$$\mathbb{E}\left[|\tilde{h}_1(\mathbf{q}_{k+1})|^2\right] = (1 + r(\mathbf{q}_k, \mathbf{q}_{k+1})(|h(\mathbf{q}_k)|^2 - 1)), \tag{3.11}$$

where $r(\cdot, \cdot)$ is the channel correlation given by (2.8). For notational simplicity, we will use interchangeably $r(\mathbf{q}_k, \mathbf{q}_j)$ and $r_{k,j}$ in the rest of the chapter. From (2.8) and (3.11) we observe that if the MR wants to maximize the power of the predicted channel at $\mathbf{q}_{k+1}$ it must move near (far) from $\mathbf{q}_k$ to experience a high (low) correlation factor $r_{k,k+1}$ if $|h(\mathbf{q}_k)|^2$ is high (low). If we implement this principle in the general IPPF-1 (3.8) then its distance function $d_1(h(\mathbf{q}_k))$ takes the following form (see Fig. 3.1):

$$d_1\left(h\left(\mathbf{q}_k\right)\right) = \mathbf{1}_{\mathbb{R}^{+*}}(|h\left(\mathbf{q}_k\right)| - \alpha)d + \mathbf{1}_{\mathbb{R}^{-}}(|h\left(\mathbf{q}_k\right)| - \alpha)D, \tag{3.12}$$

where $\mathbf{1}_{\mathbb{R}^{+*}}(\cdot)$ is the indicator function and $d < D$ and α are the parameters to be optimized according to:

$$\begin{aligned}
&\max_{d,D,\alpha} \theta\mathbb{E}\left[|h(\mathbf{q}_{opt})|\right] - (1-\theta)\mathbb{E}\left[\sum_{k=1}^{N} \|\mathbf{q}_{k+1} - \mathbf{q}_k\|_2^2\right] \\
&\text{s.t.} \\
&\mathbf{q}_{k+1} = d_1(h(\mathbf{q}_k))\mathbf{v}(k) + \mathbf{q}_k \quad k = 1, 2, \cdots, N-1, \\
&d_1\left(h\left(\mathbf{q}_k\right)\right) = \mathbf{1}_{\mathbb{R}^{+*}}(|h\left(\mathbf{q}_k\right)| - \alpha)d + \mathbf{1}_{\mathbb{R}^{-}}(|h\left(\mathbf{q}_k\right)| - \alpha)D, \\
&\mathbf{q}_{N+1} = \mathbf{q}_{opt}, \\
&\psi(k) = \psi(1).
\end{aligned} \tag{3.13}$$

This optimization problem is obtained by restricting $d_1\left(h\left(\mathbf{q}_k\right)\right)$ to take the form in (3.12) and absorbing the term $\mathcal{K}(T)$ of the mechanical energy term into the multiplying factor $1-\theta$. The optimization target in (3.1) is a convex combination between the expected value of the channel gain at $\mathbf{q}_{opt}$ and the negative of the sum the average mechanical energy (normalized by $\mathcal{K}(T)$). The design parameter θ determines the

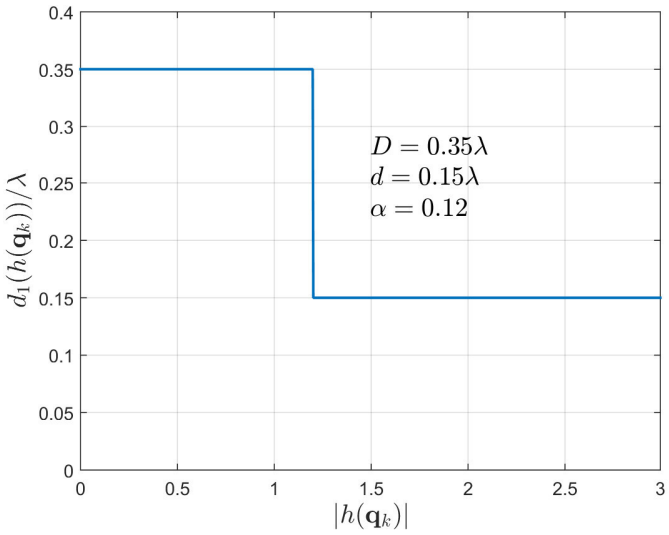

Figure 3.1: Example of the function $d_1\left(h\left(\mathbf{q}_k\right)\right)$ for $d = 0.15\lambda$, $D = 0.35\lambda$ and $\alpha = 1.2$.

relative importance of obtaining a high channel gain respect to spending mechanical energy. Therefore if we want to obtain a high channel gain but we do not mind spending too much mechanical energy then we can select θ close to 1.

This optimization problem can be solved numerically using simulated annealing. In general there is no analytical expression for the optimization target and so it must be evaluated by simulations but for the particular case of $N = 2$ stopping points we are able to derive an analytical expression for the optimization target, as we will show in subsections 3.3.2 and 3.3.3.

Note that the optimization target in (3.13) depends indirectly on the parameters d, D and α. This is because the optimization target depends on the stopping points and these are calculated using those parameters as can be seen from the first and second equality restrictions in (3.13).

Now, given $d_1\left(h\left(\mathbf{q}_k\right)\right)$, the function $\psi(k)$ determines the distance traveled by the MR during the *selection phase*[2], the distance among the stopping points and so the correlation between their wireless channels. Consequently, it also affects the statistics of $h(\mathbf{q}_{opt})$. So, a poor choice of $\psi(k)$ can significantly decrease $\mathbb{E}\left[|h(\mathbf{q}_{opt})|\right]$ and/or maximize the amount of mechanical energy used during the *selection phase*. Therefore the necessity of optimizing $\psi(k)$ is clear. Given the number of stopping points N and the optimized function $d_1\left(h\left(\mathbf{q}_k\right)\right)$ we can optimise $\psi(k)$ by solving the

[2]The distance traveled during the *searching phase* depends only on $d_1\left(h\left(\mathbf{q}_k\right)\right)$ and not on $\psi(k)$.

following problem:

$$\begin{aligned} &\max_{\psi} \theta \mathbb{E}\left[|h(\mathbf{q}_{opt})|\right] - (1-\theta)\mathbb{E}\left[\|\mathbf{q}_{opt} - \mathbf{q}_N\|_2^2\right] \\ &\text{s.t.} \\ &\mathbf{q}_{k+1} = d_1^*(h(\mathbf{q}_k))\mathbf{v}(k) + \mathbf{q}_k \quad k = 1, 2, \cdots, N-1, \\ &\psi(k+1) - \psi(k) = \psi \quad k = 1, 2, \cdots, N-2, \end{aligned} \tag{3.14}$$

where $d_1^*(h(\mathbf{q}_k))$ is the optimised distance function according to (3.13). The first term in the optimization target is the same as in (3.13) while the second term is the expected value of the distance traveled during the *selection phase*. This is because, as mentioned previously, only the distance traveled during the *selection phase* is affected by $\psi(k)$. In the optimization target, the first term will tend to spread out the stopping points to reduce the correlation among all the points and to increase $\mathbb{E}\left[|h\left(\mathbf{q}_{opt}\right)|\right]$ but the second term will tend to concentrate the stopping points around $\mathbf{q}_N$ to reduce the distance traveled during the *selection phase*. Now, the last equality restriction of (3.14) reduces the dimension of the search space from $N-2$ to 1. This is done because there is not an analytical expression for the optimization target and so reducing the search space simplifies significantly the optimization process (although it also reduces the performance). We have used this angular restriction in similar optimisation problems [37].

Note that by solving optimization problem (3.14) we are reducing the average distance between $\mathbf{q}_N$ and $\mathbf{q}_{opt}$ while avoiding a large increase in the channel correlation that could degrade significantly $\mathbb{E}\left[|h(\mathbf{q}_{opt})|\right]$.

So now that we have shown how to optimise $d_1(h(\mathbf{q}_k))$ and $\psi(k)$ in (3.8) we have concluded the design of the IPPF-1 in (3.8). In the next section we will analyse some properties of this particular IPPF-1 for the particular case when $N = 2$. We will also derive the analytical expression for the optimization target of (3.13) for the particular case when $N = 2$. Finally, it is important to mention that although the IPPF-1 will be executed online its optimization can be done off-line.

3.3 IPPF-1 Analysis

In this section we demonstrate some important properties of the IPPF-1 and fully characterize it for the special case of $N = 2$. We also obtain an analytical expression for the optimization target in (3.13) for $N = 2$.

3.3.1 Channel Gain Distributions

When the location of the stopping points is predetermined as in the previous chapter the channels at all the stopping points are identically distributed. But, when we use the IPPF-1 developed in the previous section to calculate the location of the stopping points this property does not hold anymore. Now we proceed to prove this. Consider

two stopping points $\mathbf{q}_1$ and $\mathbf{q}_2$, where $\mathbf{q}_1$ is explored first. So the p.d.f. of $|h(\mathbf{q}_1)|$ is:

$$f_1(x) = 2x \exp\left(-x^2\right). \tag{3.15}$$

We use the IPPF-1 from previous section to calculate $\mathbf{q}_2$ so the correlation between $h(\mathbf{q}_1)$ and $h(\mathbf{q}_2)$ is $r_0 = J_0\left(\frac{2\pi D}{\lambda}\right)$ if $|h(\mathbf{q}_1)| < \alpha$ and $r_1 = J_0\left(\frac{2\pi d}{\lambda}\right)$ if $|h(\mathbf{q}_1)| \geq \alpha$. Since in this case $\mathbf{q}_2$ depends on $|h(\mathbf{q}_1)|$, and in order to avoid having a cumbersome notation, instead of writing the correlation between the channels at both $\mathbf{q}_1$ and $\mathbf{q}_2$ as $r(\mathbf{q}_1, \mathbf{q}_2(|h(\mathbf{q}_1)|))$ in this section we will write $r(|h(\mathbf{q}_1)|)$, where $\mathbf{q}_1$ is the arbitrary starting point.

Now, given $h(\mathbf{q}_1)$, from (3.10), it can be demonstrated that $h(\mathbf{q}_2)$ is a complex Gaussian random variable with mean $r(|h(\mathbf{q}_1)|)h(\mathbf{q}_1)$ and variance $1 - r^2(|h(\mathbf{q}_1)|)$. Thus, we can show that the conditional p.d.f. of $|h(\mathbf{q}_2)|$ given $|h(\mathbf{q}_1)| = x$ is a Rician distribution:

$$f_{2|1}(y|x) = \tfrac{2y}{1-r^2(x)} \exp\left(\tfrac{-y^2-r^2(x)x^2}{1-r^2(x)}\right) \mathrm{I}_0\left(\tfrac{2r(x)yx}{1-r^2(x)}\right) \tag{3.16}$$

where $\mathrm{I}_0(\cdot)$ is the modified Bessel function of the first kind and zeroth order. Now, combining (3.15) and (3.16) according to the total probability theorem we have:

$$f_2(y) = \int_0^{+\infty} f_{2|1}(y|x) f_1(x) \mathrm{d}x, \tag{3.17}$$

$$f_2(y) = \int_0^{+\infty} \frac{4xy}{1-r^2(x)} \exp\left(-x^2\right) \exp\left(\frac{-y^2-r^2(x)x^2}{1-r^2(x)}\right) \mathrm{I}_0\left(\frac{2r(x)yx}{1-r^2(x)}\right) \mathrm{d}x, \tag{3.18}$$

$$\begin{aligned} f_2(y) &= \int_0^{\alpha} \frac{4xy}{1-r_0^2} \exp\left(-x^2\right) \exp\left(\frac{-y^2-r_0^2x^2}{1-r_0^2}\right) \mathrm{I}_0\left(\frac{2r_0yx}{1-r_0^2}\right) \mathrm{d}x \\ &+ \int_{\alpha}^{+\infty} \frac{4xy}{1-r_1^2} \exp\left(-x^2\right) \exp\left(\frac{-y^2-r_1^2x^2}{1-r_1^2}\right) \mathrm{I}_0\left(\frac{2r_1yx}{1-r_1^2}\right) \mathrm{d}x, \end{aligned} \tag{3.19}$$

$$\begin{aligned} f_2(y) &= \int_0^{\alpha} \frac{4xy}{1-r_0^2} \exp\left(\frac{-y^2-x^2}{1-r_0^2}\right) \mathrm{I}_0\left(\frac{2r_0yx}{1-r_0^2}\right) \mathrm{d}x \\ &+ \int_{\alpha}^{+\infty} \frac{4xy}{1-r_1^2} \exp\left(\frac{-y^2-x^2}{1-r_1^2}\right) \mathrm{I}_0\left(\frac{2r_1yx}{1-r_1^2}\right) \mathrm{d}x, \end{aligned} \tag{3.20}$$

$$\begin{aligned} f_2(y) &= 2y \exp\left(-y^2\right) \int_0^{\alpha} \frac{2x}{1-r_0^2} \exp\left(\frac{-x^2-r_0^2y^2}{1-r_0^2}\right) \mathrm{I}_0\left(\frac{2r_0yx}{1-r_0^2}\right) \mathrm{d}x \\ &+ 2\exp\left(-y^2\right) \int_{\alpha}^{+\infty} \frac{2x}{1-r_1^2} \exp\left(\frac{-x^2-r_1^2y^2}{1-r_1^2}\right) \mathrm{I}_0\left(\frac{2r_1yx}{1-r_1^2}\right) \mathrm{d}x, \end{aligned} \tag{3.21}$$

Note that the integrands in (3.21) are Rician distributions and consequently we have:

$$\begin{aligned} f_2(y) &= 2y\exp\left(-y^2\right)\left(1-\mathrm{Q}_1\left(\frac{\sqrt{2}r_0 y}{\sqrt{1-r_0^2}},\frac{\sqrt{2}\alpha}{\sqrt{1-r_0^2}}\right)\right) \\ &+ 2\exp\left(-y^2\right)\mathrm{Q}_1\left(\frac{\sqrt{2}r_1 y}{\sqrt{1-r_1^2}},\frac{\sqrt{2}\alpha}{\sqrt{1-r_1^2}}\right), \end{aligned} \tag{3.22}$$

where $\mathrm{Q}_1(\cdot,\cdot)$ is the generalized Marcum Q-function of first order and after factorizing the p.d.f. of $|h(\mathbf{q}_2)|$ is:

$$f_2(y) = \left[1-\mathrm{Q}_1\left(\frac{\sqrt{2}r_0 y}{\sqrt{1-r_0^2}},\frac{\sqrt{2}\alpha}{\sqrt{1-r_0^2}}\right)+\mathrm{Q}_1\left(\frac{\sqrt{2}r_1 y}{\sqrt{1-r_1^2}},\frac{\sqrt{2}\alpha}{\sqrt{1-r_1^2}}\right)\right]2y\exp\left(-y^2\right). \tag{3.23}$$

Comparing (3.15) with (3.23) we clearly observe that $|h(\mathbf{q}_1)|$ and $|h(\mathbf{q}_2)|$ have different distributions. This demonstrates that when the MR uses the IPPF-1 the channels are not in general identically distributed. This occurs because the correlation between the channels depends on the realization of $|h(\mathbf{q}_1)|$ - see (3.8) and (3.12) .

3.3.2 Optimum Channel Gain Properties

Now we derive the c.d.f. of $|h(\mathbf{q}_{opt})|$ which is the maximum of both channel gains $|h(\mathbf{q}_1)|$ and $|h(\mathbf{q}_2)|$. From basic probability theory we have[3]:

$$\begin{aligned} \Pr\left(|h(\mathbf{q}_{opt})|<z\right) &= \int_0^z\int_0^z f_{1,2}(x,y)dxdy \\ &= \int_0^z\int_0^z f_{2|1}(y|x)f_1(x)dxdy \end{aligned} \tag{3.24}$$

where $f_{1,2}(x,y)$ is the joint p.d.f. of the channel gains $|h(\mathbf{q}_1)|$ and $|h(\mathbf{q}_2)|$, $f_{2|1}(y|x)$ is the conditional p.d.f. of $|h(\mathbf{q}_2)|$ conditioned on $|h(\mathbf{q}_1)|=x$ given by (3.16) and $f_1(x)$ is the marginal p.d.f. of $|h(\mathbf{q}_1)|$ given by (3.15). Now, for $z<\alpha$, we have from (3.15), (3.16) and (3.24) that:

$$\Pr\left(|h(\mathbf{q}_{opt})|<z\right) = \int_0^z\int_0^z f_{2|1}(y|x)\mathrm{d}y f_1(x)\mathrm{d}x \tag{3.25}$$

$$\Pr\left(|h(\mathbf{q}_{opt})|<z\right) = \int_0^z f_1(x)\int_0^z \frac{2y}{1-r_0^2}\exp\left(\frac{-y^2-r_0^2x^2}{1-r_0^2}\right)\mathrm{I}_0\left(\frac{2r_0yx}{1-r_0^2}\right)\mathrm{d}y\mathrm{d}x \tag{3.26}$$

[3] $\Pr\left(|h(\mathbf{q}_{opt})|<z\right)$ is the probability that $|h(\mathbf{q}_{opt})|<z$ is satisfied.

the inner integrand is a Rician distribution and so:

$$\Pr\left(|h(\mathbf{q}_{opt})| < z\right) = \int_0^z f_1(x)\left(1 - Q_1\left(\frac{\sqrt{2}r_0 x}{\sqrt{1-r_0^2}}, \frac{\sqrt{2}z}{\sqrt{1-r_0^2}}\right)\right)\mathrm{d}x \tag{3.27}$$

$$\begin{aligned}\Pr\left(|h(\mathbf{q}_{opt})| < z\right) &= 1 - \exp(-z^2) \\ &- \int_0^z 2x\exp(-x^2)Q_1\left(\frac{\sqrt{2}r_0 x}{\sqrt{1-r_0^2}}, \frac{\sqrt{2}z}{\sqrt{1-r_0^2}}\right)\mathrm{d}x\end{aligned} \tag{3.28}$$

Now, in [36] we find the following integral:

$$\begin{aligned}\int_0^c x\exp(-p^2x^2/2)Q_1\left(ax, b\right)\mathrm{d}x &= \frac{1}{p^2}\exp\left(\frac{-p^2b^2}{2(a^2+p^2)}\right)Q_1\left(c\sqrt{a^2+p^2}, \frac{ab}{\sqrt{a^2+p^2}}\right) \\ &- \exp\left(\frac{-p^2c^2}{2}\right)Q_1\left(ac, b\right)\end{aligned} \tag{3.29}$$

Then, using integral (3.29) into (3.28) we obtain:

$$\begin{aligned}\Pr(|h(\mathbf{q}_{opt})| < z) &= e^{-z^2}\left(Q_1\left(\frac{\sqrt{2}r_0 z}{\sqrt{1-r_0^2}}, \frac{\sqrt{2}z}{\sqrt{1-r_0^2}}\right) - Q_1\left(\frac{\sqrt{2}z}{\sqrt{1-r_0^2}}, \frac{\sqrt{2}r_0 z}{\sqrt{1-r_0^2}}\right)\right) \\ &+ 1 - e^{-z^2},\end{aligned} \tag{3.30}$$

and for $z \geq \alpha$ we have:

$$\begin{aligned}\Pr(|h(\mathbf{q}_{opt})| < z) &= \Pr(|h(\mathbf{q}_{opt})| < \alpha) \\ &+ \Pr(|h(\mathbf{q}_1)| < \alpha, \alpha < |h(\mathbf{q}_2)| < z) \\ &+ \Pr(|h(\mathbf{q}_2)| < \alpha, \alpha < |h(\mathbf{q}_1)| < z) \\ &+ \Pr(\alpha < |h(\mathbf{q}_1)| < \alpha, \alpha < |h(\mathbf{q}_2)| < z)\end{aligned} \tag{3.31}$$

where the first probability on the right hand side is obtained by evaluating (3.30) at α while the following three probabilities can be calculated using a similar procedure as the one used to derive (3.30). Then after calculating each probability and simplifying terms we obtain:

$$\begin{aligned}\Pr(|h(\mathbf{q}_{opt})| < z) &= e^{-\alpha^2}\left(Q_1\left(\frac{r_0\alpha\sqrt{2}}{\sqrt{1-r_0^2}}, \frac{z\sqrt{2}}{\sqrt{1-r_0^2}}\right) - Q_1\left(\frac{\alpha r_1\sqrt{2}}{\sqrt{1-r_1^2}}, \frac{z\sqrt{2}}{\sqrt{1-r_1^2}}\right)\right) \\ &- e^{-z^2}\left(Q_1\left(\frac{\alpha\sqrt{2}}{\sqrt{1-r_0^2}}, \frac{r_0 z\sqrt{2}}{\sqrt{1-r_0^2}}\right) - Q_1\left(\frac{\alpha\sqrt{2}}{\sqrt{1-r_1^2}}, \frac{zr_1\sqrt{2}}{\sqrt{1-r_1^2}}\right)\right) \\ &+ e^{-z^2}\left(Q_1\left(\frac{zr_1\sqrt{2}}{\sqrt{1-r_1^2}}, \frac{z\sqrt{2}}{\sqrt{1-r_1^2}}\right) - Q_1\left(\frac{z\sqrt{2}}{\sqrt{1-r_1^2}}, \frac{zr_1\sqrt{2}}{\sqrt{1-r_1^2}}\right)\right) \\ &+ 1 - e^{-z^2}.\end{aligned} \tag{3.32}$$

And its expected value can be obtained by evaluating numerically the following integral:

$$\mathbb{E}[|h(\mathbf{q}_{opt})|] = \int_0^\infty (1 - P(|h(\mathbf{q}_{opt})| < z))\, dz. \tag{3.33}$$

This gives us an analytical expression to calculate the first term in the optimization target of (3.13) for $N = 2$. Now, when the location of both stopping points is predetermined we have $\alpha \to +\infty$ and so the c.d.f. of $|h(\mathbf{q}_{opt})|$ is given by (3.30) and by evaluating numerically its expected value with (3.33) we observe that $\mathbb{E}[|h(\mathbf{q}_{opt})|]$ its a decreasing function of r_0 and so reaches its maximum for $r_0 = 0$. Now we proceed to calculate this maximum value. When $\alpha \to +\infty$ (3.26) becomes:

$$\begin{aligned} \Pr\left(|h(\mathbf{q}_{opt})| < z\right) &= \left(\int_0^z 2x \exp\left(-x^2\right) \mathrm{d}x\right)^2 \\ &= \left(1 - \exp\left(-z^2\right)\right)^2 \\ &= 1 - 2\exp\left(-z^2\right) + \exp\left(-2z^2\right) \end{aligned} \tag{3.34}$$

and from (3.33) we have:

$$\mathbb{E}[|h(\mathbf{q}_{opt})|] = \int_0^\infty \left(2\exp\left(-z^2\right) - \exp\left(-2z^2\right)\right) dz. \tag{3.35}$$

$$\mathbb{E}[|h(\mathbf{q}_{opt})|] = 2\sqrt{\pi} \int_0^\infty \frac{1}{\sqrt{\pi}} \exp\left(-z^2\right) \mathrm{d}z - \frac{\sqrt{\pi}}{\sqrt{2}} \int_0^\infty \frac{\sqrt{2}}{\sqrt{\pi}} \exp\left(-2z^2\right) \mathrm{d}z. \tag{3.36}$$

Note that both integrands are Gaussian distributions with zero-mean and then both integrals take the value of $1/2$. Therefore we have the maximum value for $\mathbb{E}[|h(\mathbf{q}_{opt})|]$ is given by:

$$\mathbb{E}[|h(\mathbf{q}_{opt})|] = \sqrt{\pi} - \frac{\sqrt{\pi}}{\sqrt{2}} \frac{1}{2} \tag{3.37}$$

$$\mathbb{E}[|h(\mathbf{q}_{opt})|] = \sqrt{\pi} \left(1 - \frac{1}{\sqrt{8}}\right) \tag{3.38}$$

Nevertheless, if we optimize $d_1(h(\mathbf{q}_k))$ according to (3.13) with $\theta = 1$ then, for $N = 2$, we have $\mathbb{E}[|h(\mathbf{q}_{opt})|] \approx 1.561 > \sqrt{\pi}\left(1 - \frac{1}{\sqrt{8}}\right) \approx 1.458$. In other words, if we intelligently control the channel correlation (using the IPPF-1) we can surpass the expected value of the maximum channel gain obtained when both channels are independent. Even if for $N = 2$ the expected value $\mathbb{E}[|h(\mathbf{q}_{opt})|]$ is just slightly larger with respect to the case in which both channels are independent this is an important result from a theoretical perspective and we shall see the implications of this interesting property later in section 3.6. This is a unique property of the MDAs since traditional diversity techniques have their performance reduced with the introduction of channel correlation [12].

3.3.3 Mechanical Energy

The mechanical energy is proportional to the squared distance traveled by the MR between stopping points (see (2.28)). So, we first derive the statistics of the distance traveled and then we derive the statistics for the mechanical energy.

The distance l_1 traveled during the *searching phase* can be shown to have the following p.m.f.:

$$\begin{aligned} \Pr(l_1 = d) &= \Pr(|h(\mathbf{q}_1)| \geq \alpha) = \exp(-\alpha^2) \\ \Pr(l_1 = D) &= \Pr(|h(\mathbf{q}_1)| < \alpha) = 1 - \exp(-\alpha^2). \end{aligned} \tag{3.39}$$

Now, we derive the p.m.f. for the distance l_2 traveled during the *selection phase*. For $\Pr(l_2 = D)$ we have:

$$\begin{aligned} \Pr(l_2 = D) &= \Pr(\mathbf{q}_{opt} = \mathbf{q}_1,\ |h(\mathbf{q}_1)| < \alpha) \\ &= \Pr(\alpha > |h(\mathbf{q}_1)| > |h(\mathbf{q}_2)|) \\ &= \Pr(\alpha > |h(\mathbf{q}_1)|, \alpha > |h(\mathbf{q}_2)|)/2 \\ &= \frac{1}{2}e^{-\alpha^2}\left(Q_1\left(\frac{\alpha r_0\sqrt{2}}{\sqrt{1-r_0^2}}, \frac{\alpha\sqrt{2}}{\sqrt{1-r_0^2}}\right) - Q_1\left(\frac{\alpha\sqrt{2}}{\sqrt{1-r_0^2}}, \frac{\alpha r_0\sqrt{2}}{\sqrt{1-r_0^2}}\right)\right) \\ &+ \frac{1}{2} - \frac{1}{2}e^{-\alpha^2}. \end{aligned} \tag{3.40}$$

For $\Pr(l_2 = d)$ we have:

$$\begin{aligned} \Pr(l_2 = d) &= \Pr(\mathbf{q}_{opt} = \mathbf{q}_1,\ |h(\mathbf{q}_1)| \geq \alpha) \\ &= \Pr(\mathbf{q}_{opt} = \mathbf{q}_1) - \Pr(l_2 = D) \end{aligned} \tag{3.41}$$

where $\Pr(\mathbf{q}_{opt} = \mathbf{q}_1)$ can be calculated from the joint p.d.f. $f_{1,2}(x, y)$, given by the product of (3.15) and (3.16). Then by integrating $f_{1,2}(x, y)$ we have:

$$\begin{aligned} \Pr(\mathbf{q}_{opt} = \mathbf{q}_1) &= \frac{1}{2}e^{-\alpha^2}\left(Q_1\left(\frac{\alpha\sqrt{2}}{\sqrt{1-r_1^2}}, \frac{\alpha r_1\sqrt{2}}{\sqrt{1-r_1^2}}\right) + Q_1\left(\frac{\alpha r_0\sqrt{2}}{\sqrt{1-r_0^2}}, \frac{\alpha\sqrt{2}}{\sqrt{1-r_0^2}}\right)\right) \\ &- \frac{1}{2}e^{-\alpha^2}\left(Q_1\left(\frac{\alpha r_1\sqrt{2}}{\sqrt{1-r_1^2}}, \frac{\alpha\sqrt{2}}{\sqrt{1-r_1^2}}\right) + Q_1\left(\frac{\alpha\sqrt{2}}{\sqrt{1-r_0^2}}, \frac{\alpha r_0\sqrt{2}}{\sqrt{1-r_0^2}}\right)\right) \\ &+ \frac{1}{2} \end{aligned} \tag{3.42}$$

Now, regarding $\Pr(l_2 = 0)$ we have:

$$\Pr(l_2 = 0) = \Pr(\mathbf{q}_{opt} = \mathbf{q}_2) \tag{3.43}$$

where $\Pr(\mathbf{q}_{opt} = \mathbf{q}_2) = 1 - \Pr(\mathbf{q}_{opt} = \mathbf{q}_1)$. And the p.m.f. of the mechanical energy (see (2.28)) $E_m(t_1, t_3, \mathbf{u}(t))$ used during the MDA execution is:

$$\begin{aligned} \Pr\left(E_m(t_1, t_3, \mathbf{u}(t)) = \mathcal{K}(T)D^2\right) &= \Pr(\mathbf{q}_{opt} = \mathbf{q}_2,\ |h(\mathbf{q}_1)| < \alpha) \\ &= \Pr(l_1 = D) - \Pr(l_2 = D) \end{aligned} \tag{3.44}$$

$$\begin{aligned} \Pr\left(E_m(t_1, t_3, \mathbf{u}(t)) = \mathcal{K}(T)d^2\right) &= \Pr(\mathbf{q}_{opt} = \mathbf{q}_2,\ |h(\mathbf{q}_1)| \geq \alpha) \\ &= \Pr(l_1 = d) - \Pr(l_2 = d) \end{aligned} \tag{3.45}$$

$$\Pr\left(E_m(t_1, t_3, \mathbf{u}(t)) = 2\mathcal{K}(T)D^2\right) = \Pr(l_2 = D) \tag{3.46}$$

$$\Pr\left(E_m(t_1, t_3, \mathbf{u}(t)) = 2\mathcal{K}(T)d^2\right) = \Pr(l_2 = d). \tag{3.47}$$

Finally we can calculate $\mathbb{E}[E_m(t_1, t_3, \mathbf{u}(t))]$ from (3.39), (3.40), (3.41) and the above equations. So together with (3.30), (3.32) and (3.33) we have now a complete analytical expressions for both terms of the optimization target in (3.13) for $N = 2$.

3.4 Path Planners with Memory Order Two

Now that we have derived the IPPF-1 we proceed to derive the IPPF-2 in this section. As mentioned during the design of the IPPF-1, the maximization of an optimisation target which does not have an analytical expression can be problematic and computationally expensive. So, in order to derive the optimum IPPF-2 we will first develop an analytical expression for the optimisation target.

This optimization target must have two elements: the first element must take into account the optimum channel gain obtained and the second element must consider the mechanical energy used for obtaining the optimum channel. In general, due to the complexity of the problem it is not possible to obtain analytical expressions either for $\mathbb{E}[|h(\mathbf{q}_{opt})|]$ or for $\mathbb{E}[E_{mech}(t_1, t_{N+1}, \mathbf{u}(t))]$ but there are alternative choices as we shall see later.

If we try to optimize $\mathbf{f}_2\left(\mathbf{Q}_2(k), \hat{\mathbf{H}}_2(k), k\right)$ off-line then we need to optimise this function over its whole domain. On the other hand, if we optimise $\mathbf{f}_2\left(\mathbf{Q}_2(k), \hat{\mathbf{H}}_2(k), k\right)$ online at time instant t_k then $\mathbf{q}_k$, $\mathbf{q}_{k-1}$, $h(\mathbf{q}_k)$ and $h(\mathbf{q}_{k-1})$ are all known and therefore we just need to optimise the value of $\mathbf{f}_2\left(\mathbf{Q}_2(k), \hat{\mathbf{H}}_2(k), k\right)$ at a single point rather than finding the whole optimal function, thus making the optimisation process much simpler. Thus for designing IPPF-2 we are going to use the predictor (3.4) with $M(k) = 2$. In this case ($M(k) = 2$) the predictor (3.4) can be written as:

$$\tilde{h}_2(\mathbf{q}_{k+1}) = \nu_{k+1}\sqrt{1 - \frac{r_{k-1,k+1}^2 + r_{k,k+1}^2 - 2r_{k-1,k}r_{k,k+1}r_{k-1,k+1}}{1 - r_{k-1,k}^2}}$$

$$
\begin{aligned}
&+ \quad h(\mathbf{q}_k)\left(\frac{r_{k,k+1}-r_{k-1,k}r_{k-1,k+1}}{1-r_{k-1,k}^2}\right)\\
&+ \quad h(\mathbf{q}_{k-1})\left(\frac{r_{k-1,k+1}-r_{k-1,k}r_{k,k+1}}{1-r_{k-1,k}^2}\right)
\end{aligned}
\tag{3.48}
$$

where $\nu_{k+1} \sim \mathcal{CN}(0,1)$ and it is not difficult to see that $\tilde{h}_2(\mathbf{q}_{k+1})$ is a complex Gaussian random variable with mean:

$$
\begin{aligned}
\mu \quad &= \quad h(\mathbf{q}_k)\left(\frac{r_{k,k+1}-r_{k-1,k}r_{k-1,k+1}}{1-r_{k-1,k}^2}\right)\\
&+ \quad h(\mathbf{q}_{k-1})\left(\frac{r_{k-1,k+1}-r_{k-1,k}r_{k,k+1}}{1-r_{k-1,k}^2}\right),
\end{aligned}
\tag{3.49}
$$

and variance:

$$
\sigma^2 = 1 - \frac{r_{k-1,k+1}^2 + r_{k,k+1}^2 - 2r_{k-1,k}r_{k,k+1}r_{k-1,k+1}}{1-r_{k-1,k}^2} \tag{3.50}
$$

where $r_{k,j} = r(\mathbf{q}_k, \mathbf{q}_j)$ (for notational simplicity) and we will use interchangeably both terms in the rest of the chapter.

The fact that $\tilde{h}_2(\mathbf{q}_{k+1})$ is complex Gaussian distributed with such a mean and variance implies that $|\tilde{h}_2(\mathbf{q}_{k+1})|$ is Rician distributed with its two first moments given by:

$$
\mathbb{E}\left[|\tilde{h}_2(\mathbf{q}_{k+1})|\right] = \left(\frac{\sigma\sqrt{\pi}}{2}\right) e^{\frac{-|\mu|^2}{2\sigma^2}} \left[\left(1+\frac{|\mu|^2}{\sigma^2}\right) I_0\left(\frac{|\mu|^2}{2\sigma^2}\right) + \left(\frac{|\mu|^2}{\sigma^2}\right) I_1\left(\frac{|\mu|^2}{2\sigma^2}\right)\right], \tag{3.51}
$$

and:

$$
\mathbb{E}\left[|\tilde{h}_2(\mathbf{q}_{k+1})|^2\right] = \sigma^2 + |\mu|^2. \tag{3.52}
$$

Where $I_j(\cdot)$ is the modified Bessel functions of the first kind and order ith. As mentioned previously, to design the IPPF-2 we need to construct a optimization target that takes into account both the optimum channel gain obtained and the mechanical energy used. There is no analytical expression for the expected value of the optimum channel gain obtained but we can indirectly take it into account in the optimization target by using either (3.51) or (3.52). For the second term we can use $\|\mathbf{q}_{k+1} - \mathbf{q}_k\|_2$, which corresponds to the mechanical energy normalized by $\mathcal{K}(T)$ that will be used in moving from $\mathbf{q}_k$ to $\mathbf{q}_{k+1}$. So, one way to calculate $\mathbf{q}_{k+1}$ by optimising the IPPF-2 at $\mathbf{Q}_2(k)$ and $\hat{H}_2(k)$ is to solve:

$$
\begin{aligned}
&\max_{\mathbf{q}_{k+1}} \theta\mathbb{E}\left[|\tilde{h}_2(\mathbf{q}_{k+1})|^n\right] - (1-\theta)\|\mathbf{q}_{k+1} - \mathbf{q}_k\|_2\\
&\text{s.t.}\\
&(-1)^k \mathbf{o}_k^T\left(\mathbf{q}_{k+1} - \mathbf{q}_k\right) \geq 0\\
&\mathbf{o}_k = [-(y_{\mathbf{q}}(k) - y_{\mathbf{q}}(k-1)), \quad x_{\mathbf{q}}(k) - x_{\mathbf{q}}(k-1)]
\end{aligned}
\tag{3.53}
$$

where $x_{\mathbf{q}}(k)$ and $y_{\mathbf{q}}(k)$ are the x and y components of the point $\mathbf{q}_k$ and $n = 1, 2$ is a design parameter. Note that vector $\mathbf{o}_k$ is an orthogonal vector to $\mathbf{q}_k - \mathbf{q}_{k-1}$, see Fig.3.2. The optimization target of this optimization problem is symmetric with respect to the vector $\mathbf{q}_k - \mathbf{q}_{k-1}$ meaning that if the optimization target is evaluated at a particular $\mathbf{q}_{k+1}$ and also at its mirrored image respect to $\mathbf{q}_k - \mathbf{q}_{k-1}$ then the optimization target will produce the same value in both cases. Thus, we can restrict[4] the search space to one semi-plane[5] without eliminating any possible solution. This is done by the inequality restriction. The vector $\mathbf{o}_k$ defined in the second restriction (in (3.53)) is orthogonal to $\mathbf{q}_k - \mathbf{q}_{k-1}$ and the first restriction ensures that all the points $\mathbf{q}_{k+1}$ are situated in the correct semi-plane with respect to $\mathbf{q}_k - \mathbf{q}_{k-1}$. The term $(-1)^k$ in the second restriction produces a semi-plane "alternation". In other words if at the time instant t_k the search space is in the left semi-plane then when invoked again at t_{k+1} the search space is in the right semi-plane. This semi-plane alternation avoids the MR following an inwards spiral-like trajectory that clusters the stopping points, increases the correlation between the wireless channels and so reduces $\mathbb{E}[|h(\mathbf{q_{opt}})|]$ as we will show in section 3.6. Through experimentation we

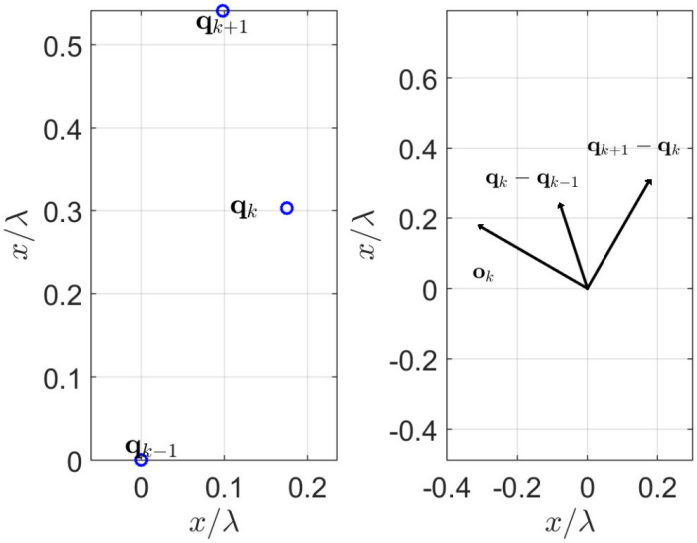

Figure 3.2: On the left we observe an example of the configuration for the stopping points $\{\mathbf{q}_j\}_{k-1}^{k+1}$ and on the right we observe their corresponding vectors $\mathbf{o}_k$, $\mathbf{q}_{k+1} - \mathbf{q}_k$ and $\mathbf{q}_k - \mathbf{q}_{k-1}$ which are considered in the optimization problem (3.53).

found that if we replace the term $\mathbb{E}\left[|\tilde{h}_2(\mathbf{p}(t_{i+1}))|^2\right]$ in the optimization target of

[4]This restriction makes smaller the searching space and so helps to accelerate the optimization process.

[5]Defined with respect to vector $\mathbf{q}_k - \mathbf{q}_{k-1}$.

(3.53) with $\mathbb{E}\left[|\tilde{h}_2(\mathbf{q}_{k+1})|^2\right]+\sigma^2 = 2\sigma^2+|\mu|^2$ then we obtain an IPPF-2 that performs significantly better in terms of $\mathbb{E}[|h(\mathbf{q_{opt}})|]$ as we shall see later in the section 3.6. This change produces:

$$\begin{array}{l} \max\limits_{\mathbf{q}_{k+1}} \theta\left(2\sigma^2+|\mu|^2\right)-(1-\theta)\|\mathbf{q}_{k+1}-\mathbf{q}_k\|_2 \\ \text{s.t.} \\ (-1)^k\mathbf{o}_k^T\left(\mathbf{q}_{k+1}-\mathbf{q}_k\right)\geq 0 \\ \mathbf{o}_k=[-(y_{\mathbf{q}}(k)-y_{\mathbf{q}}(k-1)),\quad x_{\mathbf{q}}(k)-x_{\mathbf{q}}(k-1)]. \end{array} \tag{3.54}$$

Although calculating $\mathbf{q}_{k+1}$ by optimizing online either (3.53) or (3.54) is computationally cheaper than doing it offline it still remains expensive for a MR with low computational capabilities. Thus a different approach which is computationally cheaper is desirable for these types of MRs. This approach can be derived from the superposition of the distance function (3.12) used in the IPPF-1. This produces a rule based path planner with memory order two (RBPPM-2).

Now, we present the RBPPM-2. We first assume that $\mathbf{q}_2$ is calculated using the IPPF-1 and so either $\|\mathbf{q}_2-\mathbf{q}_1\|_2=d$ or $\|\mathbf{q}_2-\mathbf{q}_1\|_2=D$. The RBPPM-2 is described by the following set of rules:

1. If $|h(\mathbf{q}_k)|<\eta$ and $|h(\mathbf{q}_{k-1})|<\eta$ then $\mathbf{q}_{k+1}$ must be chosen so that $r_{k,k+1}$ and $r_{k-1,k+1}$ are small. To achieve this we need $\|\mathbf{q}_{k+1}-\mathbf{q}_k\|_2=\|\mathbf{q}_{k+1}-\mathbf{q}_{k-1}\|_2=D$. There will be two solutions: one to the left of the vector $\mathbf{q}_k-\mathbf{q}_{k-1}$ and one to its right. We choose the left side solution if k is odd and the right side solution otherwise.

2. If $|h(\mathbf{q}_k)|\geq\eta$ and $|h(\mathbf{q}_{k-1})|<\eta$ then $\mathbf{q}_{k+1}$ must be chosen so that $r_{k,k+1}$ is large but $r_{k-1,k+1}$ is small. To do this we need $\|\mathbf{q}_{k+1}-\mathbf{q}_k\|_2=d$ and $\|\mathbf{q}_{k+1}-\mathbf{q}_{k-1}\|_2=D$, with $d<D$. There will be two solutions: one to the left of the vector $\mathbf{q}_k-\mathbf{q}_{k-1}$ and one to its right. We choose the left side solution if k is odd and the right side solution otherwise.

3. If $|h(\mathbf{q}_k)|\geq\eta$ and $|h(\mathbf{q}_{k-1})|\geq\eta$ then $\mathbf{q}_{k+1}$ must be chosen so that $r_{k,k+1}$ and $r_{k-1,k+1}$ are large. To do it we need $\|\mathbf{q}_{k+1}-\mathbf{q}_k\|_2=\|\mathbf{q}_{k+1}-\mathbf{q}_{k-1}\|_2=d$. There will be two solutions: one to the left of the vector $\mathbf{q}_k-\mathbf{q}_{k-1}$ and one to its right. We choose the left side solution if k is odd and the right side solution otherwise.

4. If $|h(\mathbf{q}_k)|<\eta$ and $|h(\mathbf{q}_{k-1})|\geq\eta$ then $\mathbf{q}_{k+1}$ must be chosen so that $r_{k,k+1}$ is small but $r_{k-1,k+1}$ is larger. This is achieved by $\|\mathbf{q}_{k+1}-\mathbf{q}_k\|_2=D$ and $\|\mathbf{q}_{k+1}-\mathbf{q}_{k-1}\|_2=D-d$.

We have to highlight that if $\|\mathbf{q}_2-\mathbf{q}_1\|_2=d$ or $\|\mathbf{q}_2-\mathbf{q}_1\|_2=D$ then this set of four rules is complete. This means that we can calculate all the future stopping points $\mathbf{q}_k$ with $k=3,4,...$ using only the four rules already presented. This is because under

the conditions mentioned above this set of rules considers all the possible scenarios and so at any time instant t_k we will have $\|\mathbf{q}_k - \mathbf{q}_{k-1}\|_2 = d$ or $\|\mathbf{q}_k - \mathbf{q}_{k-1}\|_2 = D$ and consequently we will always be able to calculate $\mathbf{q}_{k+1}$ using one of the four rules composing the RBPPM-2.

We have already shown how to obtain path planners with memory order one and two. So, in the next section we show how to derive path planners with an arbitrary memory order.

3.5 Path Planners with Arbitrary Memory Order

To do develop path planners with arbitrary memory order, we first note that according to (3.4) the prediction model $\tilde{h}_{M(k)}(\mathbf{q}_{k+1})$ is a complex Gaussian random variable with mean:

$$\mu_{M(k)} = \mathbf{p}_{M(k)+1,1:M(k)}(k+1, M(k)+1)\mathbf{P}^{-1}(k, M(k))\hat{\mathbf{H}}_{M(k)}(k), \tag{3.55}$$

and variance:

$$\sigma^2_{M(k)} = p^2_{M(k)+1,M(k)+1}(k+1, M(k)+1), \tag{3.56}$$

where $\mathbf{p}_{M(k)+1,1:M(k)}(k+1, M(k)+1)$ is a vector containing the first $M(k)$ entries of the last row of the matrix $\mathbf{P}(k+1, M(k)+1)$ and $p_{M(k)+1,M(k)+1}(k+1, M(k)+1)$ is the last entry of the the last row of the same matrix $\mathbf{P}(k+1, M(k)+1)$. Since $\tilde{h}_{M(k)}(\mathbf{q}_{k+1})$ is a complex Gaussian random variable then first two moments of its modulus are:

$$\begin{aligned}\mathbb{E}\left[|\tilde{h}_{M(k)}(\mathbf{q}_{k+1})|\right] &= \left(1 + \frac{|\mu_{M(k)}|^2}{\sigma^2_{M(k)}}\right) I_0\left(\frac{|\mu_{M(k)}|^2}{2\sigma^2_{M(k)}}\right)\left(\frac{\sigma_{M(k)}\sqrt{\pi}}{2}\right) e^{\frac{-|\mu_{M(k)}|^2}{2\sigma^2_{M(k)}}} \\ &+ \left(\frac{|\mu_{M(k)}|^2}{\sigma^2_{M(k)}}\right) I_1\left(\frac{|\mu_{M(k)}|^2}{2\sigma^2_{M(k)}}\right)\left(\frac{\sigma_{M(k)}\sqrt{\pi}}{2}\right) e^{\frac{-|\mu_{M(k)}|^2}{2\sigma^2_{M(k)}}}\end{aligned} \tag{3.57}$$

$$\mathbb{E}\left[|\tilde{h}_{M(k)}(\mathbf{q}_{k+1})|^2\right] = \sigma^2_{M(k)} + |\mu_{M(k)}|^2. \tag{3.58}$$

It is interesting to note (compare (3.57) and (3.58) with (3.51) and (3.52)) that the first two moments of the channel predictor of order $M(k)$ ($|\tilde{h}_{M(k)}(\mathbf{q}_{k+1})|$) have the same form as the two first moments of the channel predictor of order 2 ($|\tilde{h}_2(\mathbf{q}_{k+1})|$). The only differences are that $\mu_M \neq \mu$ and $\sigma^2_M \neq \sigma^2$, see (3.49), (3.50), (3.55) and (3.56). Therefore, we can use this similarity to extend the IPPF-2 to derive the IPPF-$M(k)$ with an arbitrary memory order $M(k)$ using the same approach. So we can optimize the IPPF-$M(k)$ at $\mathbf{Q}_{M(k)}(k)$ and $\hat{H}_{M(k)}(k)$ by solving:

$$\begin{aligned}&\max_{\mathbf{q}_{k+1}} \left\{\theta\mathbb{E}\left[|\tilde{h}_{M(k)}(\mathbf{q}_{k+1})|^n\right] - (1-\theta)\|\mathbf{q}_{k+1} - \mathbf{q}_k\|_2\right\} \\ &\text{s.t.} \\ &2 < M(k) \leq k, \quad n = 1, 2\end{aligned} \tag{3.59}$$

where $\theta \in [0,1]$, n and $M(k)$ are design parameters. Regarding the memory order parameter $M(k)$ we must mention that to use the IPPF-$M(k)$ with full memory order we must choose $M(k) = k$ and so the memory order of the path planner increases at each iteration. Now, similar to (3.53) if this optimization problem is solved online rather than off-line it becomes easier to solve. But as opposed to (3.53) the optimization target of (3.59) has no symmetries and so we do not reduce the search space in the same way. Another difference with (3.53) is that the optimization target is computationally more expensive to evaluate[6] but as we shall see in section 3.6 its performance is significantly better.

3.6 Simulations

In the simulations, we selected the same robot parameters as in last chapter which describe a real robot. We consider the channel estimation error to have a variance $\sigma_e^2 = 0.05$ and we select a wavelength $\lambda = 14.02$cm, corresponding to a carrier frequency of 2.14GHz, and $T = 833.775$ms.

We will first test the path planners with memory order one and compare them with the memoryless path planners. To do so we will test different path planners on the MDMTA using the *Maximum Channel Gain Rule* as the selection rule and we will not use the thresholds. So we first consider the following MDAs:

1. MDA1(N): MDMTA with predetermined the stopping points which are uniformly distributed along a straight line and the distance between adjacent stopping points is $\|\mathbf{q}_i - \mathbf{q}_{i+1}\|_2 \approx 0.3827\lambda$.

2. MDA2(N): MDMTA with the IPPF-1 derived in section 3.2. The distance function is optimized by solving off-line (3.13) for $N = 2$ with $\theta = 0.99$. In addition we select $\mathbf{v}_i = 0$ so the stopping points will lie into a straight line.

3. MDA3(N): Similar to MDA2(N) but the direction vectors $\mathbf{v}_i$ are optimized for each different number of stopping points variable N and according to (3.14) with $\theta = 0.9$.

In addition, for reference purposes we plot the upper bound for $\mathbb{E}[|h(\mathbf{q}_{opt})|^2]$ when the stopping points are predetermined. This upper bound is reached when all the N wireless channels considered are independent. Note that this upper bound also represents the upper bounds for selection combining systems.

First of all, the most striking aspect that we observe in Fig. 3.3 is that the MDA's using the IPPF-1 surpass the upper bounds for $\mathbb{E}[|h(\mathbf{q}_{opt})|^2]$ when all the channels

[6]Because the optimization target of IPPF-$M(k)$ depends on $\mu_{M(k)}$, see (3.55), and to calculate this term we first need to calculate the correlation matrix $\mathbf{C}(k, M(k))$ (see section 3.1), then we need to perform its Cholesky decomposition to obtain the matrix $\mathbf{P}(k, M(k))$ and finally we need to invert this matrix.

are independent. This shows that contrary to what has been widely accepted in the wireless communications literature, the expected value of the maximum gain of N wireless channels is not maximized when all those channels are independent. This result matches our analysis of the MDA2(2) in section 3.3.2.

From Figs. 3.3-3.4 we observe that the MDA2(N) outperforms the MDA1(N) (which uses predetermined stopping points arranged along a straight line) in terms of both $\mathbb{E}[|h(\mathbf{q}_{opt})|^2]$ and the mechanical energy used. Now, the MDA3(N) also uses an IPPF-1 with the same distance function as the MDA2(N) but instead of moving in a straight line it optimizes the direction vectors (see (3.14)) and therefore reduces the distance traveled during the *selection phase*. As we can observe in the figures, in terms of $\mathbb{E}[|h(\mathbf{q}_{opt})|^2]$ both the MDA2(N) and the MDA3(N) have practically the same performance but the MDA3(N) uses significantly less mechanical energy due to the reduction in the distance traveled during the *selection phase*. Now, we observe that for the special case of $N = 3$ stopping points MDA3(N) produces higher $\mathbb{E}[|h(\mathbf{q}_{opt})|^2]$ than MDA2(N). This is because the optimal angle of the direction vectors for this particular case is around 120 degrees and so in some cases the resultant geometries match the adaptive geometries that would be produced by a path planner with memory order two. Therefore, in this particular case for $N = 3$, the IPPF-1 used by the MDA3(N) acts as an approximation for an IPPF-2 and this is why MDA3(3) produces better $\mathbb{E}[|h(\mathbf{q}_{opt})|^2]$ than MDA2(3).

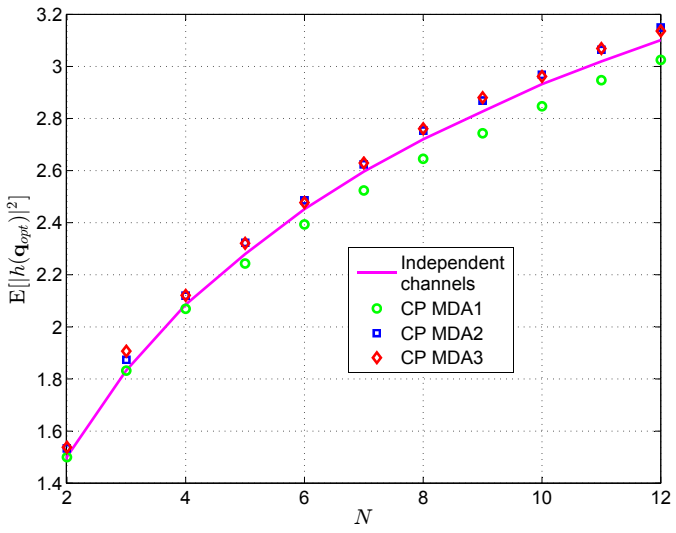

Figure 3.3: $\mathbb{E}[|h(\mathbf{q}_{opt})|^2]$ obtained by the MDAs as a function of the number (N) of stopping points.

Now, to evaluate the performance of the path planners with memory order two we consider the following variations of the MDMTA which again use the *Maximum Channel Gain Rule* as the selection rule and do not use the thresholds:

1. MDA4(N): MDMTA with an IPPF-2. The IPPF-2 is obtained by solving

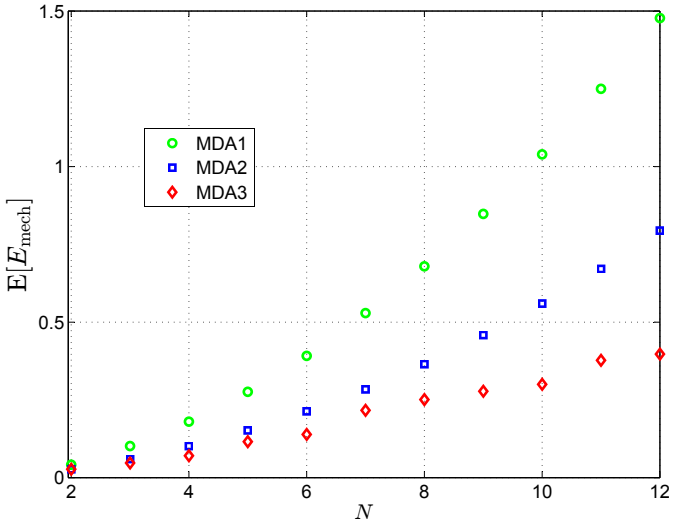

Figure 3.4: $\mathbb{E}[E_m(t_1, t_{N+1}, \mathbf{u}(t))]$ for different MDAs as a function of the number (N) of stopping points.

online (3.53) with $\theta = 0.99$ and $n = 1$.

2. MDA5(N): Similar to MDA4(N) but with $n = 2$.

3. MDA6(N): Similar to MDA5(N) but without the 'semi-plane alternation' mechanism mentioned in section 3.4.

4. MDA7(N): MDMTA with an IPPF-2. The IPPF-2 is obtained by solving online (3.54) with $\theta = 0.99$.

5. MDA8(N): MDMTA with an IPPF-2. The IPPF-2 chosen is the RBPPM-2 whose parameter values (d, D and α) are the same as the ones used for the MDA3(N).

Note that IPPF-2s require two stopping points to start working so in order to calculate the second stopping point in the MDAs 4-8 we use the IPPF-1 used in the MDA3(N) and to calculate the remaining stopping points we will use the corresponding IPPF-2.

We observe first in Figs. 3.5-3.6 that they can outperform the MDAs using IPPF-1. The MDA4(N) uses an IPPF-2 that at time instant t_k maximizes $\mathbb{E}[|\tilde{h}(\mathbf{p}(t_{k+1}))|]$. We observe that $N = 3$ produces approximately the same $\mathbb{E}[|h(\mathbf{q}_{opt})|^2]$ as MDA1(3) while using less mechanical energy but then for $N > 3$ it produces lower $\mathbb{E}[|h(\mathbf{q}_{opt})|^2]$ than the simpler MDA1(N) which uses a memoryless path planner. Now, the MDA5(N) uses a similar IPPF but instead of maximizing $\mathbb{E}[|\tilde{h}(\mathbf{p}(t_{k+1}))|]$ it maximizes $\mathbb{E}[|\tilde{h}(\mathbf{p}(t_{k+1}))|^2]$. This small difference has a significant impact on the performance and as we can see in Figs. 3.5-3.6 the MDA5(N) produces higher channel

power than the MDA4(N). In addition, for a small number of stopping points it also outperforms the MDAs using the IPPF-1 in terms of $\mathbb{E}[|h(\mathbf{q}_{opt})|^2]$ as well as in terms of the mechanical energy used. But then for $N > 6$ its performance in terms of $\mathbb{E}[|h(\mathbf{q}_{opt})|^2]$ becomes smaller than the MDAs using the IPPF-1 and even smaller than the MDA1(N). Now, the only difference between the MDA5(N) and MDA6(N) is that the MDA6(N) does not use the 'semi-plane alternation' mechanism mentioned in section 3.4. In Fig. 3.5 we observe that the lack of this 'semi-plane alternation' mechanism reduces the performance in terms of $\mathbb{E}[|h(\mathbf{q}_{opt})|^2]$ and also makes the MR consume slightly more mechanical energy, see Fig. 3.6. This is because the lack of 'semi-plane alternation' mechanism generates an inwards spiral-like trajectory that increases the correlation among the channels and therefore reduces $\mathbb{E}[|h(\mathbf{q}_{opt})|^2]$. This shows the benefits of introducing the 'semi-plane alternation' mechanism into the IPPF-2.

As we mentioned, MDA4(N) uses an IPPF-2 that maximizes the gain of the channel predictor while MDA5(N) uses an IPPF-2 that maximizes the power of the channel predictor but MDA7(N) uses an IPPF-2 that maximizes a optimization target slightly differently, see (3.54), that does not have a physical interpretation. Nevertheless we can observe in Fig. 3.5 that in terms of channel power it outperforms all the previously considered MDAs and in terms of the mechanical energy it uses less energy than the MDAs using the IPPF-1. This suggests that we might find more cost functions for (3.54) that do not necessarily have a physical interpretation but produce better results.

Now, to finish with the analysis of the IPPF-2s we consider the MDA8(N) which uses the RBPPM-2. As we can observe from Figs. 3.5-3.6 the MDA8(N) has a good performance in terms of both $\mathbb{E}[|h(\mathbf{q}_{opt})|^2]$ and the mechanical energy used. For a higher number of stopping points it produces a slightly lower $\mathbb{E}[|h(\mathbf{q}_{opt})|^2]$ than the MDAs using the IPPF-1 but uses considerably less mechanical energy. Now, the MDA8(N) is only outperformed in both aspects by the MDA7(N). Nevertheless the MDA8(N) uses a rule based IPPF-2 which does not require any complex calculation during the MDA execution while the MDA7(N) uses an IPPF which requires solving an optimization problem at each stopping point thus making it computationally more expensive.

To finish our analysis we will consider MDAs using path planners with arbitrary memory order:

1. MDA9(N): MDMTA with IPPF-$M(k)$ obtained by solving online at time instant t_k (3.59) with $\theta = 0.99$, $n = 1$ and $M(k) = k - 1$.

2. MDA10(N): Similar to MDA9(N) but with $n = 2$.

As we can observe in Figs. 3.7-3.8 the MDA9(N) and MDA10(N) outperform significantly all the previous MDAs in terms of $\mathbb{E}[|h(\mathbf{q}_{opt})|^2]$ as well as in terms of the mechanical energy used. By comparing these MDAs with those using an IPPF-2 or an IPPF-1 we note that in general an IPPF with higher memory can have better

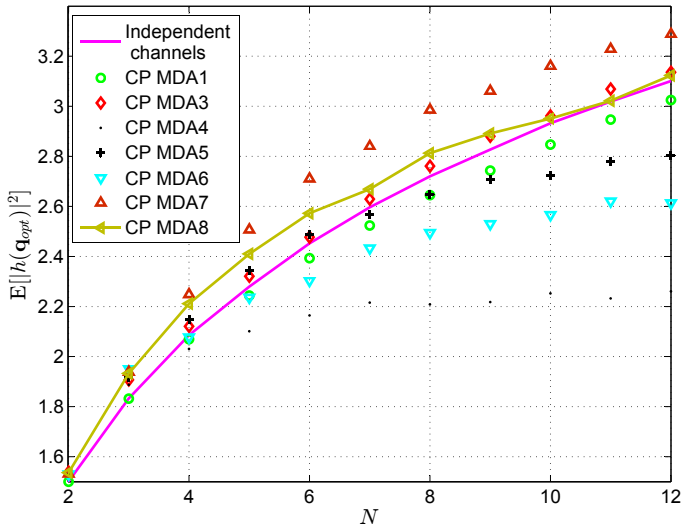

Figure 3.5: $\mathbb{E}[|h(\mathbf{q}_{opt})|^2]$ obtained by the MDAs as a function of the number (N) of stopping points.

performance. We also note that MDA10(N) performs better than MDA9(N). It is interesting to note that the IPPFs that maximize the power of the channel predictor perform better than those which optimize the gain of the channel predictor – compare MDA9(N) with MDA10(N) and MDA4(N) with MDA5(N).

So in summary, we have shown that MRs executing MDAs with adaptive path planners can achieve significantly higher wireless channel gain while using considerably less mechanical energy when compared to the case when they use predetermined stopping points.

3.7 Conclusions

One of the main contributions of this chapter is the fact that we demonstrated that the expected value of the maximum channel gain of N channels is not maximized when all the N channels are independent. From a theoretical point of view for the communications community this is an important result and in our context it implies that MDAs using path planners with memory can outperform MDAs using predetermined stopping points in terms of $\mathbb{E}[|h(\mathbf{q}_{opt})|^2]$.

Another important contribution of this chapter is the derivation of the path planners with memory using channel predictors. We solved this problem for any memory order. We also showed that when using path planners with memory there are properties of the channel that change with respect to the case in which predetermined stopping points are used. Specifically the channels at all the stopping points are no longer identically distributed. Also as mentioned above the fact that the when using these path planners with memory we can obtain higher values of $\mathbb{E}[|h(\mathbf{q}_{opt})|^2]$ than

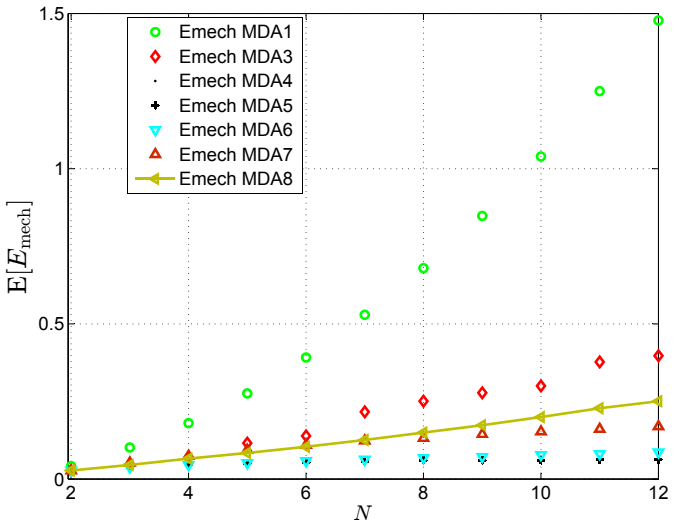

Figure 3.6: $\mathbb{E}[E_m\,(t_1, t_{N+1}, \mathbf{u}(t))]$ for different MDAs as a function of the number (N) of stopping points.

when we use predetermined stopping points. Therefore, these properties confirm that from a mathematical perspective MDAs are not equivalent to selection combining and they are indeed a new kind of diversity techniques.

For completeness we showed how the path planner fits into the MDMTA derived in the previous chapter and we showed that the predetermined stopping points considered in the previous chapter can be seen as a path planner with zero memory order. We also showed how to construct systematically path planners with any level of memory using the channel predictors. Also, as expected it was shown through simulations that MDAs using path planners with higher memory order can perform better than MDAs with lower levels of memory both in terms of $\mathbb{E}[|h(\mathbf{q}_{opt})|^2]$ and in terms of mechanical energy obtained.

Now, after observing these results we could say that path planners with memory are superior to predetermined stopping points. Nevertheless we have to take into account that as mentioned at the beginning of the chapter the path planners with memory require knowledge of the shadowing term in order to isolate the small-scale fading term. So when the MR does not have an estimate of the shadowing term it can only use predetermined stopping points. In addition, although path planners with memory can produce higher channel gains and can reduce the amount of mechanical energy used in the MDA execution, it is computationally more expensive than using predetermined stopping points.

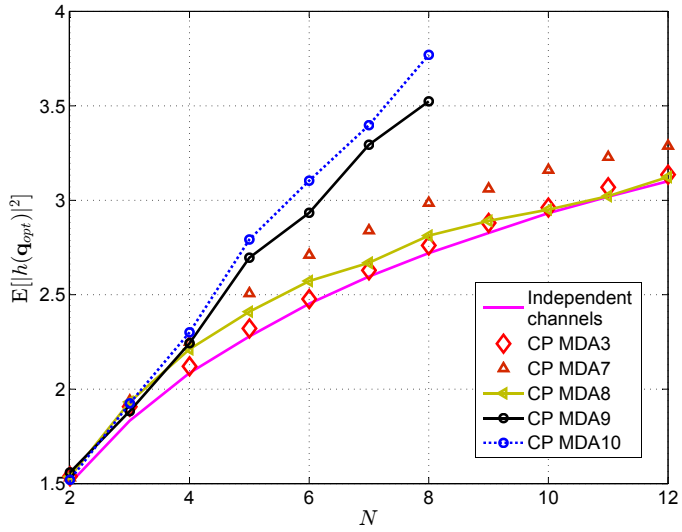

Figure 3.7: $\mathbb{E}[|h(\mathbf{q}_{opt})|^2]$ obtained by the MDAs as a function of the number (N) of stopping points.

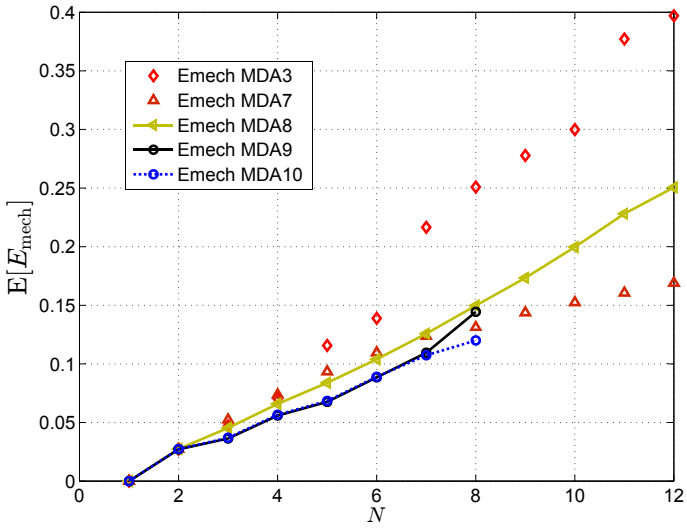

Figure 3.8: $\mathbb{E}[E_m\left(t_1, t_{N+1}, \mathbf{u}(t)\right)]$ for different MDAs as a function of the number (N) of stopping points.

Chapter 4

Multiple-links MDAs

In chapters 2 and 3 we addressed the problem of MDAs with discrete search spaces in order to compensate the small-scale fading in a single wireless link between a MR and a stationary node which may be another MR or a base station. We will refer to this kind of MDA as a single-link MDAs. Consider a robotic wireless network experiencing small-scale fading and assume we want to improve the performance of the network by compensating the small-scale fading using a single-link MDA. In general each node of the network has to communicate with more than one node (not necessarily simultaneously). In other words, each node is part of more than one wireless link. As a consequence, compensating the small-scale fading in all the wireless links of the network using single-link MDAs may be a complicated process. Therefore, in this chapter we develop MDAs that can compensate small-scale fading at multiple-links simultaneously to be used in robotic wireless networks scenarios. To do this we depart from our previous work on single-link MDAs with discrete search spaces and extend it to develop the multiple-link MDAs with discrete search spaces.

The main contributions of this chapter are the general structure of the multiple-link MDA, double-link path planners with arbitrary memory order for the double-link MDAs and also a multiple-link path planner with arbitrary memory order for multiple-link MDAs.

This multiple-link MDAs can useful in wireless robotic networks operating in environments which present small-scale fading. In this scenario some MRs may need to establish communication with more than one MR at the same time via wireless channel experiencing small-scale fading. Although, the MRs could use single-link MDAs to compensate for the fading at each wireless link separately this could take more time than using multiple-link MDAs to compensate simultaneously the small-scale fading at various wireless channels. Therefore, multiple-link MDAs could be beneficial in such multi-agent scenarios.

In section 4.1 we start by re-stating the wireless channel model notation in order to make it more convenient for the multiple-link MDAs. Then in section 4.2 we present the general structure of the multiple-link MDA for discrete search spaces. In section 4.3 we design a double-link MDA to be used by an amplify-and-forward

and robotic relay and in section 4.4 we design another double-link MDA but this time for a decode-and-forward robotic relay. Finally, in section 4.5 we show how we can extend the double-link path planner with memory order one developed in the previous sections for the double-link MDA in order to obtain first double-link path planners with arbitrary memory order and then multiple-link path planners with arbitrary memory order. Finally in 4.7 we briefly summarize the work presented in this chapter.

4.1 System Model

In this chapter we consider again the same channel model depicted in section 2.1.2 of chapter 2. We will rewrite the equations describing that model in a more suitable form for to handle the consideration of the small-scale fading at multiple wireless links simultaneously. In a robotic wireless network the signal received by the jth MR due to a transmission of the kth MR is given by:

$$y_{j,k}(t) = s(\mathbf{p}_k(t), \mathbf{p}_j(t))h(\mathbf{p}_k(t), \mathbf{p}_j(t))x_k(t) + n_j(t) \tag{4.1}$$

where $\mathbf{p}_j(t)$ and $\mathbf{p}_k(t)$ are the locations of the jth and the kth MRs; $x_k(t)$ is the narrowband signal transmitted by the kth MR; $n_j(t) \sim CN(0, \sigma^2_{n,j})$ is the additive white zero-mean Gaussian noise generated at the jth MR's receiver; $h(\mathbf{p}_k(t), \mathbf{p}_j(t))$ is the small-scale fading term in the (k-j) link (i.e., the link between the kth and jth MRs); and finally $s(\mathbf{p}_k(t), \mathbf{p}_j(t))$ is the shadowing term with $10\log_{10}(s(\mathbf{p}_k(t), \mathbf{p}_j(t))) \sim \mathcal{N}(0, \sigma^2_{s,k-j})$.

As in section 2.1.2 we assume again channel reciprocity as well as Jakes' model [28] for the small scale fading. Thus $h(\mathbf{p}_j(t), \mathbf{p}_k(t)) \sim \mathcal{CN}(0, 1)$ and its spatial normalized correlation is then given by:

$$\begin{aligned} C(\mathbf{o}, \mathbf{p}, \mathbf{o}, \mathbf{q}) &= \mathbb{E}[h(\mathbf{o}, \mathbf{p})h^*(\mathbf{o}, \mathbf{q})] \\ &= \mathbb{E}[h(\mathbf{p}, \mathbf{o})h^*(\mathbf{q}, \mathbf{o})] \\ &= J_0\left(\frac{2\pi\|\mathbf{p} - \mathbf{q}\|_2}{\lambda}\right) \end{aligned} \tag{4.2}$$

where λ is the wavelength used for the RF and $\mathbf{o}$, $\mathbf{p}$ and $\mathbf{q}$ are any three points in the space. For notational simplicity we will write in the rest of the chapter $s_{k,j}$ instead of $s(\mathbf{p}_k(t), \mathbf{p}_j(t))$ and also $h_{j,k}(\mathbf{p}_k(t))$ instead of $h(\mathbf{p}_k(t), \mathbf{p}_j(t))$ when $\mathbf{p}_j(t)$ remains constant. Also, for notational convenience we will write MR-j instead of jth MR.

4.2 Multiple-Link MDA Structure

In this section we describe the structure of the L-link MDMTA. We assume that this MDA is executed by the MR-0 to compensate simultaneously for the fading at

L wireless links with other L MRs. During the L-link MDMTA execution the MR-0 will explore N stopping points $(\mathbf{q}_1, \mathbf{q}_2, \cdots, \mathbf{q}_N)$ and it requires that all the remaining L MRs remain stationary during the algorithm execution. Before we continue let us define the fading vector as $\mathbf{h}^{(L)}(\mathbf{q}_k) = [h_{0,1}(\mathbf{q}_k),\ h_{0,2}(\mathbf{q}_k), \cdots,\ h_{0,L}(\mathbf{q}_k)]^T$ (where the superscript (L) refers to the fact that it contains L small-scale fading terms) and the shadowing matrix $S^{(L)} = \text{diag}[s_{0,1}, s_{0,2}, \cdots, s_{0,L}]$. We also define the following $M(k) \times L$ matrix:

$$\hat{\mathbf{H}}^{(L)}_{M(k)}(k) = [\mathbf{h}^{(L)}(\mathbf{q}_{k-M(k)+1}), \mathbf{h}^{(L)}(\mathbf{q}_{k-M(k)+2}), \cdots, \mathbf{h}^{(L)}(\mathbf{q}_k)]^T \tag{4.3}$$

where $M(k)$ is the memory order of the path planner used by the L-link MDMTA and, as in the previous chapter, the matrix $\mathbf{Q}_{M(k)}(k) = [\mathbf{q}_{k-M(k)+1},\ \mathbf{q}_{k-M(k)+2}, \cdots, \mathbf{q}_k]^T$ contains the last $M(k)$ visited stopping points.

The L-link MDMTA is divided into the 'exploration phase' and the 'selection phase'. During the 'exploration phase' ($t \in [t_1, t_N]$) the algorithm works as follows. The initial position $\mathbf{p}_0(t_1)$ is by definition the first stopping point, i.e., $\mathbf{q}_1$. Then at time instant t_k the MR-0 located at $\mathbf{q}_k$ (i.e., $\mathbf{p}_0(t_k) = \mathbf{q}_k$) calculates the estimate of the wireless channel (i.e., the product $S^{(L)}\mathbf{h}^{(L)}(\mathbf{q}_k)$) which will be denoted as $\hat{S}^{(L)}\hat{\mathbf{h}}^{(L)}(\mathbf{q}_k)$). Then the MR-0 evaluates a thresholding function $\mathcal{T}_{\mathcal{H}}\left(\hat{S}^{(L)}\hat{\mathbf{h}}^{(L)}(\mathbf{q}_k)\right)$ and if this function is greater than some value η_k then the MR-0 terminates the algorithm and establishes communication with the other L MRs. In this case, for notational coherence, we say that $\mathbf{q}_{opt} = \mathbf{q}_k$. On the other hand, if the thresholding function is lower than η_k then the MR-0 invokes the path planner of memory order $M(k)$ for L links in order to calculate the next stopping point $\mathbf{q}_{k+1}$ and then it moves to that point. Once the MR-0 reaches $\mathbf{q}_N$ it estimates the wireless channel at this last stopping point and so the 'exploration phase' ends while the 'selection phase' starts. Then the MR-0 invokes an L link 'selection rule' to determine the optimum stopping point $\mathbf{q}_{opt}$, moves to that point to establish communications with the other L robots and the L-link MDMTA terminates. In algorithm 4 we observe the details of the L-link MDMTA. Note that $\hat{S}^{(L)}$ is in brackets in the list of input parameters. This means that this input parameter is optional. Nevertheless, as in the single link case, if we are going to use path planners with memory we require this parameter. Otherwise we will only be able to use memoryless path planners.

After having presented the structure of the L-link MDMTA (referred to as the L-MDMTA for short) we will proceed to design its main components (i.e., the thresholding function $\mathcal{T}_{\mathcal{H}}$, the path planner $\mathbf{f}^{(L)}_{M(k)}(\cdot,\cdot,\cdot)$ and the selection rule $\mathcal{R}_s$)). We will start by designing a double-link MDMTA for two different applications. The first double-link MDMTA will be designed for an amplify-and-forward robotic relay while the second one will be designed for a decode-and-forward robotic relay. In both applications the robot executing the double-link MDMTA (i.e., the MR-0) will be referred to as the robotic relay (RR).

Algorithm 4 $L-MDMTA(N, M(k), \mathbf{f}^{(L)}_{M(k)}, \mathbf{t}, \boldsymbol{\eta}, \mathcal{R}_s, (\hat{S}^{(L)}))$

$\mathbf{p}_0(t_1) \leftarrow \mathbf{q}_1$
for $k = 1$ to $N-1$ **do**
  $\hat{S}^{(L)}\hat{\mathbf{h}}^{(L)}(\mathbf{q}_k) \leftarrow$ Estimate$[S^{(L)}\mathbf{h}^{(L)}(\mathbf{q}_k)]$ {Channel gain estimation .}
  if $\mathcal{T}_{\mathcal{H}}\left(\hat{S}^{(L)}\hat{\mathbf{h}}^{(L)}(\mathbf{q}_k)\right) \geq \eta_k$ **then**
    $\mathbf{q}_{opt} \leftarrow \mathbf{q}_k$
    Terminate Algorithm
  end if
  $\mathbf{q}_{k+1} = \mathbf{f}^{(L)}_{M(k)}\left(\mathbf{Q}_{M(k)}(k), \hat{\mathbf{H}}^{(L)}_{M(k)}(k), k\right)$ {The path planner is used to calculate the next stopping point.}
  $\mathbf{p}_0(t_{k+1}) \leftarrow \mathbf{q}_{k+1}$ {The MR moves to the next stopping point in $t_{k+1} - t_k$ seconds.}
end for
$\hat{S}^{(L)}\hat{\mathbf{h}}^{(L)}(\mathbf{q}_N) \leftarrow$ Estimate$[S^{(L)}\mathbf{h}^{(L)}(\mathbf{q}_N)]$
$\mathbf{q}_{opt} \leftarrow \mathcal{R}_s$ {A 'selection rule' is used to determine the optimum position.}
$\mathbf{p}_0(t_{N+1}) \leftarrow \mathbf{q}_{opt}$ {The MR moves to the optimum stopping point in $t_{N+1} - t_N$ seconds.}
Terminate Algorithm

4.3 Amplify-and-Forward Robotic Relay

In this section we customise the components of the double-link MDMTA for an amplify-and-forward robotic relay. In this case the RR receives a signal from MR-1, amplifies it by a factor β and then re-transmits it to MR-2. We also assume that $s_{2,1} \approx 0$ and so the signals received by RR and by the MR-2 are then:

$$y_{0,1}(t) = s_{0,1}h_{0,1}(\mathbf{p}_0(t))x_1(t) + n_0(t), \tag{4.4}$$

$$y_{2,0}(t) = s_{2,0}h_{2,0}(\mathbf{p}_0(t))\beta y_{0,1}(t) + n_2(t) \tag{4.5}$$

where $x_1(t)$ is the signal transmitted by the MR-1 and $\beta y_{0,1}(t)$ is the signal transmitted by the RR. For simplicity we will assume that all the MRs have the same type of receiver and so the power of the noise generated at each receiver is the same. So we have $\sigma^2_{n,0} = \sigma^2_{n,2} = \sigma^2_n$. We assume that both the MR-1 and the RR transmit using their maximum allowable average power (P_{max}) and so $\mathbb{E}[|x_1(t)|^2] = P_{max}$. So the amplification factor β in (4.5) becomes:

$$\beta^2 = \frac{P_{max}}{\sigma^2_n + s^2_{0,1}|h_{0,1}(\mathbf{q}_k)|^2 P_{max}}. \tag{4.6}$$

Substituting (4.4) and (4.6) into (4.5) we obtain:

$$y_{2,0}(t) = \left(\frac{h_{2,0}(\mathbf{p}_0(t))h_{0,1}(\mathbf{p}_0(t))s_{2,0}s_{0,1}\sqrt{P_{max}}}{\sqrt{\sigma^2_n + s^2_{0,1}|h_{0,1}(\mathbf{p}_0(t))|^2 P_{max}}}\right) x_1(t) \tag{4.7}$$

$$+ \quad \left(\frac{h_{2,0}(\mathbf{p}_0(t)) s_{2,0} \sqrt{P_{max}}}{\sqrt{\sigma_n^2 + s_{0,1}^2 |h_{0,1}(\mathbf{p}_0(t))|^2 P_{max}}} \right) n_0(t) + n_2(t).$$

Departing from (4.7) we start the customisation of the MDMTA components in the next subsections. We will first design the selection rule and then double-link path planner.

4.3.1 Selection Rule Design

The selection rule is invoked at time instant t_N when the RR is at $\mathbf{q}_N$ and it has already estimated the L wireless channels at all the N stopping points. It be shown from (4.7) that given the wireless channels at both links the SNR observerd by the MR-2's receiver, when the RR is located at $\mathbf{q}_k$, is given by:

$$\Gamma(\mathbf{q}_k) = \frac{\left(\frac{P_{max}}{\sigma_n^2}\right)^2 s_{2,0}^2 |h_{2,0}(\mathbf{q}_k)|^2 s_{0,1}^2 |h_{0,1}(\mathbf{q}_k)|^2}{\left(\frac{P_{max}}{\sigma_n^2}\right) (s_{2,0}^2 |h_{2,0}(\mathbf{q}_k)|^2 + s_{0,1}^2 |h_{0,1}(\mathbf{q}_k)|^2) + 1}. \tag{4.8}$$

The RR knows P_{max} and σ_n^2 which were used in the calculation for the amplification factor β (4.6). In addition, as mentioned above it also knows the wireless channels of both links at the N stopping points. Therefore the RR can calculate (4.8) for all the stopping points. In consequence the natural choice in this case for the selection rule is to select $\mathbf{q}_{opt}$ as the stopping point that maximises (4.8).

For the thresholding function $\mathcal{TH}$ we can also use (4.8) and so when one $\mathbf{q}_k$ stopping point presents an SNR higher than some value η_k the double-link MDMTA will terminate.

Note that to use this selection rule the RR only requires to know $s_{j,l}|h_{j,l}(\mathbf{q}_k)|$ but not $s_{j,l}$ and $|h_{j,l}(\mathbf{q}_k)|$ separately. In other words, to implement this selection rule the RR does not need to know the shadowing terms in order to isolate the small-scale fading terms. In the next subsection we will discuss the construction of the path planner.

4.3.2 Path Planner Design

Now we proceed to design a double-link path planner with memory order one for the amplify-and-forward RR. To do this we will follow a similar procedure as the one we used to develop the single-link path planner with memory order one developed in section (3.2). So, the general double-link path planner with memory order one has the following form:

$$\begin{aligned} \mathbf{f}_1^{(2)} \left(\mathbf{q}_k, \hat{\mathbf{h}}^{(2)}(\mathbf{q}_k), k \right) &= \mathbf{q}_k + d_1^{(2)} \left(\hat{\mathbf{h}}^{(2)}(\mathbf{q}_k) \right) \mathbf{v}_k, \quad k = 1, 2, \cdots, N-1 \\ \mathbf{v}(k) &= [\cos(\psi(k)) \quad \sin(\psi(k))]^T \end{aligned} \tag{4.9}$$

where $\psi(k)$ is the direction that the RR has to follow in order to move from $\mathbf{q}_k$ to $\mathbf{q}_{k+1}$ and $d_1^{(2)}\left(\hat{\mathbf{h}}^{(2)}(\mathbf{q}_k)\right)$ is a function that determines $\|\mathbf{q}_{k+1}-\mathbf{q}_k\|_2$ using $\hat{\mathbf{h}}^{(2)}(\mathbf{q}_k)$.

We will reasonably assume that $\|\mathbf{p}_1(t)-\mathbf{p}_2(t)\|_2 \gg \lambda$. In other words we assume that the distance between MR-1 and MR-2 is significantly greater than the distance of a wavelenght[1]. Thus, according to (4.2) we have $\mathbb{E}\left[\mathbf{h}_{2,0}(\mathbf{p}_0(t))\mathbf{h}_{0,1}^*(\mathbf{p}_0(t))\right] \approx 0$. In other words, for all practical purposes, the wireless channels from one link are independent of the wireless channel of the other link.

In the single-link case the distance function $d_1(h(\mathbf{q}_k))$ in (3.8) took a form that allowed us to improve the channel gain at the next stopping point $\mathbf{q}_{k+1}$. In the double-link case we can try to design $d_1^{(2)}\left(\hat{\mathbf{h}}^{(2)}(\mathbf{q}_k)\right)$ to maximise the SNR at the next stopping point but this is a complicated problem. A more practical and reasonable solution is to design the distance function to maximise the power of the signal received by the MR-2 and sent by the MR-1 while assuming the gain factor β constant. This problem is equivalent to finding the distance function that, at time instant t_k, maximises $s_{2,0}^2 s_{0,1}^2 \mathbb{E}[|h_{2,0}(\mathbf{q}_{k+1})|^2]\mathbb{E}[|h_{0,1}(\mathbf{q}_{k+1})|^2]$.

Since at time instant t_k the channels $h_{2,0}(\mathbf{q}_{k+1})$ and $h_{0,1}(\mathbf{q}_{k+1})$ are not known we can only maximise $s_{2,0}^2 s_{0,1}^2 \mathbb{E}[|\tilde{h}_{2,0,1}(\mathbf{q}_{k+1})|^2]\mathbb{E}[|\tilde{h}_{0,1,1}(\mathbf{q}_{k+1})|^2]$ where $\tilde{h}_{j,l,1}(\mathbf{q}_{k+1})$ is the predictor of memory order one for the channel $h_{j,l}(\mathbf{q}_{k+1})$.

Since the channels from one link are independent of the channels of the other link then we can use two separate single-link channel predictors as the ones used in (3) for the channel of each link and indirectly coupling them via the double-link distance function $d_1^{(2)}\left(\hat{\mathbf{h}}^{(2)}(\mathbf{q}_k)\right)$. Therefore the double-link channel predictor of memory order one $\mathbf{h}^{(2)}(\mathbf{q}_{k+1})$ can be written as:

$$\tilde{\mathbf{h}}_1^{(2)}(\mathbf{q}_{k+1}) = \boldsymbol{\nu}_{k+1}\sqrt{1-\rho^2\left(\hat{\mathbf{h}}^{(2)}(\mathbf{q}_k)\right)} + \hat{\mathbf{h}}^{(2)}(\mathbf{q}_k)\rho\left(\hat{\mathbf{h}}^{(2)}(\mathbf{q}_k)\right), \tag{4.10}$$

with:

$$\rho\left(\hat{\mathbf{h}}^{(2)}(\mathbf{q}_k)\right) = J_0\left(\frac{2\pi d_1^{(2)}\left(\hat{\mathbf{h}}^{(2)}(\mathbf{q}_k)\right)}{\lambda}\right), \tag{4.11}$$

where $\tilde{\mathbf{h}}_1^{(2)}(\mathbf{q}_{k+1}) = [\tilde{h}_{0,1,1}(\mathbf{q}_{k+1}) \quad \tilde{h}_{2,0,1}(\mathbf{q}_{k+1})]^T$, $\rho\left(\hat{\mathbf{h}}^{(2)}(\mathbf{q}_k)\right)$ represents the correlation between $h_{2,0}(\mathbf{q}_k)$ and $h_{2,0}(\mathbf{q}_{k+1})$ which is the same as the correlation between $h_{0,1}(\mathbf{q}_k)$ and $h_{0,1}(\mathbf{q}_{k+1})$. In addition $\boldsymbol{\nu}_{k+1} = [\nu_1(k+1) \quad \nu_2(k+1)]^T$ with $\nu 1(k+1), \nu 2(k+1), \sim \mathcal{CN}(0,1)$ and $\mathbb{E}[\boldsymbol{\nu}_{k+1}\ \boldsymbol{\nu}_{k+1}^H] = \mathbf{I}$. So, using the predictors (4.10) we have:

$$\mathbb{E}\left[|\tilde{h}_{2,0,1}(\mathbf{q}_{k+1})|^2\right]\mathbb{E}\left[|\tilde{h}_{0,1,1}(\mathbf{q}_{k+1})|^2\right] \quad = \quad (1+\rho^2\left(\hat{\mathbf{h}}^{(2)}(\mathbf{q}_k)\right)(|h_{2,0}(\mathbf{q}_k)|^2-1))$$

[1]This assumption is consistent with the fact that in this application MR-1 needs to use MR-0 as a relay in order to communicate with MR-2.

$$\times \quad (1+\rho^2\left(\hat{\mathbf{h}}^{(2)}(\mathbf{q}_k)\right)(|h_{0,1}(\mathbf{q}_k)|^2-1)). \tag{4.12}$$

We now maximise (4.12) with respect to the correlation factor $\rho\left(\hat{\mathbf{h}}^{(2)}(\mathbf{q}_k)\right)$ to give the optimum value:

$$\rho^*\left(\hat{\mathbf{h}}^{(2)}(\mathbf{q}_k)\right)=\begin{cases}0, & |h_{2,0}(\mathbf{q}_k)|^2+|h_{0,1}(\mathbf{q}_k)|^2<2\\ 1, & 2|h_{2,0}(\mathbf{q}_k)|^2|h_{0,1}(\mathbf{q}_k)|^2-|h_{2,0}(\mathbf{q}_k)|^2-|h_{0,1}(\mathbf{q}_k)|^2>0\\ \frac{2-|h_{2,0}(\mathbf{q}_k)|^2-|h_{0,1}(\mathbf{q}_k)|^2}{2(|h_{2,0}(\mathbf{q}_k)|^2-1)(|h_{0,1}(\mathbf{q}_k)|^2-1)}, & \text{otherwise.}\end{cases} \tag{4.13}$$

This equation defines three regions: In the first region the channel gain of both links is low and thus the optimal correlation factor $\rho^*\left(\hat{\mathbf{h}}^{(2)}(\mathbf{q}_k)\right)$ must be low (first line of (4.13)); in the second region the channel gain is high for both links and thus the optimal correlation factor must be high (second line of (4.13)); and finally in the third region either both links have moderate channel gains or one has a high channel gain while the other has low channel gain and in this case a moderate correlation factor is desirable (third line of (4.13)). Using this interpretation we can derive the optimum form of the distance function $d_1^{(2)}\left(\hat{\mathbf{h}}^{(2)}(\mathbf{q}_k)\right)$ which is then given by:

$$\begin{aligned} d_1^{(2)}\left(\hat{\mathbf{h}}^{(2)}(\mathbf{q}_k)\right) &= (d_s-d_m)\mathbf{1}_{\mathbf{R}^{+*}}\left(2|h_{2,0}(\mathbf{q}_k)|^2|h_{0,1}(\mathbf{q}_k)|^2-|h_{2,0}(\mathbf{q}_k)|^2-|h_{0,1}(\mathbf{q}_k)|^2\right)\\ &+ (d_m-d_b)\mathbf{1}_{\mathbf{R}^{+*}}\left(|h_{2,0}(\mathbf{q}_k)|^2+|h_{0,1}(\mathbf{q}_k)|^2-2\right)+d_b \end{aligned} \tag{4.14}$$

where $\mathbf{1}_{\mathbf{R}^{+*}}(\cdot)$ is the indicator function; and $d_b > d_m > d_s$ are design parameters that must be chosen so that when the distance function (4.14) is evaluated in (4.11) it produces low, moderate and high channel correlation according to the regions defined in (4.13).

Now that we have derived the optimum form of the distance function (4.14) we can optimise its parameters as well as the angles $\psi(k)$ in (4.9) in order to conclude with the optimisation of the double-link path planner for the amplify-and-forward RR. To do this we can follow a similar approach to the one used to optimise the parameters of the single-link path planner in section 3.2. That is, first we optimise the parameters d_b, d_m and d_s assuming $\psi(k)$ is constant and then we optimise $\psi(k)$ with the previously optimised d_b, d_m and d_s. For the first part optimisation problem (i.e., the optimisation of d_b, d_m and d_s) we can modify (3.9) by replacing $\mathbb{E}\left[|h(\mathbf{q}_{opt})|\right]$

with $\mathbb{E}\left[\max_{k=1,2,\cdots,N}|h_{2,0}(\mathbf{q}_k)h_{0,1}(\mathbf{q}_k)|^2\right]$. Thus the resulting optimisation problem is:

$$\begin{aligned}
&\max_{d_m,d_s,d_b}\theta\mathbb{E}\left[\max_{k=1,2,\cdots,N}|h_{2,0}(\mathbf{q}_k)h_{0,1}(\mathbf{q}_k)|^2\right]-(1-\theta)\mathbb{E}\left[\sum_{k=1}^{N}E_m\left(t_k,t_{k+1},\mathbf{u}_k^*(t)\right)\right]\\
&\text{s.t.}\\
&\mathbf{q}_{k+1}=\mathbf{q}_k+d_1^{(2)}\left(\hat{\mathbf{h}}^{(2)}(\mathbf{q}_k)\right)\mathbf{v}(k),\ k=1,2,\cdots,N-1\\
&\mathbf{v}(k)=[\cos(\psi(k))\quad\sin(\psi(k))]^T\\
&\psi(k)=\psi(1),\quad k=2,3\cdots,N-1\\
&d_s\le d_m\le d_b\le z_0,
\end{aligned}\tag{4.15}$$

where z_0 is the smallest value of the distance to make zero the correlation in (4.11). This is done to reduce the size of the optimisation space without eliminating any possible solution. The optimization target in (4.15) is a convex combination of the expected value of the maximum channel power gain from MR-1 to MR-2 via the RR $\mathbb{E}\left[\max_{k=1,2,\cdots,N}|h_{2,0}(\mathbf{q}_k)h_{0,1}(\mathbf{q}_k)|^2\right]$ and the negative of the average mechanical energy used by the RR during the MDA execution using the optimum control law presented in the previous chapters. This optimization target has the same form as (3.9). The design parameter $\theta\in[0,1]$ defines the importance of one term over the other.

Once we have optimised d_b, d_m and d_s we optimise the set of angles $\psi(k)$. The resulting optimisation problem is:

$$\begin{aligned}
&\max_{\psi}\theta\mathbb{E}\left[\max_{k=1,2,\cdots,N}|h_{2,0}(\mathbf{q}_k)h_{0,1}(\mathbf{q}_k)|^2\right]-(1-\theta)\mathbb{E}\left[\sum_{k=1}^{N}E_m\left(t_k,t_{k+1},\mathbf{u}_k^*(t)\right)\right]\\
&\text{s.t.}\\
&\mathbf{q}_{k+1}=\mathbf{q}_k+d_1^{(2)}\left(\hat{\mathbf{h}}^{(2)}(\mathbf{q}_k)\right)\mathbf{v}(k),\ k=1,2,\cdots,N-1\\
&\mathbf{v}(k)=[\cos(\psi(k))\quad\sin(\psi(k))]^T\\
&\psi(k+1)-\psi(k)=\psi\quad k=1,2,\cdots,N-2,
\end{aligned}\tag{4.16}$$

where the distance function uses the values of d_b, d_m and d_s optimised according to (4.16). Since there is no analytical expression for the optimization target in (4.16) we have to evaluate it by simulations which can increase significantly the computational load. To alleviate this problem and reduce the computational load we add the third constraint in (4.16) to reduce the dimensionality of the optimisation problem[2] just as it was done in the optimisation problem (3.14). Both (4.15) and (4.16) can be solved using simulated annealing.

With the optimisation of the double-link path planner we conclude the design of the double-link MDMTA for the amplify-and-forward RR. In the next section we design the double link MDMTA for the decode-and-forward RR.

[2]This reduction in the dimensionality of the problem will reduce the performance of the solution but it will also reduce the computational load and as a consequence it will make the problem more manageable.

4.4 Decode-and-Forward Relay

In this subsection the RR operates as a decode-and-forward relay. So, the RR decodes the signal transmitted by the MR-1 and then it forwards the decoded signal to the MR-2. Thus the signal received by RR and the MR-2 are respectively:

$$\begin{aligned} y_0(t) &= s_{0,1}h_{0,1}(\mathbf{p}_0(t))x_1(t) + n_0(t), \\ y_2(t) &= s_{2,0}h_{2,0}(\mathbf{p}_0(t))\bar{x}_1(t) + n_2(t), \end{aligned} \tag{4.17}$$

where $\bar{x}_1(t)$ is the decoded version of $x_1(t)$. We could try to devise the selection rule and the path planner to minimise the BER at MR-2 but this would be too complicated and it will also make the components of the MDMTA dependent on the modulation scheme selected. We can find an alternative approach if we note that in this application when one of the links has a low channel gain the resultant BER will be high independently if the other link has a high channel gain or not.

Therefore, a good choice for the selection rule is to select $\mathbf{q}_{opt}$ as the stopping point that maximises the minimum channel gain of both links:

$$m(\mathbf{q}_k) = \min\{s_{2,0}|h_{2,0}(\mathbf{q}_k)|, s_{0,1}|h_{0,1}(\mathbf{q}_k)|\}. \tag{4.18}$$

For the thresholding function $\mathcal{TH}$ we can also use (4.18) and so when one at some stopping point $\mathbf{q}_k$ we have $m(\mathbf{q}_k) > \eta_k$ the algorithm will terminate.

The double-link path planner for the decode-and-forward RR takes the form (4.9) but with the distance function $d_1^{(2)}\left(\hat{\mathbf{h}}^{(2)}(\mathbf{q}_k)\right)$ takes a particular form which we will now develop. But before continuing the design of the path planner let us first define the following random variable:

$$\tilde{m}_1(\mathbf{q}_k) = \min\{s_{2,0}|\tilde{h}_{2,0,1}(\mathbf{q}_k)|, s_{0,1}|\tilde{h}_{0,1,1}(\mathbf{q}_k)|\} \tag{4.19}$$

where $\tilde{h}_{2,0,1}(\mathbf{q}_k)$ and $\tilde{h}_{0,1,1}(\mathbf{q}_k)$ are the channel predictors of order one for $h_{2,0}(\mathbf{q}_k)$ and $h_{0,1}(\mathbf{q}_k)$ given by (4.10) and (4.11).

A reasonable and simple solution to derive the form of the path planner is to devise it to maximise the second moment[3] of $\tilde{m}_1(\mathbf{q}_{k+1})$ at time instant t_k. This moment is given by:

$$\mathbb{E}[\tilde{m}_1^2(k+1)] = \int_0^{+\infty} \left(1 - \Pr(\tilde{m}_1^2(k+1) \leq z)\right) dz, \tag{4.20}$$

with:

$$\begin{aligned} \Pr(\tilde{m}_1^2(k+1) \leq z) &= \Pr(s_{2,0}^2|\tilde{h}_{2,0,1}(\mathbf{q}_{k+1})|^2 \leq z) \\ &+ \Pr(s_{0,1}^2|\tilde{h}_{0,1,1}(\mathbf{q}_{k+1})|^2 \leq z) \\ &- \Pr(s_{2,0}^2|\tilde{h}_{2,0,1}(\mathbf{q}_{k+1})|^2 \leq z)\Pr(s_{0,1}^2|\tilde{h}_{0,1,1}(\mathbf{q}_{k+1})|^2 \leq z), \end{aligned} \tag{4.21}$$

[3]We choose the second moment because its analytical expression is easier to handle than the expression for the first moment.

and so:

$$\begin{aligned}\mathbb{E}[\tilde{m}_1^2(k+1)] &\leq \mathbb{E}[s_{2,0}^2|\tilde{h}_{2,0,1}(\mathbf{q}_{k+1})|^2] + \mathbb{E}[s_{0,1}^2|\tilde{h}_{0,1,1}(\mathbf{q}_{k+1})|^2] \\ &= s_{2,0}^2\left(1+\rho^2(\hat{\mathbf{h}}^{(2)}(\mathbf{q}_k))(|\hat{h}_{2,0}(\mathbf{q}_k)|^2-1)\right) \\ &+ s_{0,1}^2\left(1+\rho^2(\hat{\mathbf{h}}^{(2)}(\mathbf{q}_k))(|\hat{h}_{0,1}(\mathbf{q}_k)|^2-1)\right). \end{aligned} \tag{4.22}$$

Then we optimise the right hand term of (4.22) with respect to $\rho(\hat{\mathbf{h}}^{(2)}(\mathbf{q}_k))$ in order to derive the optimum form of the distance function for the path planner. It can be shown that the optimum $\rho(\hat{\mathbf{h}}^{(2)}(\mathbf{q}_k))$ that maximises the right hand term of (4.22) is

$$\rho^*\left(\hat{\mathbf{h}}^{(2)}(\mathbf{q}_k)\right) = \begin{cases} 0, & s_{0,1}^2(|\hat{h}_{0,1}(\mathbf{q}_k)|^2-1) + s_{2,0+1}^2(|\hat{h}_{2,0}(\mathbf{q}_k)|^2-1) < 0 \\ 1, & \text{otherwise.} \end{cases} \tag{4.23}$$

This equation defines two regions, one inside the ellipse $s_{0,1}^2(|\hat{h}_{0,1}(\mathbf{q}_k)|^2-1)+s_{2,0+1}^2(|\hat{h}_{2,0}(\mathbf{q}_k)|^2-1)$ and another outside of it. In the outer region of the ellipse the upper bound for $\mathbb{E}[\tilde{m}_1^2(k+1)]$ is maximized by choosing a low correlation factor while in the inner region this bound maximized by choosing a high correlation factor. Therefore, for the decode-and-forward relay case this motivates the following distance function form:

$$d_1^{(2)}\left(\hat{\mathbf{h}}^{(2)}(\mathbf{q}_k)\right) = (d_s-d_b)\mathbf{1}_{\mathbf{R}^{+*}}\left(\frac{s_{2,0}^2(|\hat{h}_{2,0}(\mathbf{q}_k)|^2-1)+s_{0,1}^2(|\hat{h}_{0,1}(\mathbf{q}_k)|^2-1)}{s_{2,0}^2+s_{0,1}^2}\right)+d_b \tag{4.24}$$

with $d_b > d_s$. Then we insert (4.24) into (4.9) and obtain the full path planner form for the decode-and-forward relay. To optimise its parameters we can follow the same procedure as for the amplify-and-forward case in the previous section by only substituting the first term in (4.15) and (4.16) by a more suitable term like $\mathbb{E}\left[\max_{k=1,2,\cdots,N} m(\mathbf{q}_k)^2\right]$. This finalises the design of 2-MDMTA for both the amplify- and forward RR as well as for the decode-and-forward RR.

4.5 Other Path Planners

In the previous sections we designed double-link MDAs and in the process we developed double-link path planners with memory order one. In this section we show first how to extend the memory of the path planners and then we show to extend the number of links considered.

4.5.1 Double-link Path Planner with Higher Memory Order

To develop the double-link path planner with arbitrary memory order we use the channel predictors of chapter 3 for each link and combine them. So we first extend

the single-link channel predictor with arbitrary memory order in (3.10) to obtain the double-link channel predictor of arbitrary memory order. As we mentioned earlier the channels from one link are independent to the channels at the other link and so the predictor with arbitrary memory order for $\mathbf{h}^{(2)}(\mathbf{q}_{k+1})$ at time instant t_k is given by:

$$\tilde{\mathbf{h}}^{(2)}_{M(k)}(\mathbf{q}_{k+1}) = \begin{bmatrix} \mathbf{P}^{-1}(k, M(k))\hat{\mathbf{H}}^{(2)}_{M(k)}(k) \\ \boldsymbol{\nu}^{(2)} \end{bmatrix}^T \mathbf{p}^T(k+1, M(k)+1) \tag{4.25}$$

where $\boldsymbol{\nu}^{(2)}(k+1) = [\nu_1 \;\; \nu_2]$ with $\nu_1, \nu_2 \sim \mathcal{CN}(0,1)$ and ν_1 is statistically independent to ν_2. Then $\hat{\mathbf{H}}^{(2)}_{M(k)}(k)$ is defined in (4.3), with the matrix $\mathbf{P}^{-1}(k, M(k))$ and the vector $\mathbf{p}(k+1, M(k)+1)$ defined in section 3.1. It is not difficult to see that:

$$\boldsymbol{\mu}^{(2)} = \mathbb{E}[\tilde{\mathbf{h}}^{(2)}_{M(k)}] = \left(\mathbf{P}^{-1}(k, M(k))\hat{\mathbf{H}}^{(2)}_{M(k)}(k)\right)^T \mathbf{p}^T_{1:M(k)}(k+1, M(k)+1) \tag{4.26}$$

where $\mathbf{p}_{1:M(k)}(k+1, M(k)+1)$ contains the first $M(k)$ entries of the vector $\mathbf{p}(k+1, M(k)+1)$ and the covariance matrix $\mathbf{C}$ of $\tilde{\mathbf{h}}^{(2)}_{M(k)}$ is given by:

$$\mathbf{C} = \mathbf{I}\mathbf{p}^2_{M(k):M(k)}(k+1, M(k)+1) \tag{4.27}$$

with $\mathbf{I}$ the identity matrix and $\mathbf{p}_{M(k):M(k)}(k+1, M(k)+1)$ is the last entry of the vector $\mathbf{p}(k+1, M(k)+1)$. From (4.26) and (4.27) the second moment of the predictors for both channels can be written as:

$$\begin{aligned} \mathbb{E}\left[|\tilde{h}_{0,1,M(k)}(\mathbf{q}_{k+1})|^2\right] &= \mathbf{p}^2_{M(k):M(k)}(k+1, M(k)+1) + |\mu^{(2)}_1|^2, \\ \mathbb{E}\left[|\tilde{h}_{2,0,M(k)}(\mathbf{q}_{k+1})|^2\right] &= \mathbf{p}^2_{M(k):M(k)}(k+1, M(k)+1) + |\mu^{(2)}_2|^2 \end{aligned} \tag{4.28}$$

with $\mu^{(2)}_1$ and $\mu^{(2)}_2$ the first and the second entries of $\boldsymbol{\mu}^{(2)}$ in (4.26).

Finally we modify (3.59) by replacing the single-link path planner with memory order one of section 3.5 with the double-link path planner with arbitrary memory order in (4.25). So we can calculate the optimum $\mathbf{q}_{k+1}$ by solving:

$$\begin{aligned} &\max_{\mathbf{q}_{k+1}} \theta g\left(\tilde{\mathbf{h}}^{(2)}_{M(k)}(\mathbf{q}_{k+1}), S^{(2)}\right) - (1-\theta)\|\mathbf{q}_{k+1} - \mathbf{q}_k\|_2 \\ &\text{s.t.} \\ &M(k) \leq k-1, \end{aligned} \tag{4.29}$$

where $g\left(\tilde{\mathbf{h}}^{(2)}_{M(k)}(\mathbf{q}_{k+1}), S^{(2)}\right)$ is a general function that takes into account the channel gain at both links and can be customized according to the particular applicaltion. For example, in the case of the amplify-and-forward relay we can set this function to be :

$$g\left(\tilde{\mathbf{h}}^{(2)}_{M(k)}(\mathbf{q}_{k+1}), S^{(2)}\right) = \mathbb{E}\left[|\tilde{h}_{2,0,M(k)}(\mathbf{q}_{k+1})|^2\right] \mathbb{E}\left[|\tilde{h}_{0,1,M(k)}(\mathbf{q}_{k+1})|^2\right]. \tag{4.30}$$

And for the case of the decode-and-forward we can select $g\left(\tilde{\mathbf{h}}^{(2)}_{M(k)}(\mathbf{q}_{k+1}), S^{(2)}\right)$ to represent the upper bound for the minimum channel gain of both wireless links, see section 4.4, and thus we have:

$$g\left(\tilde{\mathbf{h}}^{(2)}_{M(k)}(\mathbf{q}_{k+1}), S^{(2)}\right) = \frac{s^2_{2,0}\mathbb{E}\left[|\tilde{h}_{2,0,M(k)}(\mathbf{q}_{k+1})|^2\right] + s^2_{0,1}\mathbb{E}\left[|\tilde{h}_{0,1,M(k)}(\mathbf{q}_{k+1})|^2\right]}{s^2_{2,0} + s^2_{0,1}}. \tag{4.31}$$

So we have derived a double-link path planner with arbitrary memory order by using double-link channel predictors. In the next subsection we show how we can extend these planners even further to obtain multiple-link path planners with arbitrary memory order.

4.5.2 Multiple-link Path Planner

In the previous subsection we showed how to obtain the double-link path planner with arbitrary memory order so now we show how to obtain a multiple-link path planner with arbitrary memory order. To do this we first extend the double-link channel predictor with arbitrary memory order in (4.25) to the multiple-link channel predictor with arbitrary memory order. By analysing the form of (4.25) it is straightforward to note that the multiple-link channel predictor with arbitrary memory order is:

$$\tilde{\mathbf{h}}^{(L)}_{M(k)}(\mathbf{q}_{k+1}) = \begin{bmatrix} \mathbf{P}^{-1}(k, M(k))\hat{\mathbf{H}}^{(L)}_{M(k)}(k) \\ \boldsymbol{\nu}^{(L)} \end{bmatrix}^T \mathbf{p}^T(k+1, M(k)+1) \tag{4.32}$$

where L is the number of wireless links considered.

A good objective for a multiple-link MDA can be to try to find a stopping point where the minimum channel gain of all L the wireless links considered is not poor. In other words, a good strategy (but not the only one) for a multiple-link MDA could be to maximize the minimum channel gain of the L links. To achieve this a multiple-link path planner that maximises the upper bound of the minimum channel gain of the predicted channels could be used. To do this we first define the following random variable:

$$\tilde{m}^{(L)}_{M(k)}(k) = \min_{j=1,2,\cdots,L}\{s_{0,j}|\tilde{h}_{0,j,M(k)}(\mathbf{q}_k)|\}. \tag{4.33}$$

We also remember that due to the reciprocity assumption $\tilde{h}_{0,j,M(k)}(\mathbf{q}_k) = \tilde{h}_{j,0,M(k)}(\mathbf{q}_k)$. Now, it can be shown that:

$$\begin{aligned} \Pr\left(\tilde{m}^{(L)}_{M(k)}(k+1) < z\right) &= \sum_{j=1}^{L} \Pr\left(s^2_{0,j}|\tilde{h}_{0,j}(\mathbf{q}_{k+1})|^2 < z\right) \\ &- (L-1)\prod_{j=1}^{L} \Pr\left(s^2_{0,j}|\tilde{h}_{0,j}(\mathbf{q}_{k+1})|^2 < z\right). \end{aligned} \tag{4.34}$$

So we also have:

$$\mathbb{E}\left[\tilde{m}^{(L)}_{M(k)}(k+1)\right] < \sum_{j=1}^{L} s^2_{0,j}\mathbb{E}\left[|\tilde{h}_{0,j}(\mathbf{q}_{k+1})|^2\right] \tag{4.35}$$

which becomes:

$$\sum_{j=1}^{L} s^2_{0,j}\mathbb{E}\left[|\tilde{h}_{0,j}(\mathbf{q}_{k+1})|^2\right] = \sum_{j=1}^{L} s^2_{0,j}\left(\mathbf{p}^2_{M(k):M(k)}(k+1, M(k)+1) + |\mu^{(2)}_j|^2\right). \tag{4.36}$$

Finally, in order to calculate $\mathbf{q}_k$ with the multiple-link path planner with arbitrary memory order we can first select $g\left(\tilde{\mathbf{h}}^{(L)}_{M(k)}(\mathbf{q}_{k+1}), S^{(L)}\right)$ as:

$$g\left(\tilde{\mathbf{h}}^{(L)}_{M(k)}(\mathbf{q}_{k+1}), S^{(L)}\right) = \frac{\sum_{j=1}^{L} s^2_{0,j}\mathbb{E}\left[|\tilde{h}_{0,j}(\mathbf{q}_{k+1})|^2\right]}{\sum_{j=1}^{L} s^2_{0,j}}. \tag{4.37}$$

Then we use this function in (4.29) and solve it to obtain a multiple-link path planner arbitrary memory order that maximises the upper bound of the minimum channel gain. By observing the shape of (4.37) we can note that a more general optimization target for the path planner could be as follows:

$$g\left(\tilde{\mathbf{h}}^{(L)}_{M(k)}(\mathbf{q}_{k+1}), S^{(L)}\right) = \sum_{j=1}^{L} \theta_j\mathbb{E}\left[|\tilde{h}_{0,j}(\mathbf{q}_{k+1})|^2\right] \tag{4.38}$$

where $\theta_j \in [0,1]$ and $\sum_j^L \theta_j = 1$. In other words (4.38) represents a convex combination of all the channel power predicted for all the L wireless links. The parameters θ_j represent then relative the importance of compensating the small-scale fading term at each channel. So we can calculate $\mathbf{q}_{k+1}$ with a more general multiple-link path planner with arbitrary memory order by solving online:

$$\begin{aligned} &\max_{\mathbf{q}_{k+1}} \theta \sum_{j=1}^{L} \theta_j\mathbb{E}\left[|\tilde{h}_{0,j}(\mathbf{q}_{k+1})|^2\right] - (1-\theta)\|\mathbf{q}_{k+1} - \mathbf{q}_k\|_2 \\ &\text{s.t.} \\ &M(k) \leq k-1. \end{aligned} \tag{4.39}$$

Note that the channel gain is the product of the shadowing term $s_{0,j}$ multiplied by the magnitude of the small-scale fading term. Then it makes more sense to give more importance in (4.39) to the links with lower values of the shadowing term. So a possible choice (but not the only one) for the parameters θ_j could be:

$$\theta_j = \frac{s^{-1}_{0,j}}{\sum_{k=1}^{L} s^{-1}_{0,k}}. \tag{4.40}$$

Finally, (4.39) constitutes the more general path planner for the discrete search spaces presented in this thesis since it is has arbitrary memory order and takes simultaneously into account as many channels as possible.

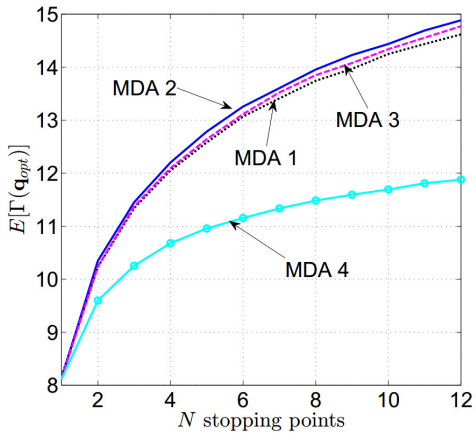

Figure 4.1: Expected value of the SNR at MR-2 after the execution of various double-link MDAs.

4.6 Simulations

In order to provide more insight into the multiple-links MDAs we present in this section some simulations of a double-link MDA. Particularly we will present results for the double-link MDA designed in section 4.3 for amplify-and-forward robotic relays. For the simulations we will assume that the shadowing has a variance of 16dB, which is a realistic value measured in [56]; $P_m/\sigma_n^2 = 20$, which corresponds to a moderate SNR; and a channel estimation error with 0.01 variance, which corresponds to a low estimation error.

Let us first consider the following two MDAs:

1. **MDA-1**: it uses the selection rule that maximizes (4.8) but uses a predetermined geometry with all the N stopping points uniformly arranged in a straight line and separated by a distance z_0.

2. **MDA-2**: it uses the selection rule that maximizes (4.8) and the double-link adaptive path planner with memory order one presented in section 4.3.2. The path planner is optimized according to (4.15) with $\theta = 1$, i.e., it is optimized to obtain the best possible channel gain.

From Fig. 4.1 we note that MDA-2 produces an SNR at the MR-2 moderately superior to MDA-1, and from Fig. 4.2 we note that it also requires the MR to move a significantly smaller distance. This shows that the adaptive double-link path planner with memory order one that we have designed improves the performance of the double-link MDA. In particular: (i) the statistics of the channels are improved at each iteration of the adaptive path planner and so the resulting SNR at MR 2 is

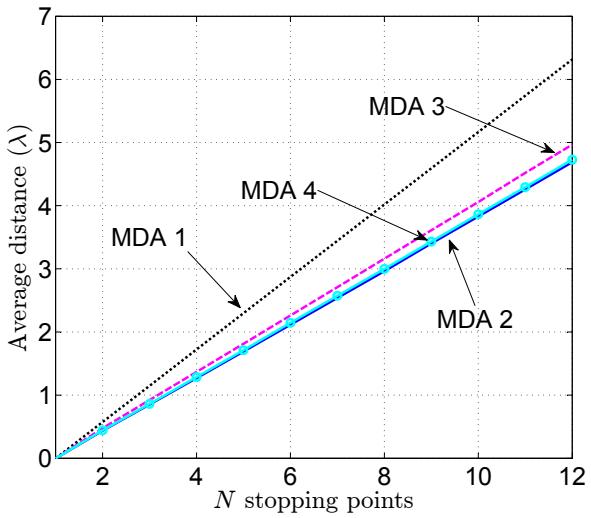

Figure 4.2: Expected value of the distance travelled by the RR for various double-link MDAs.

better than for the case in which the stopping points are predetermined; (ii) the total distance travelled by the RR while using the adaptive path planner is reduced and consequently the mechanical energy used is also reduced making the MDA-2 more energy efficient.

Note that these results are similar to the results in chapter 3 when we compared the single-link adaptive path planner with memory order one against the predetermined stopping point geometries.

Now, let us consider two more MDAS:

1. **MDA-3**: uses the same selection rule as MDA-2 but uses the optimized single-link adaptive path planner with memory order one derived in 3 to improve the wireless channel in the link between MR-1 and RR.

2. **MDA-4**: uses the same path planner as the MDA-2 but uses a single-link selection rule that maximizes the channel gain of the link between RR and MR-2.

From Figs. 4.1 and 4.2 we observe that both MDA-3 and MDA-4 perform worse than MDA-2. This is because the MDA-3 uses a single-link path planner instead of a double-link path planner while the MDA-4 uses a single-link selection rule instead of a single-link one. Nevertheless we observe that the degradations are considerably different. The degradation for the MDA-4 in terms of the SNR is quite significant (see Fig. 4.1) while the degradation of the MDA-3 with respec to the MDA-2 is small. This implies that when designing double-link MDAs (and multiple-link MDAs) we need to use double-link selection rules. But we can use single-link path planners

(which are simpler) instead of double-link ones at the cost of only a small degradation in the performance.

4.7 Summary

In this chapter we departed from the theory of single-link MDAs that we developed in chapters 2 and 3 in order to develop a theory for multiple-link MDAs. We started by designing double-link MDAs for robotic relays with all their components including the double-link path planners. Then we showed how to derive the double-link path planners with arbitrary memory order and finally we derived a general multiple-link path planner with arbitrary memory order.

This chapter concludes the first part of this thesis in which we have studied in detail all different aspects of MDAs with discrete search spaces.

Chapter 5

MDA for Energy Harvesting

In the first part of this thesis, composing chapters 2 to 4, we developed and studied in detail MDAs with discrete search spaces. In the second part of this thesis we develop MDAs with continuous search spaces (particularly predetermined continuous search spaces). As mentioned earlier, in MDAs with discrete search spaces MRs move from one point to the other, then stop at each point (this is why we refer to them as stopping points) and collect as many noisy samples from the wireless receiver as needed in order to obtain a channel estimate with sufficient accuracy. On the other hand, in MDAs with continuous search spaces MRs follow a continuous path without stopping (until the end) while collecting samples of the wireless channel.

The main motivation to develop MDAs with a continuous search space is that from a mechanical energy point of view MDAs with discrete search spaces are not so efficient. To illustrate this consider a set of N points $\{\mathbf{q}_j\}_{j=1}^{N}$ and then make the MR explore them all only once in a time T and in a certain order. If we were using an MDA with a discrete search space then we would design the control law so that the MR moves from point $\mathbf{q}_j$ to point $\mathbf{q}_{j+1}$ using a minimum amount of energy in a time T_j (such that $\sum_{j=1}^{N} T_j = T$) and stopping at each of the N points. Now assume that we eliminate the restriction of stopping at each point, then we could design a control law that makes the MR pass through all of the N points in a time T using minimum energy and stopping only at the end. It is intuitive that the amount of energy used by the second control law will be either lower or equal (in the worst case scenario) than the energy consumed by the first control law. This is because both control laws execute the same task (passing through all N points in a time T) but the first control law has additional restrictions (stopping at each point). Note that the second control law describes how the MR would operate in an MDA with a continuous search space. This implies that MDAs with continuous search spaces are more efficient from a mechanical energy consumption point of view. This could lead the reader to think that MDAs with continuous search spaces are better than MDAs with discrete search spaces. But we remind the reader that in the case of MDAs with discrete search spaces the MR stops at each point and can collect as many noisy samples from the wireless receiver as needed in order to satisfy

a certain accuracy in the channel estimate while in the case of the MDA with a discrete search space the MR can only collect one noisy sample per point. As a consequence, MDAs with a discrete search space are more robust against noise than MDAs with a continuous search space. Therefore MDAs with a continuous search space are conceptually the complement to MDAs with discrete search space.

We start our treatment of MDAs with continuous search space in this chapter by restricting the shape of the continuous search space to be a straight line, which is the simplest shape. Although the shape of the discrete search space will remain a straight line in this chapter we will optimise its length. In previous chapters we have focused on the spatial aspects of the MDA (i.e., the search space) and we have briefly discussed the temporal aspects of the MDA (i.e., execution time and its partition for the different phases). In this chapter we will pay more attention regarding the effect of the execution time and its partition on the MDA. Another difference with the previous chapters is that here we will show how the MDA can be used to improve RF energy harvesting [38], [39].

Before we explain how we can improve RF energy harvesting using MDAs let us briefly discuss some generalities about energy harvesting and the energy consumption of MRs. Untethered MRs draw their energy exclusively from an onboard battery. The amount of tasks that they can execute depends on the energy stored in its battery. Hence energy, in the context of untethered MRs, is a very scarce and important resource. There are many approaches that allow the robots to increase the time duration over which an untethered MR can operate without having to return to its base for recharging its battery. These include using energy conservation techniques to make the robot more energy efficient [40] or adding energy harvesting capabilities to the MR [41]. Now, wireless energy harvesting [42] is a technique that is being studied for sensor networks but it could be applied to small untethered MRs requiring low power. This can be done by using a dedicated base station to transmit RF energy and adding a rectifier antenna [43] to the MR so that it stores the wireless energy transmitted by the base station. Although the amount of energy stored by this method may not be as high as with other energy harvesting techniques (e.g., solar or wind energy) it is cheap to implement and it requires only a very small area on the robot's surface. Because of this latter property wireless energy harvesting systems can easily be implemented on small MRs (e.g. the micro-robot Alice [41], [44]). Moreover, the key advantage in RF energy harvesting is that it imposes minimal hardware requirements for MRs, as they are already provided with on-board radio communication capabilities.

In this chapter, we consider an untethered MR with an antenna which uses the integrated receiver architecture presented in [45] that provisions simultaneous data and wireless energy reception from the command-and-control center base station. This base station is charged to maintain communications for control purposes or just to exchange data with the MR. More specifically, we consider a scenario where

a MR, that is harvesting wireless energy most of the time[1] thanks to the receiver mentioned earlier, is deployed in the field. The robot has to perform a series of tasks demanded by the BS. Now, we assume that there are 'dead times' between the tasks which are demanded by the BS. This means that once the MR completes one task it will not be required to perform any further action for a 'dead time' of duration T seconds until the BS requests execution of the next task. During the execution of a task the MR will harvest wireless energy while completing it.

During the 'dead times' the base station transmits an RF signal so that the MR can harvest energy from it. Generally, MRs may observe many scatterers in their near vicinity and that there may not be a line of sight between the MR and the base station antenna. Therefore, the wireless channel from the base station to the MR will experience small scale fading which will affect the amount of radio energy that can be harvested. Thus, the key challenge posed in this scenario is to devise a MR algorithm which maximizes the energy stored during these 'dead times' in the presence of fading. In this chapter we achieve this by customising a continuous search space MDA to execute this task during the 'dead times'.

The contributions of this chapter is the customisation of a continuous search space MDA to improve RF energy harvesting and also the optimisation of the continuous search space size.

This chapter is organized as follows. In section 5.1 we describe the model for the MR, for the wireless channel model and for the energy storage system. Then in section 5.2 we propose a continuous search space MDA for improving the RF energy harvesting. In section 5.3 we optimize the parameters of this MDA. An explanation about how to find the optimal point from which to harvest the energy is presented in section 5.4. Finally, simulation results are given in section 5.5 and conclusions are presented in section 5.6.

5.1 System and Channel Model

5.1.1 MR Model

In this chapter, we consider a differential drive robot[2] (DDR) [46] furnished with a rectifier antenna[3] (rectenna) [43]. It is assumed that the rectenna is installed on the geometric center of the robot (see Fig. 5.1) such that it can harvest the energy received from the base station. A DDR is a MR that has two wheels (each with

[1] The only times when the MR is not harvesting wireless energy could be when the it is transmitting. This is because at that time the antenna could be connected to the transmitter instead of the receiver (depending on the transceiver architecture.)

[2] Although we restrict our analysis to a DDR the technique presented in this chapter can be easily extended to other types of MR like (for example) a three wheeled omni-directional robot as in the previous chapters.

[3] An antenna which is connected directly to a rectifier composed of a Schottky diode and a lowpass filter.

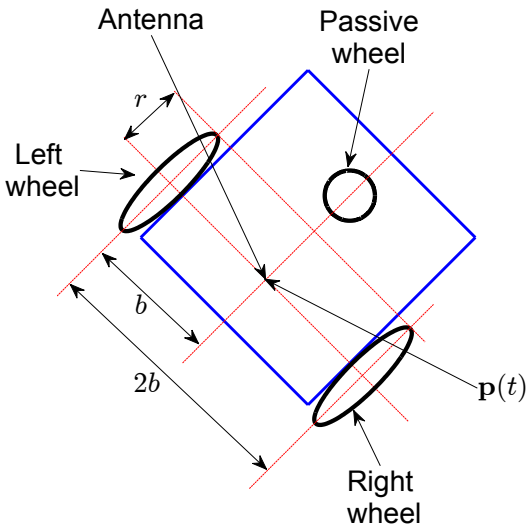

Figure 5.1: Diferential drive robot (DDR).

radius r controlled by its own motor). The distance between the two motorized wheels is $2b$. In addition, it may have a third passive[4] omnidirectional[5] wheel which serves as support for the robot (see Fig. 5.1). The DDR model considered in this chapter is a version of the model presented in [47].

The position of the MR is $\mathbf{p}(t)$ and its translational velocity $v(t)$ is controlled by the motor's input vector $\mathbf{u}(t) = [u^R(t) \quad u^L(t)]^T$ where $u^R(t)$ and $u^L(t)$ are the control inputs for the right and left motors respectively. The following state equation describes how the translational velocity $v(t)$ is controlled by $\mathbf{u}(t)$:

$$\dot{v}(t) + [1 \;\; 0]\bar{\mathbf{A}}[v(t) \;\; 0]^T = [1 \;\; 0]\bar{\mathbf{B}}\mathbf{u}(t), \tag{5.1}$$

where $\bar{\mathbf{A}} = c_A\mathbf{T_q}\mathbf{J}^{-1}\mathbf{T_q}^{-1}$ and $\bar{\mathbf{B}} = c_B\mathbf{T_q}\mathbf{J}^{-1}$, with c_A and c_B two constants depending on the electromechanical characteristics of the robot; the matrix $\mathbf{J}$ is the equivalent inertia matrix of the robot's motors:

$$\mathbf{J} = \begin{bmatrix} J_1 & J_2 \\ J_2 & J_1 \end{bmatrix}, \tag{5.2}$$

and $\mathbf{T_q}$ depends on the geometry of the robot and is given by:

$$\mathbf{T_q} = \begin{bmatrix} r/2 & r/2 \\ r/2b & -r/2b \end{bmatrix}. \tag{5.3}$$

Finally, the energy consumed by the MR due to its mechanical movement from any time t_0 to time t_1 is:

$$E_{mech}(t_0, t_1, \mathbf{u}(t)) \;\; = \;\; \int_{t_0}^{t_1} c_1\mathbf{u}^T(t)\mathbf{u}(t)\mathrm{d}t \tag{5.4}$$

[4] A passive wheel is a wheel which is not controlled by any motor.
[5] An omnidirectional wheel can roll in any direction at any time.

$$- \int_{t_0}^{t_1} c_2[v(t) \;\; 0]\mathbf{T}_{\mathbf{q}}^{-T}\mathbf{u}(t)\mathrm{d}t,$$

where c_1 and c_2 are constants which depend on the electrical parameters of the robot's motors.

5.1.2 Channel Model

In this chapter, we consider that during the dead time of duration T the base station is constantly transmitting a narrowband RF signal so that the robot can replenish its battery with RF harvested energy. A narrowband signal will produce less interference to adjacent wireless systems than a broadband signal. Now while narrowband signals will experience flat fading, which in turn will produce losses[6] in the wireless energy harvested by the system, this impairment will be compensated through the MR movement (as we will see later in the chapter).

Now, we assume that the MR receiver follows the architecture proposed in [45]. On the MR, the energy is received by a rectenna. The output of the rectifier is connected to both the robot's battery and an analog-to-digital converter (ADC) (see Fig. 5.2). In general, the receiver in Fig. 5.2 serves to receive information (through the ADC) while simultaneously harvesting radio energy, but during the dead times the receiver will just be used to harvest radio energy. We also assume that most of the energy generated at the output of the rectifier is fed to the battery and only a small amount is absorbed by the ADC's input. This may be achieved by inserting (at the rectifier's output) a well-designed three-port matching network [48] (not shown in Fig. 5.2) with one input and two outputs. Consequently, the on-board battery is charged by employing the radio signal, while the MR simultaneously monitors the amount of energy that arrives into its battery.

Since the radio signal transmitted by the base station is narrow band the wireless channel experiences flat fading. Furthermore, it is assumed that during the dead time the environment remains stationary and consequently the duration T of the dead time is smaller than the coherence time of the channel and so the channel will be considered approximately time-invariant over this duration. Note that this can only be achieved if the MR works on environments with physical features that experience low mobility. So the low-pass, complex equivalent baseband signal received by the robot's antenna at position $\mathbf{p}(t)$ is given by:

$$y_e(\mathbf{p}(t), t) = s(\mathbf{p}(t))h(\mathbf{p}(t))x_e(t) + n_y(t), \tag{5.5}$$

where $n_y(t) \sim \mathcal{CN}(0, \sigma_y^2)$ is complex, zero-mean, additive white Gaussian noise, $s(\mathbf{p}(t))$ and $h(\mathbf{p}(t))$ are the shadowing experienced and small-scale fading observed at $\mathbf{p}(t)$ while $x_e(t)$ is the lowpass equivalent of a pure RF tone with amplitude a transmitted by the base station.

[6] Due to the deep fades.

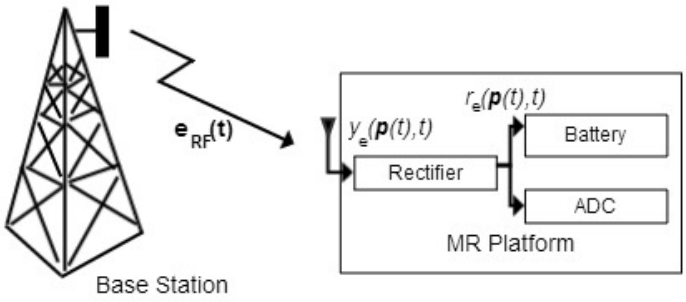

Figure 5.2: Energy receiver architecture [45].

If the movement of the robot during the dead times is in a small region then we have $s(\mathbf{p}(t)) = s$, a constant, i.e., the shadowing term is constant for all the positions in which the robot moves during the dead times. With all these considerations then (5.5) simplifies to:

$$y_e(\mathbf{p}(t), t) = h(\mathbf{p}(t))a_y + n_y(t), \tag{5.6}$$

where $a_y = sa$. We will consider that the small scale fading follows Jakes' model [28] and so $|h(\mathbf{p}(t))| \sim \mathcal{R}\left(\frac{1}{\sqrt{2}}\right)$ is Rayleigh distributed and the normalized spatial covariance function of the channel gain is:

$$\begin{aligned} C(\mathbf{p}, \mathbf{q}) &= \frac{\mathbb{E}[(|h(\mathbf{p})| - \mathbb{E}[|h(\mathbf{p})|])(|h(\mathbf{q})| - \mathbb{E}[|h(\mathbf{q})|])]}{\sqrt{\text{var}\left(|h(\mathbf{p})|\right)\text{var}\left(|h(\mathbf{q})|\right)}}, \\ &= J_0^2\left(\frac{2\pi\|\mathbf{p}-\mathbf{q}\|_2}{\lambda}\right), \end{aligned} \tag{5.7}$$

where λ is the wavelength of the RF signal transmitted by the BS. The signal at the output of the rectifier in Fig. 5.2 is [45]:

$$r_e(\mathbf{p}(t), t) = |y_e(\mathbf{p}(t), t)|^2 + n_r(t), \tag{5.8}$$

where $n_r(t) \sim \mathcal{N}(0, \sigma_r^2)$ is the real zero-mean additive Gaussian noise at the output of the rectifier. We will refer to $n_r(t)$ as the post-rectifier noise and to $n_y(t)$ in (5.5) as the pre-rectifier noise in order to differentiate between them. Finally, the signal at the output of the ADC can be characterised as $r_e(\mathbf{p}(k\Delta_s), k\Delta_s)$ with $k\Delta_s$ being the discrete sampling time. We will use $r_e(k)$ as the shorthand notation for $r_e(\mathbf{p}(k\Delta_s), k\Delta_s)$, and the same reasoning will apply for all the discrete-time signals in the rest of this chapter.

Also, note that both the pre-rectifier $n_y(t)$ and post-rectifier $n_y(t)$ noises have the same variance at all times and it is independent of the robot's movement. This is because those noises are generated inside the MR's receiver. We have also to mention that since the time necessary to take one sample from (5.8) is always constant then the same pre and pos rectifier noises also have constant variance after the being sampled.

5.1.3 Energy Storage System

The energy storage system is a vital component of the MR. The net amount of energy stored from any time t_0 to t_1 can be written as

$$E_s(t_0, t_1) = E_r(\mathbf{p}(t), t_0, t_1) - E_{mech}(t_0, t_1, \mathbf{u}(t)), \tag{5.9}$$

where $E_r(\mathbf{p}(t), t_0, t_1)$ is the energy harvested over this time period using the rectenna. Mathematically, this can be written as:

$$E_r(\mathbf{p}(t), t_0, t_1) = \eta \int_{t_0}^{t_1} r_e(\mathbf{p}(\tau), \tau) d\tau, \tag{5.10}$$

where $\eta \in (0, 1]$ is the energy charging efficiency parameter [49]. The energy storage efficiency of the MR depends on the impedance matching network at the rectifier's output and also on the energy charging system for the battery. Although the battery has finite capacity we will not consider this on our model because we assume that the amount of energy stored in the battery at the beginning of the dead time is not high enough so that the battery can be completely replenished at the end of this period. In the same manner, we will assume that the battery level at the beginning of the dead time is not low enough so that the MR runs out of energy because of the motion carried out during this period of time.

5.2 MDA for Energy Harvesting

As we will define later in this section, the dead time of T secs (from $t = 0$ to $t = T$) when the MR is attempting to find an optimal position from which to "re-energize" itself, will comprise of three phases. Only during the third phase will the MR actually be stationary. The objective is to maximise $\mathbb{E}[E_s(0, T)]$ in (5.9). Now, due to the small scale fading, the radio energy harvested by the MR using its rectenna can be very low if the MR is located at a position where the channel gain is poor. Thus, we will design a continuous search space MDA in order to compensate the small-scale fading and consequently maximize the energy stored by the MR during the dead time.

During the dead time, the more the MR moves the higher the probability of obtaining a point with a high channel gain and so increasing the radio energy harvested, $E_r(\mathbf{p}(t), 0, T)$. But also the greater the search space the higher the consumption of mechanical energy, see (5.4). This consumption in turn depletes the

energy from the MR's battery. This implies that although moving can significantly increase $E_r(\mathbf{p}(t), 0, T)$ it also increases $E_{mech}(0, T, \mathbf{u}(t))$ and consequently the net energy $E_s(0, T)$ (see (5.9)) can be low or even negative. This encourages intelligent mobility control such that the energy stored during the dead time is maximized. This intelligent control will be implemented by a continuous search space MDA. In short, in the RF energy harvesting problem for MRs the net energy stored is highly dependent on the actual exploration strategy.

The MDA is then executed during the dead time. Let us we define the design parameters $T_s < T$ and $\alpha \in (0, 1)$, which will be optimized in section 5.3. We divide the dead time into three distinct phases:

1. **Phase 1 - Searching Time** $(t \in [0, \alpha T_s])$ During this period the MR moves along the continuous search space of the MDA while simultaneously monitoring the channel gain and harvesting energy. This constitutes the first part of the MDA.

2. **Phase 2 - Positioning Time** $(t \in (\alpha T_s, T_s])$ During this phase the MR executes the last part of the MDA. The MR continues harvesting energy while moving from its current location $\mathbf{p}(\alpha T_s)$ to the optimal operating point $\hat{\mathbf{p}}_{opt}$, where $\hat{\mathbf{p}}_{opt}$ is the estimation of $\mathbf{p}_{opt}$ defined as:

$$\mathbf{p}_{opt} = \arg \max_{\substack{\mathbf{p}(t) \\ t \in [0, \alpha T_s]}} |h(\mathbf{p}(t))|. \tag{5.11}$$

3. **Phase 3 - Resting Time** $(t \in (T_s, T])$ In this period the robot remains motionless at $\hat{\mathbf{p}}_{opt}$ harvesting energy through its rectenna.

Note that, the MDA is executed in the first and second phases while in the third phase the MR enjoys the benefits of having obtained a high channel gain by executing the MDA. Now, following (5.9) the net energy stored during the harvesting time (i.e., over the total pause period of T seconds) is:

$$\begin{aligned} E_s(0,T) &= \overbrace{E_r(\mathbf{p}(t), 0, \alpha T_s) + E_r(\mathbf{p}(t), \alpha T_s, T_s)}^{\text{Harvested energy (Phases 1\& 2)}} \\ &+ \overbrace{E_r(\hat{\mathbf{p}}_{opt}, T_s, T)}^{\text{Harvested energy (Phase 3)}} \\ &- \underbrace{E_{mech}(0, \alpha T_s, \mathbf{u}_1(t)) - E_{mech}(\alpha T_s, T_s, \mathbf{u}_2(t))}_{\text{Energy consumed due to mobility in Phases 1 \& 2}} . \end{aligned} \tag{5.12}$$

where $\mathbf{u}_1(t)$ and $\mathbf{u}_2(t)$ are the control inputs (see (5.1)) employed during the first and second phases[7]. Let us define the continuous searching space of the MDA as follows:

$$\mathcal{S} = \{\mathbf{q} \mid \mathbf{q} = \mathbf{p}(t) \text{ for } t \in [0, T]\}. \tag{5.13}$$

[7]Note that energy is harvested during all three phases of the dead time but it is during phase 3 that the most significant harvesting actually takes place.

In this chapter, for simplicity, we restrict the search space $\mathcal{S}$ to be a straight segment with finite length, to consider a linear search space with finite length L. So, in this chapter we select $\mathcal{S}$ to be:

$$\mathcal{S} = \{[l \;\; 0]^T \mid l \in [0, L]\}. \tag{5.14}$$

This implies that:

1. The control input $\mathbf{u}_1(t)$ has to follow a control law that takes the robot from its initial linear velocity $v(0) = 0$ and initial pose $\mathbf{p}_o(0) = \mathbf{0}$ to the final linear velocity $v(\alpha T_s) = 0$ and final pose $\mathbf{p}_o(\alpha T_s) = [L \;\; 0 \;\; 0]^T$ while moving in a straight line.

2. The control input $\mathbf{u}_2(t)$ has to follow a control law that takes the robot from the initial linear velocity $v(\alpha T_s) = 0$ and initial pose $\mathbf{p}_o(\alpha T_s) = [L \;\; 0 \;\; 0]^T$ to the final linear velocity $v(T_s) = 0$ and final pose $\mathbf{p}_o(T_s) = [\hat{\mathbf{p}}_{opt} \;\; 0]^T$. Since $\mathbf{p}_{opt}$ and $\hat{\mathbf{p}}_{opt}$ are both random variables the control law $\mathbf{u}_2(t)$ is a stochastic process (as opposed to $\mathbf{u}_1(t)$ which is deterministic).

While in this chapter we are arbitrarily restricting the shape of the continuous search space for the MDA in the next chapter we will show how to optimise its shape.

5.3 Optimization of the MDA

In this section, our objective is to optimize the MDA so that the expected value of the net energy stored during the dead time is maximized. In other words, we want to maximize the average net stored energy $\mathbb{E}[E_s(0, T)]$. The optimization process will ensure that the average energy level of the MR battery at the end of the dead time will be maximized.

For this section, we assume that at the second subphase $\mathbf{p}_{opt}$ is known and therefore $\hat{\mathbf{p}}_{opt} = \mathbf{p}_{opt}$ (In section 5.4, we provide further details of the estimation process for $\mathbf{p}_{opt}$). Finally, we assume that we know a_y in (5.6).

Substituting (5.10) into (5.12) and taking the expectation:

$$\begin{aligned}
\mathbb{E}[E_s(0,T)] &= \eta \int_0^{\alpha T_s} \mathbb{E}[r_e(\mathbf{p}(\tau), \tau)] d\tau + \eta \int_{\alpha T_s}^{T_s} \mathbb{E}[r_e(\mathbf{p}(\tau), \tau)] d\tau \\
&+ \eta \int_{T_s}^{T} \mathbb{E}[r_e(\mathbf{p}_{opt}, \tau)] d\tau - E_{mech}(0, \alpha T_s, \mathbf{u}_1(t)) \\
&- \mathbb{E}[E_{mech}(\alpha T_s, T_s, \mathbf{u}_2(t))].
\end{aligned} \tag{5.15}$$

We will now examine in turn each of the five terms on the right hand side of (5.15). The first term corresponds to the energy harvested during the first phase and we can demonstrate that:

$$\mathbb{E}[r_e(\mathbf{p}(\tau), \tau)] = a_y^2 + \sigma_y^2. \tag{5.16}$$

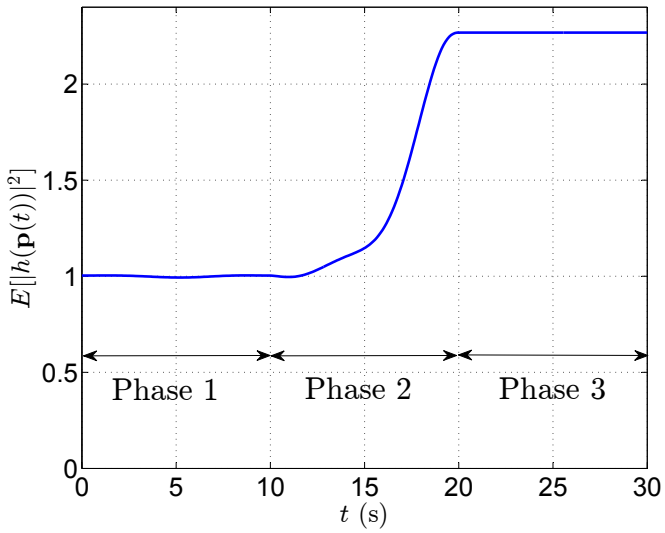

Figure 5.3: Evolution of $\mathbb{E}[|h(\mathbf{p}(t))|^2]$, obtained from Monte Carlo simulations, during the execution of the three phases (see start of section 5.2) with $T = 30$s, $T_s = 20$s, $\alpha = 0.5$ and $L = 1\lambda$.

The second term on the right hand side of (5.15) corresponds to the energy harvested during the second phase. In this phase the MR starts at position $\mathbf{p}(\alpha T_s)$ (which is a deterministic position) and finishes at $\mathbf{p}(T_s) = \mathbf{p}_{opt}$ (which is a random position). Now, $|h(\mathbf{p}(\alpha T_s))| \sim \mathcal{R}\left(\frac{1}{\sqrt{2}}\right)$ and so $\mathbb{E}[|h(\mathbf{p}(\alpha T_s))|^2] = 1$. Also, due to the definition of $\mathbf{p}_{opt}$ then, for $L > 0$, $\mathbb{E}[|h(\mathbf{p}(T_s))|^2] > 1$. During this phase, if at time instant t the MR is 'near' to $\mathbf{p}_{opt}$ then $h(\mathbf{p}(t))$ will be highly correlated with $h(\mathbf{p}(T_s)) = h(\mathbf{p}_{opt})$ and so $\mathbb{E}[|h(\mathbf{p}(t))|^2]$ will be just slightly inferior to $\mathbb{E}[|h(\mathbf{p}_{opt})|^2]$. On the other hand, if at time instant t the MR is 'far' from $\mathbf{p}_{opt}$ then $h(\mathbf{p}(t))$ will be almost uncorrelated with $h(\mathbf{p}(T_s)) = h(\mathbf{p}_{opt})$ and so $\mathbb{E}[|h(\mathbf{p}(t))|^2] \approx 1$. This all means that during this second phase $\mathbb{E}[|h(\mathbf{p}(t))|^2] > 1$ and $\mathbb{E}[|h(\mathbf{p}(t))|^2]$ increases from 1 to $\mathbb{E}[|h(\mathbf{p}_{opt})|^2]$. In Fig. 5.3 we illustrate this temporal evolution. These results imply that $\mathbb{E}[r_e(\mathbf{p}(\tau), \tau)]$ is bounded as follows:

$$a_y^2 + \sigma_y^2 \leq \mathbb{E}[r_e(\mathbf{p}(\tau), \tau)] \leq a_y^2 \mathbb{E}[|h(\mathbf{p}_{opt})|^2] + \sigma_y^2. \tag{5.17}$$

Now, the third term on the right hand side of (5.15) depends on $\mathbf{p}_{opt}$ which further depends on $\mathcal{S}$ in (5.14). Analytical evaluation of $\mathbb{E}[r_e(\mathbf{p}_{opt}, \tau)]$ is a complicated and non-trivial task that implies calculating $\mathbb{E}[|h(\mathbf{p}_{opt})|^2]$. Nevertheless, by extensive simulations and numerical analysis we realised that $\mathbb{E}[|h(\mathbf{p}_{opt})|^2]$ seemed to be a logarithmic function of L. Hence we observed that a good fitting for $\mathbb{E}[|h(\mathbf{p}_{opt})|^2]$ is:

$$\mathbb{E}[|h(\mathbf{p}_{opt})|^2] \approx a_h \ln\left(\frac{b_h \cdot L}{\lambda} + 1\right) + 1 \tag{5.18}$$

Table 5.1: Evaluation (by simulation) of functionals a_h and b_h in (5.18) for different spatial sampling rates, $S_r = \alpha T_s \lambda / \Delta_s L$

S_r	1	2	4	8	16
a_h	0.9909	1.03	1.061	1.092	1.14
b_h	0.6494	1.057	1.698	1.987	1.907

where a_h (not to be confused with the amplitude a_y) and b_h are the shorthand notations for $a_h(\mathbf{p}(k\Delta_s), \Delta_s)$ and $b_h(\mathbf{p}(k\Delta_s), \Delta_s)$, which are two functionals of $\mathbf{p}(k\Delta_s)$ parameterized on Δ_s. For the case in which

$$\mathbf{p}(k\Delta_s) = \begin{bmatrix} \frac{k\Delta_s L}{\alpha T_s} & 0 \end{bmatrix}^T \quad \text{for} \quad k = 0, 1, \cdots, \frac{\alpha T_s}{\Delta_s} \tag{5.19}$$

we used simulations to evaluate a_h and b_h for different spatial sampling rates[8] given by:

$$S_r = \frac{\alpha T_s \lambda}{\Delta_s L}. \tag{5.20}$$

To obtain this approximation we first noted that $\mathbb{E}[|h(\mathbf{p}_{opt})|^2]$ depends only on the search space $\mathcal{S}$ and the spatial sampling rate S_r in (5.20). Since we have selected the search space $\mathcal{S}$ to be a line it is uniquely characterized by its length L. After performing an extensive amount of simulations and plotting the results we noted that for any fixed value of S_r the plot of $\mathbb{E}[|h(\mathbf{p}_{opt})|^2]$ versus L seems to be logarithmic with respect to L. Considering that for $L = 0$ we must have $\mathbb{E}[|h(\mathbf{p}_{opt})|^2] = \mathbb{E}[|h(0)|^2] = 1$ then we proposed the approximation (5.18) and later we optimized numerically the parameters a_h and b_h for each sampling rate.

The results are summarized in table 5.1. In addition, as illustrated by Fig. 5.4, the proposed analytical approximation in (5.18) is virtually indistinguishable from the actual mean $\mathbb{E}[|h(\mathbf{p}_{opt})|^2]$, and this shows the validity of our approximations. Note that in (5.19) the number $\frac{\alpha T_s}{\Delta_s}$ must be an integer, and so we can write:

$$\Delta_s = \frac{\alpha T_s}{N} \tag{5.21}$$

where N a positive integer.

Now consider the fourth and fifth terms on the right hand side of (5.15). We need a control law that takes the robot from its initial position along a straight line of length L, stops the robot at the end of that line and finally makes it move to $\mathbf{p}_{opt}$. In addition, this must be done by using the minimum amount of mechanical energy. So we first derive the optimum control law that makes the DDR described by equations (5.1)-(5.4) start still at an initial time instant t_i, then move in a straight

[8]The spatial sampling rate is measured samples per wavelength.

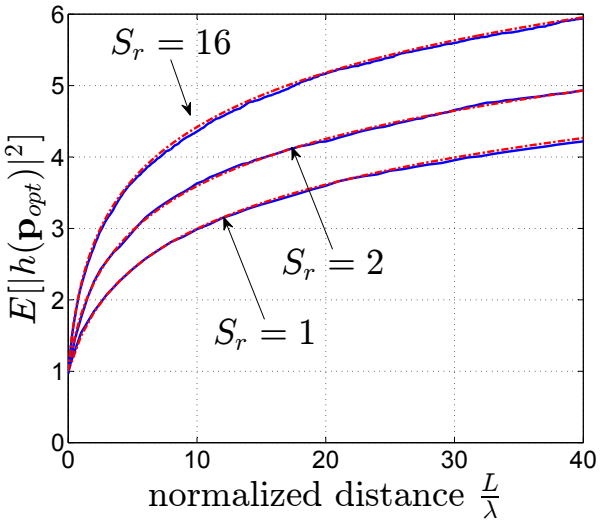

Figure 5.4: Comparison between the simulated $\mathbb{E}[|h(\mathbf{p}_{opt})|^2]$ (in blue) and its analytical approximation (in red) given by (5.18) for different spatial sampling rates, S_r.

line a distance l then stop at a final time instant t_f and perform all this using a minimum amount of energy. Mathematically this optimization problem can be stated as follows:

$$\min_{u_R(t)} \int_{t_i}^{t_f} \left(c_1 \mathbf{u}^T(t)\mathbf{u}(t) - c_2[v(t) \;\; 0]\mathbf{T}_{\mathbf{q}}^{-T}\mathbf{u}(t)\right)dt \tag{5.22}$$

s.t.

$$\dot{v}(t) + [1 \;\; 0]\bar{\mathbf{A}}[v(t) \;\; 0]^T = [1 \;\; 0]\bar{\mathbf{B}}\mathbf{u}(t), \tag{5.23}$$

$$\int_{t_i}^{t_f} v(t)dt = l, \tag{5.24}$$

$$u_R(t) = u_L(t) \tag{5.25}$$

$$v(t_i) = 0, \qquad v(t_f) = 0. \tag{5.26}$$

The differential constraint (5.23) corresponds to the state equation that describes how the velocity $v(t)$ is controlled by the control input $\mathbf{u}(t)$. We must also satisfy the isoperimetric [35] constraint (5.24) that makes the robot advance a distance l, and satisfy the boundary conditions (5.26) which state that the robot starts from rest and finishes at rest. Finally, we must satisfy the constraint (5.25) to ensure that the robot moves in straight line.

The optimization problem (5.22)-(5.26) is a classical optimum control problem and can be solved using calculus of variations [35], [50]. By applying this method we

arrive at the following second order differential equation:

$$\ddot{v}(t) - [1 \;\; 0]\left(\mathbf{Q}^T\mathbf{Q}[v(t) \;\; 0]^T + \bar{\mathbf{B}}\bar{\mathbf{B}}^T\left[\frac{\alpha}{2c_1} \;\; 0\right]^T\right) = 0 \tag{5.27}$$

where α is the Lagrange multiplier for constraint (5.24) and

$$\mathbf{Q}^T\mathbf{Q} = \bar{\mathbf{A}}^T\bar{\mathbf{A}} - \left(\frac{c_2}{c_1}\right)\bar{\mathbf{B}}\bar{\mathbf{B}}^T\mathbf{T}_{\mathbf{q}}^{-T}\bar{\mathbf{B}}^{-1}\bar{\mathbf{A}}. \tag{5.28}$$

By solving (5.27) and satisfying the conditions (5.26) we get:

$$v(t) = \left(K_{v1}(t_f - t_i)e^{\frac{-t}{\sqrt{\tau_v}}} + K_{v2}(t_f - t_i)e^{\frac{t}{\sqrt{\tau_v}}} + K_{v3}(t_f - t_i)\right)\cdot l \tag{5.29}$$

where $\tau_v = \frac{c_A(c_1c_A - c_2c_B)}{c_1(J_1+J_2)^2}$ and:

$$\begin{aligned}
K_{v1}(t_f - t_i) &= \frac{1 - e^{\frac{t_f - t_i}{\sqrt{\tau_v}}}}{4\sqrt{\tau_v}\left(1 - \cosh\left(\frac{t_f - t_i}{\sqrt{\tau_v}}\right)\right) + 2(t_f - t_i)\sinh\left(\frac{t_f - t_i}{\sqrt{\tau_v}}\right)},\\
K_{v2}(t_f - t_i) &= \frac{e^{\frac{-(t_f - t_i)}{\sqrt{\tau_v}}} - 1}{4\sqrt{\tau_v}\left(1 - \cosh\left(\frac{t_f - t_i}{\sqrt{\tau_v}}\right)\right) + 2(t_f - t_i)\sinh\left(\frac{t_f - t_i}{\sqrt{\tau_v}}\right)},\\
K_{v3}(t_f - t_i) &= \frac{2\sinh\left(\frac{t_f - t_i}{\sqrt{\tau_v}}\right)}{4\sqrt{\tau_v}\left(1 - \cosh\left(\frac{t_f - t_i}{\sqrt{\tau_v}}\right)\right) + 2(t_f - t_i)\sinh\left(\frac{t_f - t_i}{\sqrt{\tau_v}}\right)}.
\end{aligned} \tag{5.30}$$

Finally, using (5.29) with (5.25) and (5.23) we obtain the optimal control law:

$$\mathbf{u}^*(t) = \begin{bmatrix} K_{u1}(t_f - t_i)e^{\frac{-t}{\sqrt{\tau_v}}} + K_{u2}(t_f - t_i)e^{\frac{t}{\sqrt{\tau_v}}} + K_{u3}(t_f - t_i) \\ K_{u1}(t_f - t_i)e^{\frac{-t}{\sqrt{\tau_v}}} + K_{u2}(t_f - t_i)e^{\frac{t}{\sqrt{\tau_v}}} + K_{u3}(t_f - t_i) \end{bmatrix}\cdot l \tag{5.31}$$

where:

$$\begin{aligned}
K_{u1}(t_f - t_i) &= \left(\frac{c_A - \frac{J_1+J_2}{\sqrt{\tau_v}}}{c_B r}\right)K_{v1}(t_f - t_i),\\
K_{u2}(t_f - t_i) &= \left(\frac{c_A + \frac{J_1+J_2}{\sqrt{\tau_v}}}{c_B r}\right)K_{v2}(t_f - t_i),\\
K_{u3}(t_f - t_i) &= \left(\frac{c_A}{c_B r}\right)K_{v3}(t_f - t_i).
\end{aligned} \tag{5.32}$$

Using (5.31) it is not difficult to show that the optimal control law for phase 1 is given by:

$$\mathbf{u}_1^*(t) \;\; = \;\; L\cdot[1 \; 1]^T\left(K_{u1}(\alpha T_s)e^{\frac{-t}{\sqrt{\tau_v}}} + K_{u2}(\alpha T_s)e^{\frac{t}{\sqrt{\tau_v}}} + K_{u3}(\alpha T_s)\right), \tag{5.33}$$

where $t \in [0, \alpha T_s]$. Similarly, for the phase 2 it is:

$$\begin{aligned}
\mathbf{u}_2^*(t) \;\; &= \;\; \left(K_{u1}((1-\alpha)T_s)e^{\frac{-(t-\alpha T_s)}{\sqrt{\tau_v}}} + K_{u2}((1-\alpha)T_s)e^{\frac{t-\alpha T_s}{\sqrt{\tau_v}}} + K_{u3}((1-\alpha)T_s)\right)\\
&\cdot \;\; \|[L \; 0]^T - \mathbf{q}_{opt}\|_2\cdot[1 \; 1]^T,
\end{aligned} \tag{5.34}$$

where $t \in (\alpha T_s, T_s]$. Using these optimal control laws and by performing some cumbersome algebra on (5.1) and (5.4), we can show that the mechanical energy consumed during phase 1 is:

$$E_{mech}(0, \alpha T_s, \mathbf{u}_1(t)) = m_2(\alpha T_s)L^2 \tag{5.35}$$

and the mechanical energy consumed during phase 2 is:

$$E_{mech}(\alpha T_s, T_s, \mathbf{u}_2(t)) = m_2((1-\alpha)T_s)\|[L\ 0]^T - \mathbf{q}_{opt}\|_2^2 \tag{5.36}$$

where $m_2(t)$ is given by (5.37) with $K_{v1}(t_0)$, $K_{v2}(t_0)$ and $K_{v3}(t_0)$ defined in (5.30):

$$\begin{aligned} m_2(t_0) &= 2\Big[\left(\frac{\sqrt{\tau_v}K_{u1}(t_0)}{2}\right)\cdot\left(c_1K_{u1}(t_0) - \frac{c_2}{r}K_{v1}(t_0)\right)\cdot\left(1 - e^{\frac{-2t_0}{\sqrt{\tau_v}}}\right) \\ &+ \sqrt{\tau_v}\Big(2c_1K_{u1}(t_0)K_{u3}(t_0) - \frac{c_2}{r}\left(K_{u1}(t_0)K_{v3}(t_0) + K_{v1}(t_0)K_{u3}(t_0)\right)\Big) \\ &\cdot \left(1 - e^{\frac{-t_0}{\sqrt{\tau_v}}}\right) + \left(c_1(2K_{u1}(t_0)K_{u2}(t_0) + K_{u3}^2(t_0))\right)t_0 \\ &- \left(\frac{c_2}{r}(K_{u1}(t_0)K_{v2}(t_0) + K_{v1}(t_0)K_{u2}(t_0) + K_{u3}(t_0)K_{v3}(t_0))\right)t_0 \\ &+ \sqrt{\tau_v}\Big(2c_1K_{u2}(t_0)K_{u3}(t_0) - \frac{c_2}{r}(K_{u2}(t_0)K_{v3}(t_0) + K_{v2}(t_0)K_{u3}(t_0))\Big) \\ &\cdot \left(e^{\frac{t_0}{\sqrt{\tau_v}}} - 1\right) + \left(\frac{\sqrt{\tau_v}K_{u2}(t_0)}{2}\right)\cdot\left(c_1K_{u2}(t_0) - \frac{c_2}{r}K_{v2}(t_0)\right)\cdot\left(e^{\frac{2t_0}{\sqrt{\tau_v}}} - 1\right)\Big]. \end{aligned} \tag{5.37}$$

Now, using the proposed approximation (5.18), and substituting (5.16), (5.35) and (5.36) into (5.15) we obtain

$$\begin{aligned} \mathbb{E}[E_s(0,T)] &\approx \eta\alpha T_s\left(a_y^2 + \sigma_y^2\right) + \eta\int_{\alpha T_s}^{T_s}\mathbb{E}[r_e(\mathbf{p}(\tau),\tau)]d\tau \\ &+ \eta(T - T_s)a_y^2\left(a_h\ln\left(\frac{b_h\cdot L}{\lambda} + 1\right) + 1\right) + \eta(T-T_s)\sigma_y^2 - m_2(\alpha T_s)L^2 \\ &- m_2((1-\alpha)T_s)\mathbb{E}[\|[L\ 0]^T - \mathbf{q}_{opt}\|_2^2]. \end{aligned} \tag{5.38}$$

For the case where $S_r \to \infty$ in (5.20) (according to experimental results $S_r \geq 8Sa/\lambda$ will perform similarly to $S_r \to \infty$) then $\|[L\ 0]^T - \mathbf{q}_{opt}\|_2$ becomes a continuous random variable uniformly distributed between 0 and L. Thus, $\mathbb{E}[\|[L\ 0]^T - \mathbf{q}_{opt}\|_2^2] = \frac{L^2}{3}$ and if we use the inequality (5.17) in (5.38) then we can derive a lower bound:

$$\begin{aligned} \mathbb{E}[E_s(0,T)] &> \eta\alpha T_s\left(a_y^2 + \sigma_y^2\right) + \eta\int_{\alpha T_s}^{T_s}(a_y^2 + \sigma_y^2)d\tau \\ &+ \eta(T - T_s)a_y^2\left(a_h\ln\left(\frac{b_h\cdot L}{\lambda} + 1\right) + 1\right) + \eta(T-T_s)\sigma_y^2 - m_2(\alpha T_s)L^2 \\ &- m_2((1-\alpha)T_s)\mathbb{E}[\|[L\ 0]^T - \mathbf{q}_{opt}\|_2^2], \end{aligned} \tag{5.39}$$

$$\begin{aligned}\mathbb{E}[E_s(0,T)] &> \eta\alpha T_s\Big(a_y^2+\sigma_y^2\Big)+\eta(T_s-\alpha T_s)(a_y^2+\sigma_y^2)\\ &+ \eta(T-T_s)a_y^2\Big(a_h\ln\Big(\frac{b_h\cdot L}{\lambda}+1\Big)+1\Big)+\eta(T-T_s)\sigma_y^2-m_2(\alpha T_s)L^2\\ &- m_2((1-\alpha)T_s)\frac{L^2}{3},\end{aligned} \tag{5.40}$$

$$\begin{aligned}\mathbb{E}[E_s(0,T)] &> \eta T_s(a_y^2+\sigma_y^2)+\eta(T-T_s)a_y^2+\eta(T-T_s)\sigma_y^2\\ &+ \eta(T-T_s)a_y^2a_h\ln\Big(\frac{b_h\cdot L}{\lambda}+1\Big)\\ &- \Big(m_2(\alpha T_s)+\frac{1}{3}m_2((1-\alpha)T_s)\Big)\cdot L^2,\end{aligned} \tag{5.41}$$

$$\begin{aligned}\mathbb{E}[E_s(0,T)] &> \eta T_s(a_y^2+\sigma_y^2)+\eta(T-T_s)(a_y^2+\sigma_y^2)\\ &+ \eta(T-T_s)a_y^2a_h\ln\Big(\frac{b_h\cdot L}{\lambda}+1\Big)\\ &- \Big(m_2(\alpha T_s)+\frac{1}{3}m_2((1-\alpha)T_s)\Big)\cdot L^2,\end{aligned} \tag{5.42}$$

and then the lower bounds becomes:

$$\begin{aligned}\mathbb{E}[E_s(0,T)] &> \eta T\Big(a_y^2+\sigma_y^2\Big)+\eta(T-T_s)a_y^2a_h\ln\Big(\frac{b_h\cdot L}{\lambda}+1\Big)\\ &- \Big(m_2(\alpha T_s)+\frac{1}{3}m_2((1-\alpha)T_s)\Big)\cdot L^2\\ &= f_L(L,\alpha,T_s),\end{aligned} \tag{5.43}$$

Now, for the upper bound we use again the inequality (5.17) in (5.38) to obtain:

$$\begin{aligned}\mathbb{E}[E_s(0,T)] &< \eta\alpha T_s\Big(a_y^2+\sigma_y^2\Big)+\eta\int_{\alpha T_s}^{T_s}(a_y^2\mathbb{E}[|h(\mathbf{q}_{opt})|^2]+\sigma_y^2)d\tau\\ &+ \eta(T-T_s)a_y^2\Big(a_h\ln\Big(\frac{b_h\cdot L}{\lambda}+1\Big)+1\Big)+\eta(T-T_s)\sigma_y^2\\ &- \Big(m_2(\alpha T_s)+\frac{1}{3}m_2((1-\alpha)T_s)\Big)\cdot L^2,\end{aligned} \tag{5.44}$$

then using the approximation (5.18) to replace $\mathbb{E}[|h(\mathbf{q}_{opt})|^2]$ in (5.44) we have:

$$\begin{aligned}\mathbb{E}[E_s(0,T)] &< \eta\alpha T_s\Big(a_y^2+\sigma_y^2\Big)+\eta\int_{\alpha T_s}^{T_s}\left(a_y^2\Big(a_h\ln\Big(\frac{b_h\cdot L}{\lambda}+1\Big)+1\Big)+\sigma_y^2\right)d\tau\\ &+ \eta(T-T_s)a_y^2\Big(a_h\ln\Big(\frac{b_h\cdot L}{\lambda}+1\Big)+1\Big)+\eta(T-T_s)\sigma_y^2\\ &- \Big(m_2(\alpha T_s)+\frac{1}{3}m_2((1-\alpha)T_s)\Big)\cdot L^2,\end{aligned} \tag{5.45}$$

$$\begin{aligned}\mathbb{E}[E_s(0,T)] &< \eta\alpha T_s\Big(a_y^2+\sigma_y^2\Big)+\eta(T-\alpha T_s)\sigma_y^2 \\ &+ \eta(T-\alpha T_s)a_y^2\Big(a_h\ln\Big(\frac{b_h\cdot L}{\lambda}+1\Big)+1\Big) \\ &- \Big(m_2(\alpha T_s)+\frac{1}{3}m_2((1-\alpha)T_s)\Big)\cdot L^2, \end{aligned} \tag{5.46}$$

$$\begin{aligned}\mathbb{E}[E_s(0,T)] &< \eta\alpha T_s\Big(a_y^2+\sigma_y^2\Big)+\eta(T-\alpha T_s)\sigma_y^2+\eta(T-\alpha T_s)a_y^2 \\ &+ \eta(T-\alpha T_s)a_y^2a_h\ln\Big(\frac{b_h\cdot L}{\lambda}+1\Big) \\ &- \Big(m_2(\alpha T_s)+\frac{1}{3}m_2((1-\alpha)T_s)\Big)\cdot L^2, \end{aligned} \tag{5.47}$$

and so the upper bound becomes:

$$\begin{aligned}\mathbb{E}[E_s(0,T)] &< \eta T\Big(a_y^2+\sigma_y^2\Big)+\eta(T-\alpha T_s)a_y^2a_h\ln\Big(\frac{b_h\cdot L}{\lambda}+1\Big) \\ &- \Big(m_2(\alpha T_s)+\frac{1}{3}m_2((1-\alpha)T_s)\Big)\cdot L^2 \\ &= f_U(L,\alpha,T_s). \end{aligned} \tag{5.48}$$

Therefore instead of maximizing $\mathbb{E}[E_s(0,T)]$, for which we do not have an analytical expression, we can optimize its bounds, i.e., either $f_L(L,\alpha,T_s)$ or $f_U(L,\alpha,T_s)$. If we optimize the upper bound $f_U(L,\alpha,T_s)$ we risk obtaining a behaviour in which the average of the energy harvested is lower than the average energy used for the motion, because the energy harvested is over-estimated in this bound. On the other hand if we optimize the lower bound $f_L(L,\alpha,T_s)$ then we eliminate this risk because the energy harvested is under-estimated in this other bound. Therefore we will proceed to maximize the lower bound $f_L(L,\alpha,T_s)$.

Now, we can maximise $f_L(L,\alpha,T_s)$ by simultaneously solving the following set of equations:

$$\begin{aligned}&\tfrac{\partial f_L(L,\alpha,T_s)}{\partial L}=0,\\ &\tfrac{\partial f_L(L,\alpha,T_s)}{\partial \alpha}=0,\\ &\tfrac{\partial f_L(L,\alpha,T_s)}{\partial T_s}=0.\end{aligned} \tag{5.49}$$

Solving for the optimal length L the first equation in (5.49) gives:

$$L_{opt}(\alpha,T_s)=\frac{1}{2}\sqrt{\frac{\lambda^2}{b_h^2}+\frac{2\eta(T-T_s)a_y^2a_h}{m_2(\alpha T_s)+\frac{1}{3}m_2((1-\alpha)T_s)}}-\frac{\lambda}{2b_h}. \tag{5.50}$$

The objective of this technique is to obtain gain from the small-scale fading which varies considerably over small distances. In practice if L is too big then the shadowing and the path-loss effects cannot be considered constant anymore (as we have

assumed at the beginning of this chapter) and consequently this technique may not work properly anymore. Therefore in order to avoid this problem we will limit the maximum value of L to some predefined value L_{max} and so the bounded optimal value for L is:

$$L^b_{opt}(\alpha, T_s) = \begin{cases} L_{opt}(\alpha, T_s), & \forall\ L_{opt}(\alpha, T_s) < L_{max} \\ L_{max}, & \text{otherwise.} \end{cases} \tag{5.51}$$

Since the shadowing can usually be considered constant for distances of a few wavelengths then we would suggest selecting $L_{max} < 10\lambda$.

Now, if we substitute for L in $f_L(L, \alpha, T_s)$ with (5.51) then we obtain the modified optimization target $f_m(\alpha, T_s)$. We have to note that since $\alpha \in (0, 1)$ and $T_s \in (0, T)$ the domain of $f_m(\alpha, T_s)$ is finite. If we discretize this domain by applying a fine enough grid and then we use simulated annealing [32] to maximize $f_m(\alpha, T_s)$ over this grid we can ensure that we obtain a solution sufficiently close to the global maximum.

Finally, note that T_s is the execution time of the MDA and α determines the portion of T_s that one part of the MDA lasts (with $(1 - \alpha)$ the other part), see definition of phases 1 and 2 in section 5.2. Therefore by maximising $f_m(\alpha, T_s)$ we are optimising the execution time and the temporal duration of both parts of the MDA. In other words we are optimising the temporal aspects of the MDA (unlike in previous chapter) and by using (5.51) we are optimising the size of its continuous search space.

So now we have completed the optimization of the MDA to maximize the net average stored energy, $\mathbb{E}[E_s(0, T)]$. In the next section we will look at the estimator for $\mathbf{p}_{opt}$.

5.4 Estimation of Optimal Location $\mathbf{p}_{opt}$

In this section, we illustrate how the optimal location $\mathbf{p}_{opt}$ can be estimated from the noisy signal $r_e(k)$ in (5.8) (shorthand for $r_e(\mathbf{p}(k\Delta_s), k\Delta_s)$). This process is done once the robot finishes the first part of the MDA (phase 1 of the dead time). Let the sampling period be $\Delta_s = \frac{\alpha T_s}{N}$ and so the robot will use $N + 1$ measurements $[r_e(0),\ r_e(1), \ldots, r_e(N)]$. The MR can use a linear smoother to reduce the effect of the noise. Then it can employ the output of the smoother $r_s(k)$ instead of the signal $r_e(k)$ to obtain a better estimate for $\mathbf{p}_{opt}$. So, the estimation of $\mathbf{p}_{opt}$ can be performed as follows:

$$\hat{\mathbf{p}}_{opt} = \mathbf{p}(k_{opt}), \tag{5.52}$$

where

$$k_{opt} = \arg\max_k r_s(k), \tag{5.53}$$

and

$$r_s(k) = \sum_{m=0}^{N} \beta_{k,m}^* r_e(m). \tag{5.54}$$

Now, the optimal weights ($\beta_{k,m}^*$) for the linear smoother are calculated as follows:

$$\boldsymbol{\beta}_k^* = \arg\min_{\boldsymbol{\beta}_k} J(\boldsymbol{\beta}_k) \tag{5.55}$$

with

$$J(\boldsymbol{\beta}_k) = \mathbb{E}\left[\left(r_s(k) - a_y^2|h(\mathbf{p}(k))|^2\right)^2\right] \tag{5.56}$$

where $\boldsymbol{\beta}_k = [\beta_{k,0},\ \beta_{k,1},\ \ldots, \beta_{k,N}]^T$ and

$$\begin{aligned} J(\boldsymbol{\beta}_k) &= \mathbb{E}\left[r_s^2(k) - 2a_y^2 r_s(k)|h(\mathbf{p}(k))|^2 + a_y^4|h(\mathbf{p}(k))|^4\right] \\ &= \mathbb{E}\left[\left(\sum_{m=0}^{N} \beta_{k,m} r_e(m)\right)^2\right] - 2a_y^2 \sum_{m=0}^{N} \beta_{k,m}\mathbb{E}\left[r_e(m)|h(\mathbf{p}(k))|^2\right] \\ &+ a_y^4\mathbb{E}\left[|h(\mathbf{p}(k))|^4\right]. \end{aligned} \tag{5.57}$$

So setting

$$\nabla_{\boldsymbol{\beta}_k} J(\boldsymbol{\beta}_k) = \mathbf{0}, \tag{5.58}$$

where $\nabla_{\boldsymbol{\beta}_k} = [\frac{\partial}{\partial\beta_{k,0}},\ \frac{\partial}{\partial\beta_{k,1}}, \ldots,\ \frac{\partial}{\partial\beta_{k,N}}]^T$ and:

$$\frac{\partial J(\boldsymbol{\beta}_k)}{\partial \beta_{k,i}} = 2\sum_{m=0}^{N} \beta_{k,m}\mathbb{E}\left[r_e(m)r_e(i)\right] - 2a_y^2\mathbb{E}\left[r_e(i)|h(\mathbf{p}(k))|^2\right] \tag{5.59}$$

then it is not difficult to show that:

$$\begin{aligned} \mathbb{E}\left[r_e(i)|h(\mathbf{p}(k))|^2\right] &= a_y^2\mathbb{E}\left[|h(\mathbf{p}(i))|^2|h(\mathbf{p}(k))|^2\right] + \sigma_y^2 \\ &= a_y^2 J_0^2\left(\frac{2\pi\|\mathbf{p}(i) - \mathbf{p}(k)\|_2}{\lambda}\right) + a_y^2 + \sigma_y^2 \end{aligned} \tag{5.60}$$

$$\begin{aligned} \mathbb{E}\left[r_e(i)r_e(m)\right] &= a_y^4\left(J_0^2\left(\frac{2\pi\|\mathbf{p}(i) - \mathbf{p}(m)\|_2}{\lambda}\right) + 1\right) \\ &+ 2a_y^2\sigma_y^2 + \sigma_y^4 + \sigma_r^2,\ i \neq m \end{aligned} \tag{5.61}$$

and

$$\mathbb{E}\left[r_e^2(i)\right] = 2a_y^4 + 8a_y^2\sigma_y^2 + 8\sigma_y^4 + \sigma_r^2,\ i = m. \tag{5.62}$$

Therefore, if we know σ_y^2, σ_r^2 and a_y^2 (or we can estimate them) then we can evaluate (5.60), (5.61) and (5.62) and use in (5.59) to calculate an analytical expression for the gradient $\nabla_{\boldsymbol{\beta}_k} J(\boldsymbol{\beta}_k)$. So, we can solve (5.58) and obtain the optimal weights for the smoother in (5.54) in order to estimate $\mathbf{p}_{opt}$ with (5.52).

Table 5.2: Mobile robot parameters

$c_1 = 202.8169$W	$c_2 = 14.8885$N	$r = 9.5$cm
$c_A = 1.1279$Nm	$c_B = 14.8885$Nm	$b = 16.5$cm
$J_1 = 7 \cdot 10^{-2}$	$J_2 = 1.3 \cdot 10^{-3}$	

5.5 Simulation and Results

With the analytical framework developed in the previous sections, our objective now is to provide further insights by employing extensive simulations. To this end, we divide this section into two parts. In the first part, we analyze the energy harvesting technique that we have designed in this chapter in a noiseless scenario, that is assuming that $\hat{\mathbf{p}}_{opt} = \mathbf{p}_{opt}$. Then, in the second part we consider a noisy scenario and we analyze how the estimation error in $\hat{\mathbf{p}}_{opt}$ affects the energy harvested during the resting time in phase 3. We also observe how the optimal smoother described in section 5.4 can mitigate this degradation due to estimation error.

We will take the parameter values of [47] for the DDR since these values were obtained experimentally and therefore represent a real robot. This will allow us to get more realistic results in our simulations. In table 5.2 we show the MR's parameters. In addition, since the performance of the system depends on ηa_y^2 and $\eta \sigma_y^2$ and not on individual values of η we can assume for simulation purposes, and without any loss of generality, that $\eta = 1$ in (5.10).

5.5.1 Energy Harvesting Performance without Noise

Although ignoring the noise for the proposed technique would seem unrealistic, it is of practical interest to analyze the energy harvesting technique under such a consideration since it represents an upper bound on the performance of the proposed algorithm and also describes the behaviour of our technique when $SNR = \frac{a_y^2}{\sigma_y^2 + \sigma_r^2}$ is high.

In order to evaluate the performance of the energy harvesting technique, we now define a new metric called the "Energy Mobility Improvement Factor" (EMIF):

$$EMIF = \frac{\mathbb{E}[E_s(0,T)]}{\eta a_y^2 T}. \tag{5.63}$$

The numerator in (5.63) corresponds to the average net energy stored during the total dead time T while using mobility to harvest energy. The denominator is the expected value of the energy that the robot would harvest if it did not move at all. This metric quantifies how much the average net stored energy has been increased by moving the robot in comparison to the case where the robot does not move at all, and so we want $EMIF > 1$.

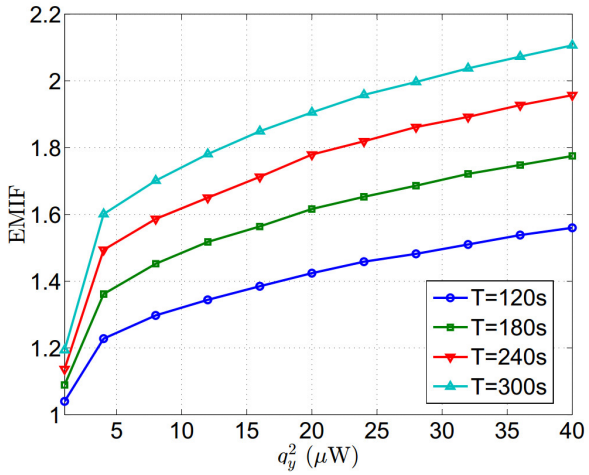

Figure 5.5: Comparison of EMIF vs a_y^2 (i.e., average received power) for different dead times T, with $N = \lceil \frac{16L_{opt}}{\lambda} \rceil$ and $\lambda = 6$cm (which corresponds to a carrier frequency of 5GHz).

We consider first the case in which the signal transmitted by the BS uses a carrier frequency of 5GHz (corresponding to a wavelength of 6cm). In Figs. 5.5 and 5.6 we can see the performance of the MR-EHT for a spatial sampling rate[9] $S_r > 16Sa/\lambda$, different dead times T and different average powers received a_y^2.

From these figures we first observe that indeed $EMIF > 1$ which shows that the optimal energy harvesting approach is to use intelligent motion. We also observe that EMIF is a nonlinear increasing function of both the dead time T and a_y^2, and so the higher the dead time T and/or the higher is a_y^2 then the larger will be the EMIF. In other words, when the dead time and/or the average received power are above a certain minimum our technique is more beneficial. Now, it is interesting to observe in Fig. 5.5 that if the robot has a dead time T of just 2 minutes and receives an average power $a_y^2 = 40\mu W$ then $EMIF > 1.5$. This implies that by optimally moving the robot the stored energy has increased by more than 50%. In a more beneficial case, for example with a dead time of $T = 5$min and an average receiving power of $a_y^2 = 50\mu W$, the benefit of moving the robot is even greater producing an EMIF higher than 2, i.e., an increase of more than 100% (see Fig. 5.6).

Now, in order to observe the effect of the wavelength of the RF signal transmitted by the BS we repeated exactly the same simulations but changed the wavelength to 14.02cm (which corresponds to a carrier frequency of 2.14GHz). So comparing Figs. 5.5 and 5.6 with 5.7 and 5.8 we observe that EMIF is considerably lower for the carrier frequency of 2.14GHz than for 5GHz.

This can be explained as follows: consider two robots using the same EHT de-

[9]This is obtained by making $N = \lceil \frac{16L_{opt}}{\lambda} \rceil$ in (5.21) with L_{opt} the optimal line length.

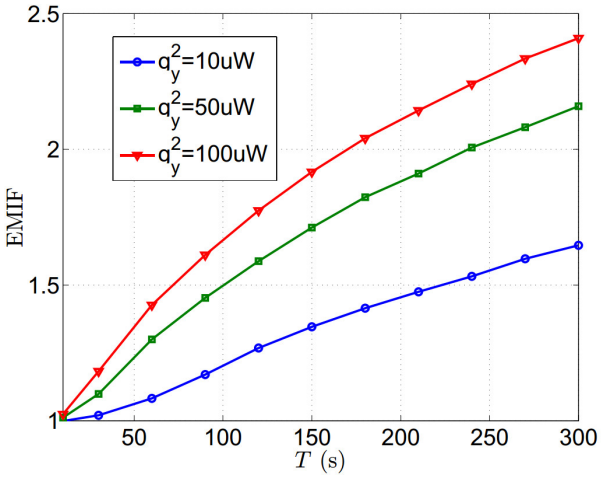

Figure 5.6: Comparison of EMIF vs T for different average received powers a_y^2, with $N = \lceil \frac{16L_{opt}}{\lambda} \rceil$ and $\lambda = 6$cm (which corresponds to a carrier frequency of 5GHz).

scribed in this chapter. Let the first robot receive a signal with wavelength λ_1 and let the second robot receive a signal of wavelength $\lambda_2 > \lambda_1$. If both robots move just one wavelength then the energy harvested will be the same since this energy depends only on the normalized distance (see (5.18)) but the second robot will have to travel a longer distance than the first one and so it will use a greater amount of mechanical energy. Thus the net energy stored (see (5.9)) by the second robot will be lower. This means that given the same conditions of received power and dead time duration our harvesting technique works better for small wavelengths. Nevertheless we should remark that the path loss increases with frequency [51]. Thus in the system using a smaller wavelength either the MR would have to be closer to the BS or the BS would have to transmit with higher power to meet the same conditions of received power as the system using a higher wavelength.

In Fig. 5.9, we observe the behaviour of $\mathbb{E}[|h_{\mathbf{opt}}|^2]$ as a function of the sampling rate S_r. We can observe it tends to saturate for a certain value of S_r and then in the noiseless case there is no reason to select S_r greater than $\approx 8Sa/\lambda$. But, as we shall see in the next subsection, higher values of S_r help to better estimate $\mathbf{p}_{opt}$ when noise is present.

We illustrate the behaviour of the optimal values of L, α and T_s in the figures 5.10 and 5.11. It is worth noticing that although L_{opt} is an increasing function of a_y^2 and T, we observe that $T_{s_{opt}}$ is an increasing function of a_y^2 but a decreasing function of T. This behaviour of T_s means that for a fixed received power a_y^2, if we increase the dead time T the robot will complete phases 1 and 2 slower to save more mechanical energy and increase the net stored energy. On the other hand if the dead time T is fixed but we increase the received power a_y^2 then the robot will complete phases

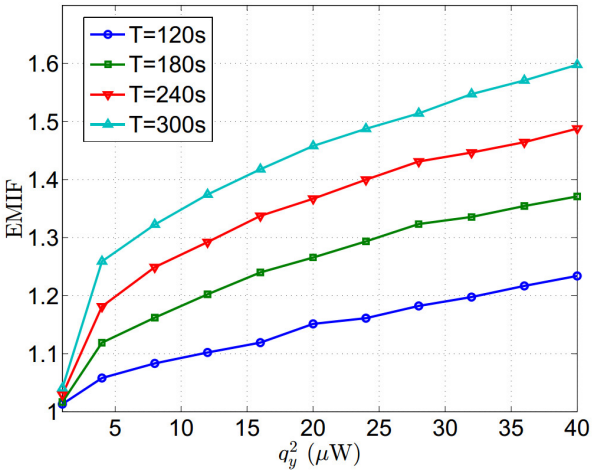

Figure 5.7: Comparison of EMIF vs a_y^2 (i.e., average received power) for different dead times T, with $N = \lceil \frac{16L_{opt}}{\lambda} \rceil$ and $\lambda = 14.02$cm (which corresponds to a carrier frequency of 2.14GHz).

1 and 2 faster to increase the duration of the resting time (phase 3). By doing so the robot increases the amount of energy harvested during this last phase and thus increases the net stored energy. Finally, it is also interesting to note that α_{opt} is independent of a_y^2 and is almost constant[10] for $T > 60$secs.

As mentioned earlier the channel coherence time is considered longer than the dead time (see definition in the Introduction and at the start of section III). So according to the values T presented in this simulation section it would seem that we are considering unrealistic values since in mobile communications coherence times are at most on the order of a couple of seconds or even miliseconds. Nevertheless, as mentioned earlier in the chapter, we are considering that the MR works in a extremely low mobility environment. Now, in [52] a narrow band wireless channel operating at a 2.4GHz in an environment with very little movement was experimentally characterized and the coherence time (referred to as time duration for which the temporal autocorrelation is higher than 90% of its maximum value) is 50 seconds. Therefore it seems natural that environments with extremely low mobility like museums at night or caves without people can exhibit coherence times on the order of a couple of minutes or at least tens of seconds.

[10]The optimal value of α was derived by optimizing $f_T(L, \alpha, T_s)$ which is a valid approximation for $\mathbb{E}[E_s(0,T)]$ as long as $S_r \geq 8Sa\lambda$. Therefore for values $S_r < 8Sa\lambda$ this behaviour may change slightly.

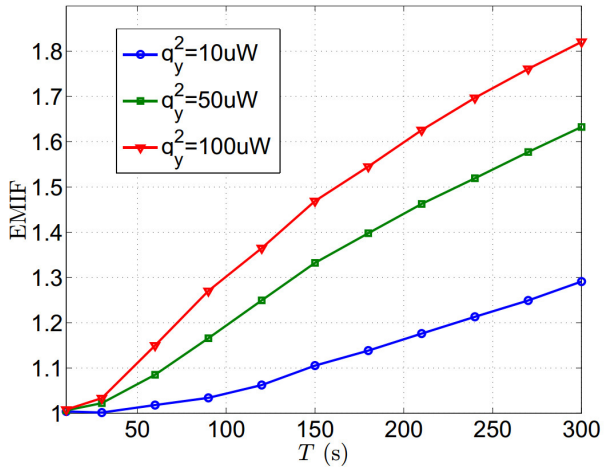

Figure 5.8: Comparison of EMIF vs T for different average received powers a_y^2, with $N = \lceil \frac{16L_{opt}}{\lambda} \rceil$ and $\lambda = 14.02$cm (which corresponds to a carrier frequency of 2.14GHz).

5.5.2 Energy Harvesting Performance with Noise

In this section, we consider the effect of the noise on the estimation of $\mathbf{p_{opt}}$ and its effect on the harvested energy (5.10) during the resting time (i.e., $t \in [T_s, T]$). Define $P_n = \sigma_y^2 + \sigma_r^2$ as the total noise power, i.e., the power of the pre-rectifier noise plus the power of the post-rectifier noise . Also let $\sigma_y^2 = \alpha_n P_n$ and $\sigma_r^2 = (1-\alpha_n)P_n$ with $\alpha_n \in (0,1)$. Finally define the SNR as $10\log_{10}\left(\frac{a_y^2}{P_n}\right)$. Let us consider three cases: (i) in the first case we consider that $\mathbf{p}_{opt}$ is estimated as in (5.52) using the optimal smoother of section 5.4 and we will denote this estimate by $\hat{\mathbf{p}}'_{opt}$; (ii) in the second case we consider that $\mathbf{p}_{opt}$ is estimated as in (5.52) but using the signal $r_e(k)$ instead of $r_s(k)$, the output of the smoother (5.54). We will denote this estimate by $\hat{\mathbf{p}}''_{opt}$; (iii) in the last case assume that the robot knows exactly $\mathbf{p}_{opt}$. While this case is unrealistic it will serve us for comparison.

We consider two scenarios with a low SNR of 0dB, line length $L = 1\lambda$, different values of α_n (for $\sigma_y^2 = \alpha_n P_n$ and for $\sigma_r^2 = (1-\alpha_n)P_n$) and two values of the spatial sampling rate: $S_r = 16Sa/\lambda$ and $S_r = 8Sa/\lambda$. In table 5.3 we observe the degradation[11] of the energy harvested during the third phase. In the first row we observe the degradation suffered when the MR uses the estimate $\hat{\mathbf{p}}'_{opt}$ and in the second row we observe the degradation when the MR uses the estimate $\hat{\mathbf{p}}''_{opt}$ mentioned above.

[11]The degradation is mathematically expressed as the ratio of the energy harvested during the resting time when $\hat{\mathbf{p}}_{opt} \neq \mathbf{p}_{opt}$ over the energy harvested during the resting time when $\hat{\mathbf{p}}_{opt} = \mathbf{p}_{opt}$. This ratio shows us how much the energy harvested has decreased due to the estimation error in $\hat{\mathbf{p}}_{opt}$.

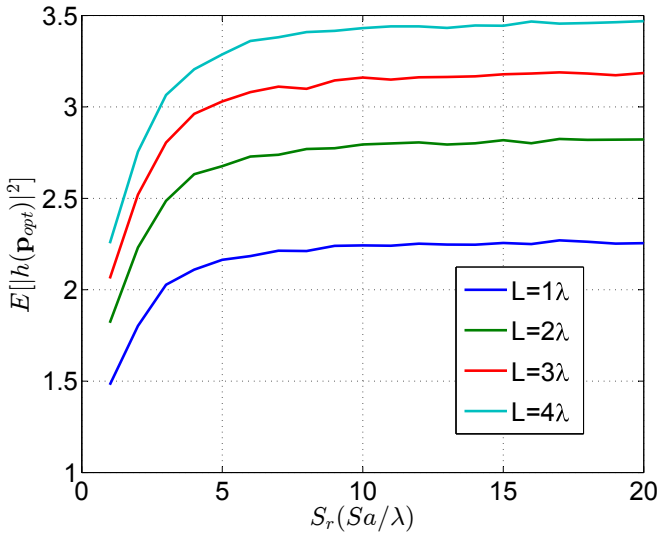

Figure 5.9: Behaviour of $\mathbb{E}[|h(\mathbf{p}_{opt})|^2]$ as a function of the spatial sampling rate S_r parameterized on different lengths of the exploration line (L).

Table 5.3: Harvested Energy degradation for $S_r = 16Sa/\lambda$

α_n	0.3	0.5	0.9
$\frac{\mathbb{E}[E_r(\hat{\mathbf{p}}'_{opt},T_s,T)]}{\mathbb{E}[E_r(\mathbf{p}_{opt},T_s,T)]}$	0.8731	0.8761	0.9004
$\frac{\mathbb{E}[E_r(\hat{\mathbf{p}}''_{opt},T_s,T)]}{\mathbb{E}[E_r(\mathbf{p}_{opt},T_s,T)]}$	0.8209	0.8070	0.8315

From tables 5.3 and 5.4 we see that the harvested energy degradation is lower for higher values of the spatial sampling rate S_r. This means that while in the noiseless scenario there is no reason to select a value of $S_r > 8Sa/\lambda$, in the noisy scenario taking higher values of S_r helps to combat the degradation of the energy harvested.

It is also interesting that the degradation of the energy harvested is not only a function of the SNR but also a function of α_n, (i.e., depending on the individual powers of the pre-rectifier noise $\sigma_y^2 = \alpha_n P_n$ and the power of the post-rectifier noise $\sigma_r^2 = (1-\alpha_n)P_n$). The degradation is higher for low values of α_n (see tables 5.3 and 5.4) which implies that the post-rectifier noise is more harmful to our technique than the pre-rectifier noise. Therefore, the RF designers should pay more attention to reducing the post-rectifier noise than the pre-rectifier noise when designing the energy harvesting receiver of figure 5.2.

5.6 Conclusions

We have shown that when harvesting radio energy with a MR the average, net amount of energy stored (i.e., the average energy harvested minus the average energy

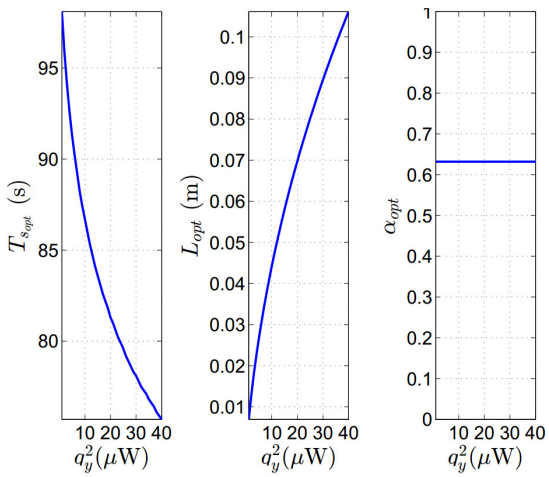

Figure 5.10: Optimal parameter values of $f_L(L, \alpha, T_s)$ vs a_y^2 for $T = 300$s, with $\lambda = 14.02$cm (which corresponds to a carrier frequency of 2.14GHz).

Table 5.4: Harvested Energy degradation for $S_r = 8Sa/\lambda$

α_n	0.3	0.5	0.9
$\frac{\mathbb{E}[E_r(\hat{\mathbf{p}}'_{opt}, T_s, T)]}{\mathbb{E}[E_r(\mathbf{p}_{opt}, T_s, T)]}$	0.8296	0.8449	0.8580
$\frac{\mathbb{E}[E_r(\hat{\mathbf{p}}''_{opt}, T_s, T)]}{\mathbb{E}[E_r(\mathbf{p}_{opt}, T_s, T)]}$	0.8018	0.8139	0.8222

used for movement) is higher when the robot is moved in an optimal way than when the robot simply stands still. This implies that the optimal behaviour for a MR using wireless energy harvesting under a flat-fading wireless channel is to move in an optimal way rather than not moving. That is an MDA can actually enhance RF energy harvesting under fading channels. We also showed how to optimise the size of the continuous search space of the MDA and also how to optimise its duration. While in this chapter we restricted the shape of the continuous search space and we limited ourselves to optimise only its size, in the next chapter we will show how we can also optimise the shape of the continuous search space.

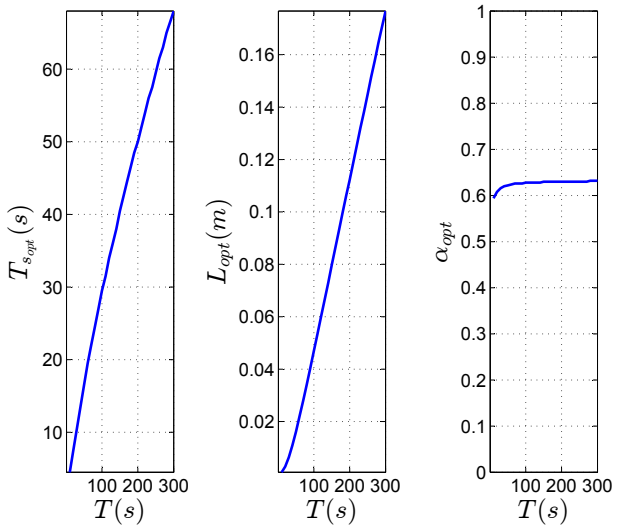

Figure 5.11: Optimal parameter values of $f_L(L, \alpha, T_s)$ vs T for $a_y^2 = 100\mu$W, with $\lambda = 14.02$cm (which corresponds to a carrier frequency of 2.14GHz).

Chapter 6

Continuous Search Space MDA

In general, MDAs work by ensuring that the MR estimates the channel gain over a search space in its close vicinity and then determines the optimum position using those channel gain estimates. The search space, the method used to explore it and the way to estimate the wireless channel gains all depend on the particular type of MDA. These algorithms can be divided depending on the class of search space which can be either discrete or continuous. In chapters 2 to 4, which forms the first part of this thesis, we treated the problem of MDAs with discrete search spaces and we provided different solutions to determine its shape for any number of stopping points. Then in chapter 5 we started treating the case of MDAs with continuous search space (but restricted to be a straight line). There we optimised only the length of the line.

In this chapter we consider a MR equipped with a single antenna wanting to establish communications, in a static environment, with a stationary node (also equipped with a single antenna) through a wireless channel experiencing small-scale fading. To compensate the small-scale fading we develop a continuous search space MDA which we will refer to as the continuous MDA (CMDA). Here, as opposed to the previous chapter, we will optimise the shape of its continuous search space. In addition we will also design the control law for the MR to explore such a continuous search space. So the main contribution of this chapter is the optimisation of the continuous search space shape.

In section 6.1 we present the models for the wireless channel and the MR. Then in section 6.2 we optimise the CMDA including its continuous search space and in section 6.3 we evaluate the performance of the CMDA under different conditions. Finally in section 6.4, some conclusions are given.

6.1 System Model

In this chapter we will consider again the three-wheel MR considered in chapters 2 and 3 and we will use also the same channel model, but for his respective convenience we will briefly again review these models.

6.1.1 MR Model

We will consider an omnidirectional MR, but in particular we select a three-wheel omnidirectional MR (TOMR) [24] for illustration purposes. However, the results of this chapter apply to any wheeled omnidirectional MR. A TOMR is a MR with three omnidirectional wheels [25] each of radius r and each wheel is driven by its own motor. The distance from the center of the robot to each wheel is L. The robot is equipped with a single antenna installed on its geometrical center. The TOMR model described in this subsection is a condensed version of the model presented in [47].

The TOMR position at time t is $\mathbf{p}(t) = [p_x(t) \;\; p_y(t)]^T$ and its pose is $\mathbf{p_o}(t) = [\mathbf{p}(t) \;\; \phi(t)]^T$ where $\phi(t)$ is its orientation. The TOMR pose is related to the control inputs as follows:

$$\ddot{\mathbf{p}}_\mathbf{o}(t) = \left(\mathbf{R}(t)\dot{\mathbf{R}}^T(t) - \mathbf{A}^{-1}\mathbf{C}\right)\dot{\mathbf{p}}_\mathbf{o}(t) + \mathbf{A}^{-1}\mathbf{R}(t)\mathbf{D}\mathbf{u}(t), \tag{6.1}$$

where $\mathbf{u}(t) = [u_1(t) \;\; u_2(t) \;\; u_3(t)]^T$ is the control input vector and $u_i(t)$ is the input for the ith motor; $\mathbf{A} = \text{diag}\left[m + \frac{3J_w}{2r^2}, m + \frac{3J_w}{2r^2}, J_c + \frac{3J_wL^2}{r^2}\right]$ where m is the total mass of the robot, r is the radius of the wheels, L is the distance from the geometric center of the robot to each wheel, and J_c and J_w are the inertia for the robot rotation and for each wheel respectively. We also have $\mathbf{C} = k_1\text{diag}[1, 1, 2L^2]$ with k_1 a robot-specific parameter. The matrix $\mathbf{D}$ is:

$$\mathbf{D} = k_2 \begin{bmatrix} 0 & -\sin(\pi/3) & \sin(\pi/3) \\ 1 & -\cos(\pi/3) & -\cos(\pi/3) \\ L & L & L \end{bmatrix}, \tag{6.2}$$

where k_2 is a robot-specific parameter. And the rotation matrix $\mathbf{R}(t)$ is given by:

$$\mathbf{R}(t) = \begin{bmatrix} \cos(\phi(t)) & -\sin(\phi(t)) & 0 \\ \sin(\phi(t)) & \cos(\phi(t)) & 0 \\ 0 & 0 & 1 \end{bmatrix}. \tag{6.3}$$

The energy drawn from the battery by the MR due to motion overtime period t_0 to t_f is:

$$\begin{aligned} E_{mech}(t_0, t_f, \mathbf{u}(t)) &= k_3 \int_{t_0}^{t_f} \mathbf{u}^T(t)\mathbf{u}(t)dt \\ &- k_4 \int_{t_0}^{t_f} \dot{\mathbf{p}}_\mathbf{o}^T(t)\mathbf{R}(t)\mathbf{D}\mathbf{u}(t)dt, \end{aligned} \tag{6.4}$$

where k_3 and k_4 are also robot-specific parameters.

6.1.2 Wireless Channel Model

We assume that there is no line of sight between the stationary node[1] and the MR; that the signal transmitted by the stationary node to the MR is narrowband (i.e., the bandwidth of the signal is significantly smaller than the radio frequency carrier frequency used in the transmission); that the MR's environment is stationary (i.e., it does not change with time during the execution of the MDA) and presents a large number of scatterers (which produce the small-scale fading). Consequently, the wireless channel is time invariant (for a given MR position) and presents Rayleigh flat fading [12]. Thus, the signal received by the MR at time instant t, when located at $\mathbf{p}(t)$, is:

$$z(t) = h(\mathbf{p}(t)) \cdot w(t) + n(t), \tag{6.5}$$

where $w(t)$ is the narrowband signal transmitted by the stationary node, $n(t) \sim \mathcal{CN}(0, \sigma_n^2)$ is the additive white Gaussian noise generated at the MR's receiver and $h(\mathbf{p}(t))$ represents the small-scale fading. We will assume Jakes' model [28] for the small scale fading term and so $h(\mathbf{p}(t)) \sim \mathcal{CN}(0, 1)$. The spatial normalized correlation function is thus:

$$r(\mathbf{p}, \mathbf{q}) = \mathbb{E}\left[h(\mathbf{p})h^*(\mathbf{q})\right] = J_0\left(2\pi\|\mathbf{p} - \mathbf{q}\|_2/\lambda\right), \tag{6.6}$$

where λ is the wavelength used in the RF transmission and $\mathbf{p}, \mathbf{q} \in \mathbb{R}^2$ are any two points in the space.

6.2 Continuous Mobility Diversity Algorithm

For this algorithm the stationary node initially works as a transmitter over T_f seconds ($t \in [0, T_f]$) and transmits a pure tone to allow the MR to collect wireless channel measurements during the CMDA execution. Thus the signal received by the MR during that period is:

$$z(t) = h(\mathbf{p}(t))K + n(t) \tag{6.7}$$

where K is the amplitude of the received tone. Once this period finishes the stationary node recalibrates its behaviour as a receiver and waits for a reply from the MR to establish communication.

Note that for MDAs with continuous search space their search space is a continuous path and so, for the rest of the chapter, we will refer to the continuous search space of the CMDA as the continuous exploration path $\mathcal{P}$.

The CMDA starts when the stationary node initiates its transmission and it is divided into the 'exploration phase' $t \in [0, T_e]$ and the 'positioning phase' $t \in [T_e, T_f]$. The MR initiates the algorithm from a stationary position at the start of the continuous exploration path $\mathcal{P}$. During the 'exploration phase' the MR follows

[1] The stationary node can be a base station or another MR which remains stationary during the CMDA execution.

the continuous path $\mathcal{P}$ while estimating the wireless channel all along it. At time instant T_e the MR stops at the end of the continuous exploration path $\mathcal{P}$. Then it invokes a selection rule to determine the optimum point $\mathbf{q}_{opt} \in \mathcal{P}$ and moves from the end of $\mathcal{P}$ to $\mathbf{q}_{opt}$ in a time $T_f - T_e$ in order to establish communications with the stationary node. This last stage is called the 'positioning phase'. Note that the MDA of the previous chapter was also divided into two phases and operated in a similar manner.

In the next subsection we show how to optimize the continuous exploration path $\mathcal{P}$ for the CMDA.

6.2.1 Optimum Exploration Path

We want to optimize the exploration path $\mathcal{P}$ so that when used within the CMDA it generates a high expected value for the channel gain at $\mathbf{q}_{opt}$ (i.e., $\mathbb{E}[|h(\mathbf{q}_{opt})|]$). The main problem for achieving this is that in general there is not an analytical expression for $\mathbb{E}[|h(\mathbf{q}_{opt})|]$ as a function of the continuous path $\mathcal{P}$. So, in practice[2] we cannot optimize $\mathcal{P}$ directly. Nevertheless there is an alternative approach. To do this let us first define the set of path points $\mathcal{D}_N = \{\mathbf{d}_1, \mathbf{d}_2, \cdots, \mathbf{d}_N\}$ associated with the following restriction:

$$\|\mathbf{d}_j - \mathbf{d}_{j+1}\|_2 = \frac{L_p}{N-1}, \quad j = 1, 2, \cdots, N-1. \tag{6.8}$$

Note that for any given continuous path $\mathcal{P}$ with length L_p and a value N high enough there exists a set $\mathcal{D}_N$ with the restriction (6.8) such that:

$$\mathcal{I}\{\mathcal{D}_N\} \approx \mathcal{P}. \tag{6.9}$$

where $\mathcal{I}\{\mathcal{D}_N\}$ is an interpolation of $\mathcal{D}_N$. It is intuitive that the higher a value for N the better the approximation (6.9) will be.

Consider now that a particular set $\mathcal{D}_N$ has a large enough value of N which according to (6.9) is a good approximation for the particular continuous path $\mathcal{P}$. If instead of allowing $\mathbf{q}_{opt} \in \mathcal{P}$ we impose the restriction $\mathbf{q}_{opt} \in \mathcal{D}_N$ then we still do not have an analytical expression for $\mathbb{E}[|h(\mathbf{q}_{opt})|]$. But the results of [53] imply that if the norm of the spatial correlation matrix of the wireless channels at the path points $\mathcal{D}_N$ is high (low) then $\mathbb{E}[|h(\mathbf{q}_{opt})|]$ will be low (high). So if given N, the set $\mathcal{D}_N$ minimizes the Frobenius norm of the spatial correlation matrix of the wireless channels at the path points then $\mathbb{E}[|h(\mathbf{q}_{opt})|]$ will be high under the constraint $\mathbf{q}_{opt} \in \mathcal{D}_N$. This implies that $\mathbb{E}[|h(\mathbf{q}_{opt})|]$ (with $\mathbf{q}_{opt} \in \mathcal{P}$) will also be higher. In other words, the continuous path $\mathcal{P}$ obtained from the interpolation of $\mathcal{D}_N$ will produce a high channel gain. Therefore a practical way to indirectly optimize the continuous

[2]Theoretically we could obtain by simulations an approximation to the term $\mathbb{E}[|h(\mathbf{q}_{opt})|]$ for each continuous path but this would require an extremely large amount of calculations, thus making the direct optimization of $\mathbb{E}[|h(\mathbf{q}_{opt})|]$ prohibitive in practice.

path $\mathcal{P}$ is to optimize the set $\mathcal{D}_N$ to minimize its spatial correlation matrix and then interpolate the path points to obtain the optimum continuous path $\mathcal{P}$. This optimum continuous path $\mathcal{P}$ will be referred to as the minimum correlation path (MCP). Taking all this into account we can optimize $\mathcal{D}_N$ as follows:

$$\begin{aligned} &\min_{\phi_1,\phi_2,\cdots,\phi_{N-1}} \|\mathbf{C}_N\|_F^2 \\ &\text{s.t.} \\ &\|\mathbf{d}_{j+1}-\mathbf{d}_j\|_2 = \tfrac{L_p}{N-1}, \quad j=1,2,\cdots,N-1, \\ &\measuredangle\{\mathbf{d}_{j+1}-\mathbf{d}_j\} = \phi_j \in [0,2\pi), \quad j=1,2,\cdots,N-1 \end{aligned} \tag{6.10}$$

where $\mathbf{C}_N$ is the spatial correlation matrix of the wireless channel at the path points with the (m,n) entry being given by $r(\mathbf{d}_m,\mathbf{d}_n)$ (see (6.6)) and $\|\cdot\|_F$ is the Frobenius norm. When this norm is low the expected value of the channel gain at $\mathbf{q}_{opt} \in \mathcal{P}$ will be large. Since the domain of the optimization space for (6.10) is bounded and we have an analytical expression to calculate the cost function we can solve this problem numerically using simulated annealing [32].

For the special case when $L_p/\lambda \leq z_0$, and where z_0 is the smallest value of z that satisfies $J_0(2\pi z)=0$, we can demonstrate that the general solution of (6.10) for any N is $\mathbf{d}_j = \mathbf{d}_1 + \frac{(j-1)L_p}{N-1}[\cos(\phi_1)\ \sin(\phi_1)]^T$ for all $1 < j \leq N$.

Now we show how to interpolate the path points $\mathcal{D}_N$ using splines [54] to obtain the continuous exploration path $\mathcal{P}$. We want the MR to be able to move through the continuous exploration path without stopping until it reaches the end of the path. To achieve this, the continuous path $\mathcal{P}$ should be significantly smooth. So we will use second-order[3] splines to perform the interpolation of the path points $\mathcal{D}_N$ to obtain $\mathcal{P}$. The parameterized function for the continuous path $\mathcal{P}$ is then obtained by:

$$\mathbf{g}(s) = \begin{cases} \Pi_j(s-j), \ \forall s \in [j,j+1), \ j=1,2,\ldots,N-1 \\ \Pi_{N-1}(1), \ \text{otherwise} \end{cases} \tag{6.11}$$

where $s \in [0,N-1]$ is a free parameter and $\Pi_j(s)$ is a two-dimensional second-order polynomial vector:

$$\Pi_j(s) = \mathbf{a}_j + \mathbf{b}_j s + \mathbf{c}_j s^2 \tag{6.12}$$

where $\mathbf{a}_j$, $\mathbf{b}_j$ and $\mathbf{c}_j$ are vector coefficients to be calculated below. In addition the polynomials must satisfy the following restrictions:

$$\Pi_j(1) = \Pi_{j+1}(0) = \mathbf{d}_{j+1}, \quad j=1,2,\cdots,N-2 \tag{6.13}$$

$$\frac{\mathrm{d}\Pi_j(s)}{\mathrm{d}s}\Big|_{s=1} = \frac{\mathrm{d}\Pi_{j+1}(s)}{\mathrm{d}s}\Big|_{s=0}, \quad j=1,2,\cdots,N-2 \tag{6.14}$$

$$\Pi_1(0) = \mathbf{d}_1, \quad \Pi_{N-1}(1) = \mathbf{d}_N. \tag{6.15}$$

[3]Second-order splines are enough to allow the MR to traverse the continuous path $\mathcal{P}$ with continuous velocity and without needing to stop due to abrupt direction changes.

The restriction (6.13) ensures the continuity of the exploration path; restriction (6.14) ensures the smoothness of the exploration path $\mathcal{P}$; and (6.15) ensures that the starting and ending points of the exploration path $\mathcal{P}$ are $\mathbf{d}_1$ and $\mathbf{d}_N$. Later we will explain how to decide which one is the starting point and which one is the ending point. To satisfy these restrictions we can select either $\Pi_1(s)$ to be a first-order polynomial vector (i.e., $\mathbf{c}_1 = \mathbf{0}$) and then calculate the coefficient of the polynomial vectors or select $\Pi_{N-1}(s)$ to be a first-order polynomial (i.e., $\mathbf{c}_{N-1} = \mathbf{0}$) and then calculate the coefficient of the polynomial vectors. Without loss of generality we will arbitrarily choose the first option, i.e., $\mathbf{c}_1 = \mathbf{0}$.

Now, after choosing $\mathbf{c}_1 = \mathbf{0}$, in order to satisfy restrictions (6.13)-(6.15) we can calculate $\mathbf{a}_1$ and $\mathbf{b}_1$ as follows:

$$\mathbf{a}_1 = \mathbf{d}_1, \tag{6.16}$$
$$\mathbf{b}_1 = \mathbf{d}_2 - \mathbf{d}_1, \tag{6.17}$$

and then we can calculate iteratively in ascending order of j the rest of the coefficients of $\Pi_j(s)$ as follows:

$$\mathbf{a}_j = \mathbf{d}_j, \tag{6.18}$$
$$\mathbf{b}_j = \mathbf{b}_{j-1} + 2\mathbf{c}_{j-1}, \tag{6.19}$$
$$\mathbf{c}_j = \mathbf{d}_{j+1} - \mathbf{a}_j - \mathbf{b}_j. \tag{6.20}$$

Finally, note that the real length L'_p of the continuous exploration path $\mathcal{P}$ is:

$$L'_p = \int_0^{N-1} \left\| \frac{\mathrm{d}\mathbf{g}(s)}{\mathrm{d}s} \right\|_2 \mathrm{d}s, \tag{6.21}$$

and in general we have $L'_p \geq L_p$ where the equality only holds if $\mathbf{c}_j = \mathbf{0}$ for all $j = 1, 2, \cdots, N-1$.

From Fig. 6.1 we can observe how the shape of the MCP changes significantly as L_p increases. We demonstrated before that for $L_p/\lambda \leq z_0$ the optimum path is a straight line and from Fig. 6.1 we observe that at least until $L_p \leq 0.6\lambda$ the optimum path remains an straight line. We have to mention that as L_p increases, solving (6.10) becomes more problematic since the number of local minima seems to increase. So for this chapter we solved (6.10) only up to $L_p = 1.8\lambda$.

Finally, we briefly discuss the sense in which the MR will traverse the exploration path $\mathcal{P}$. Consider now the set $\mathcal{D}_N^* = \{\mathbf{d}_1^*, \mathbf{d}_2^*, \cdots, \mathbf{d}_N^*\}$ that minimizes (6.10). The question is, whether the MR must traverse the path $\mathcal{P}$ from $\mathbf{d}_1^*$ to $\mathbf{d}_N^*$ or from $\mathbf{d}_N^*$ to $\mathbf{d}_1^*$. The optimum traversing sense is the one that minimizes the average distance to be travelled during the positioning phase. So we chose the sense that minimizes the average distance from its final end point to $\mathbf{q}_{opt}$. Now, since the wireless channel at all the path points is identically distributed it can be shown that $\mathbf{q}_{opt} \in \mathcal{D}_N^*$ is a

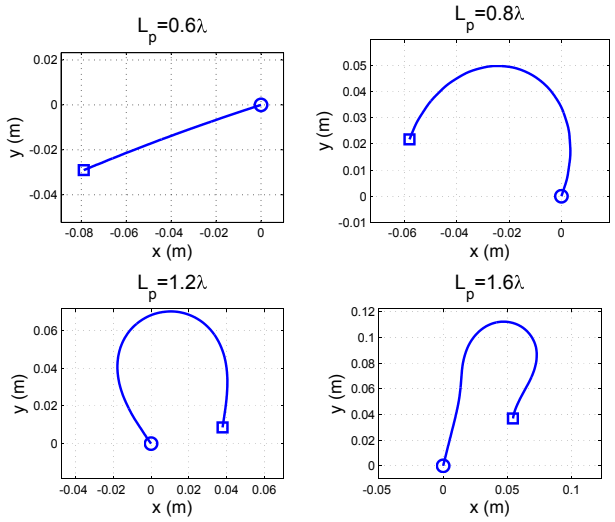

Figure 6.1: Optimized continuous path $\mathcal{P}$ for $N = 25$, $\lambda = 14.02$cm and different values of L_p. The start point $\mathbf{d}_1$ and the end point $\mathbf{d}_N$ are represented with a circle and a square respectively.

discrete random variable (almost) uniformly distributed across all the path points in $\mathbf{D}_N^*$ and so the average distance between the ending point and $\mathbf{q}_{opt}$ is:

$$J(k) \approx \frac{1}{N} \sum_{j=1}^{N} \|\mathbf{d}_j^* - \mathbf{d}_k^*\|_2, \quad k = 1 \text{ and } N \tag{6.22}$$

So if $J(1) < J(N)$ we choose $\mathbf{d}_1^*$ as the starting point and $\mathbf{d}_N^*$ as the ending point; we do the opposite if $J(1) > J(N)$. Nevertheless, if the continuous path presents some symmetry we can have $J(1) = J(N)$ in which case we can arbitrarily choose either.

By optimizing the sense in which the MR explores the continuous path $\mathcal{P}$ we minimise the distance that it has to travel during the positioning phase and consequently minimise the energy used for motion during that phase. For the rest of the chapter, for simplicity purposes and without loss of generality, we assume that the sense in which the MR traverses $\mathcal{P}$ has already been optimised resulting in $\mathbf{d}_1$ and $\mathbf{d}_N$ being the start and end points respectively of the exploration path $\mathcal{P}$.

Note that the mechanical energy is not considered in the optimisation of the exploration path but it will be considered in the optimisation of the trajectory that will traverse the optimum path that we have designed. This is because the joint optimisation of the path and the mechanical energy is too complex. This approach gives more importance to obtaining a high channel gain from the continuous exploration path than to the minimisation of the mechanical energy. Nevertheless, even with this approach the mechanical energy used can be indirectly controlled by selecting the length L_p of the path. In addition we have to note from Fig. 6.1 that the curvatureof the optimized path $\mathcal{P}$ (when the path is not a straight line) shortens the

average distance travelled during the positioning phase by the MR and consequently reduces the mechanical energy used with respect to the case in a straight line path of the same length is selected. Therefore although the optimization of the path $\mathcal{P}$ indirectly reduces and limits the mechanical energy expenditure even if it does not considers it explicitly.

6.2.2 Trajectory Design

Once we have the continuous exploration path $\mathcal{P}$ (described by its parameterized function $g(s)$) we need to design the optimum control law that makes the MR follow $\mathcal{P}$ during the searching phase. To obtain such a control law we first use the computed torque technique [24] to control directly the acceleration of the MR. This produces the following control law:

$$\mathbf{u}(t) = \mathbf{D}^{-1}\mathbf{R}^{-1}(t)\mathbf{A}\left(\left(\mathbf{A}^{-1}\mathbf{C} - \mathbf{R}(t)\dot{\mathbf{R}}^{T}(t)\right)\dot{\mathbf{p}}_o(t) + \mathbf{w}(t)\right), \tag{6.23}$$

$$\mathbf{w}(t) = \left[\ddot{\mathbf{g}}^{T}(s(t)), \quad 0\right]^{T}, \tag{6.24}$$

where $s(t)$ is a continuous function to be optimized that satisfies $s(0) = 1$ and $s(T_e) = N$. Then by substituting (6.23) and (6.24) into (6.1) we obtain:

$$\ddot{\mathbf{p}}_{\mathbf{o}}^{\mathbf{T}}(t) = \left[\ddot{\mathbf{g}}^{T}(s(t)), \quad 0\right]^{T}. \tag{6.25}$$

This equation implies that the MR will follow the continuous exploration path $\mathcal{P}$ described by its parametrization $\mathbf{g}(s(t))$.

To finish the design of the MR trajectory for the exploration phase we need to determine $s(t)$. In order to make the MR follow the complete exploration path $\mathcal{P}$ and ensure that it is still at the starting ($\mathbf{d}_1$) and ending ($\mathbf{d}_N$) points of the exploration path $\mathcal{P}$ we need to satisfy $s(0) = 1$, $s(T_e) = N$, $\dot{s}(0) = 0$ and $\dot{s}(T_e) = 0$. A simple way to satisfy these restrictions is to restrict the velocity $\dot{s}(t)$ to be a trapezoidal function, and so $s(t)$ becomes:

$$s(t) = \begin{cases} \frac{t^2\beta}{2\alpha} + 1 & 0 \leq t < \alpha \\ \beta t - \frac{\alpha\beta}{2} + 1 & \alpha \leq t \leq T_e - \alpha \\ \frac{-\beta(T_e - t)^2}{2\alpha} + \beta(T_e - \alpha) + 1 & T_e - \alpha < t \leq T_e \end{cases} \tag{6.26}$$

with:

$$\beta = \frac{N-1}{T_e - \alpha} \tag{6.27}$$

where $\alpha \in (0, T_e/2]$. The control law described by (6.23) and (6.24) with $s(t)$ given by (6.26) and (6.27) will be denoted as $\mathbf{u}_{ep}(t)$. And $\mathbf{u}^*_{ep}(t)$ will be the optimized control law with respect to α so that it minimizes the amount of energy used in motion during the exploration phase.

Now regarding the positioning phase, the MR must move from $\mathbf{d}_N$ to the optimum point $\mathbf{q}_{opt}$ in $T_f - T_e$ seconds and then stop. Since we are considering an omnidirectional MR then it can move in a straight line between those points. An optimum control law that executes this movement using minimum energy for this MR can be found in chapter 2 and it will be referred to as $\mathbf{u}^*_{pp}(t)$.

Now, if we assume that no early stopping mechanism is used then we can optimize T_e, the duration of the exploration phase, to minimize the total energy consumed during the CMDA execution as follows:

$$\begin{aligned} &\min_{T_e} E_{mech}(0, T_e, \mathbf{u}^*_{ep}(t)) + \mathbb{E}\left[E_{mech}(T_e, T_f, \mathbf{u}^*_{pp}(t))\right] \\ &s.t. \\ &0 < T_e < T_f \end{aligned} \tag{6.28}$$

with:

$$\mathbb{E}\left[E_{mech}(T_e, T_f, \mathbf{u}^*_{pp}(t))\right] = \mathcal{K}(T_f - T_e)\mathbb{E}[\|\mathbf{q}_{opt} - \mathbf{d}_N\|_2^2] \tag{6.29}$$

where the expression for $\mathcal{K}(T_f - T_e)$ can be found in [16]. Now, for the paths that we have designed, we observed from numerous simulation results that $\mathbf{q}_{opt} \in \mathcal{P}$ is a random variable which for practical purposes is almost[4] uniformly distributed along the exploration path $\mathcal{P}$. Hence we can make the following approximation:

$$\mathbb{E}[\|\mathbf{q}_{opt} - \mathbf{d}_N\|_2^2] \approx \frac{1}{N}\sum_{j=1}^{N} \|\mathbf{d}_j - \mathbf{d}_N\|_2^2 . \tag{6.30}$$

Note that this is not a general result and so for other types of exploration paths the random variable $\mathbf{q}_{opt}$ may be significantly far from being uniformly distributed.

By substituting the approximation (6.30) into (6.29) we have now a complete analytical expression for the cost function of (6.28). It can be seen that the first term in (6.28) is a strictly decreasing positive function of T_e while the second term is a strictly increasing positive function of T_e. Therefore, unless the cost function of (6.28) is constant, it has a unique minimum and then we can minimize this cost function by adapting the hill-climbing search algorithm [32].

This concludes the design of the control laws for both the exploration and positioning phases. In the next subsection we will show how to collect and process the wireless channel measurements to determine $\mathbf{q}_{opt}$.

[4]The main reason why $\mathbf{q}_{opt}$ is not exactly uniformly distributed is because according to the simulations the probability that $\mathbf{q}_{opt} = \mathbf{q}_1$ or $\mathbf{q}_{opt} = \mathbf{q}_N$ is slightly higher than the other posibilities. This is may be due their location the channels at these points are less correlated to the rest of the channels.

6.2.3 $\mathbf{q}_{opt}$ Determination and Channel Estimation

In this subsection we first show how the MR estimates the wireless channel along $\mathcal{P}$ and then we explain how it can use these estimates to determine $\mathbf{q}_{opt}$.

During the exploration phase the stationary node transmits a pure tone so that the MR estimates the wireless channel along $\mathcal{P}$ and so the signal (see (6.5)) received by the MR during this phase becomes:

$$z(t_s(k)) = Kh(\mathbf{p}(t_s(k))) + n(t_s(k)), \tag{6.31}$$

where K is the amplitude of the tone transmitted and $t_s(k)$ are the sampling instants. The sampling instants are chosen so that the samples are uniformly distributed along the path $\mathcal{P}$ and so:

$$\int_{s(t_s(k))}^{s(t_s(k+1))} \left\| \frac{\mathrm{d}\mathbf{g}(s)}{\mathrm{d}s} \right\|_2 \mathrm{d}s = \frac{L'_p}{M-1}, \quad k = 1, 2, \cdots, M-1 \tag{6.32}$$

where M is the number of samples taken along the continuous path $\mathcal{P}$. Note that the temporal sampling rate in general is not uniform. In the CMDA the MR moves continuously along the exploration path $\mathcal{P}$ without stopping while collecting only one noisy measurement of the wireless channel per point as opposed to the MDMTA of chapter 2 where the MR can collect various wireless channel measurements per stopping point. To obtain a good channel estimate at the sampling point $\mathbf{p}(t_s(k))$ the MR needs to combine the measurement collected at the sampling point $\mathbf{p}(t_s(k))$ with the measurements collected at other sampling points as follows:

$$\hat{h}_s(\mathbf{p}(t_s(k)), \mathcal{S}_k(d)) = \sum_{j \in \mathcal{S}_k(d)} a_{k,j} z(t_s(j)) \tag{6.33}$$

where $\hat{h}_s(\mathbf{p}(t_s(k)), \mathcal{S}_k(d))$ is the estimate for $h(\mathbf{p}(t_s(k)))$ using the measurements collected at $\mathcal{S}_k(d)$ which contains all sampling points included in a ball of radius d centered at the sampling point $\mathbf{p}(t_s(k))$:

$$\mathcal{S}_k(d) = \{\mathbf{p}(t_s(j)) \ : \ \|\mathbf{p}(t_s(j)) - \mathbf{p}(t_s(k))\|_2 \leq d\}. \tag{6.34}$$

By using only the measurements collected at $\mathcal{S}_k(d)$, and using the appropriate value of d, the MR uses only measurements that are highly correlated to $h(\mathbf{p}(t_s(k)))$ and neglects the rest, thus reducing the computational load of the estimation process.

Now, to optimize the coefficients $a_{k,j}$ for the estimator in (6.33) we minimize the following error:

$$e_k = \mathbb{E}\left[\left| Kh(\mathbf{p}(t_s(k))) - \sum_{j \in \mathcal{S}_k(d)} a_{k,j} z(t_s(j)) \right|^2 \right]. \tag{6.35}$$

It can be shown that the optimal coefficients $a^*_{k,j}$ that minimize (6.35) are given by:

$$\mathbf{a}^* = \left(\mathbf{C}_{\mathcal{S}_k(d)} + \frac{\sigma_n^2}{K^2}\mathbf{I}\right)^{-1} \mathbf{C}_{\mathcal{S}_k(d)}(:,k) \tag{6.36}$$

where $\mathbf{a}^* = [a^*_{k,1},\ a^*_{k,2}, \cdots, a^*_{k,N_s}]^T$, $\mathbf{C}_{\mathcal{S}_k(d)}$ is spatial correlation matrix of the wireless channels at $\mathcal{S}_k(d)$ whose entries can be calculated using (6.6) and $\mathbf{C}_{\mathcal{S}_k(d)}(:,k)$ is the kth column of this matrix.

Once we have estimates for all the channel gains we can use a selection rule that chooses $\mathbf{q}_{opt}$ as the point with the highest estimated channel gain. This concludes the discussion on the theoretical development of the CMDA.

6.3 Simulations

We first show the benefits of executing the CMDA with the optimum path obtained by solving (6.28). We then execute the CMDA, for comparison purposes, with the linear path (LP) used in [55] and [16] or the circular path (CP) used in [13] and [16].

As mentioned in section 6.2.1 we optimise indirectly the exploration path $\mathcal{P}$ by first optimising the set of path points $\mathcal{D}_\mathcal{N}$ according to (6.10) and then interpolating them instead of directly optimising the continuous path $\mathcal{P}$. In order to make the indirect optimisation of $\mathcal{P}$ a good approximation to its direct optimisation we need to select N large enough. To do this, for a given length L_p, we optimise the set of path points $\mathcal{D}_\mathcal{N}$ and interpolate them for different values of N. Then as N is increased we observe how the shape of the resulting path changes. Once the shape of the exploration path remains unchanged we can assume that we have reached a value of N large enough so that the indirect optimisation[5] of $\mathcal{P}$ results in a good approximation to its direct optimisation.

Now, in these simulations we will obtain the MCP for $0.2\lambda \leq L_p \leq 1.8\lambda$. To do this we will optimise the path points $\mathcal{D}_\mathcal{N}$ according to (6.10) with $N = 25$, which according to the explanation given above is a sufficiently large enough value of N for $L_p \leq 1.8\lambda$.

For this section we set $T_f = 3$s while T_e is optimized according to (6.28) for every path. The number of sampling points is selected as follows:

$$M = \left\lceil \frac{L'_p}{\Delta} \right\rceil + 1 \tag{6.37}$$

where Δ is the desired distance between sampling points. Due to the ceiling function in (6.37) the real distance between sampling points along the continuous path (6.32)

[5]The optimum continuous path derived via the indirect optimisation explained in 6.2.1 is called the minimum correlation path (MCP).

Table 6.1: TOMR parameters

$m = 1.989\text{kg}$	$J_c = 0.020691\text{kg} \cdot \text{m}^2$	$J_w = 0.060\text{g} \cdot \text{m}^2$
$r = 3\text{cm}$	$L = 12.55\text{cm}$	$k_1 = 35.0330\text{N/m}$
$k_2 = 38.7342\text{N}$	$k_3 = 72.9114\text{W}$	$k_4 = 1$

will be just marginally inferior to Δ. According to (6.7) the signal-to-noise ratio during the 'exploration phase' is:

$$\text{SNR} = 10 \log_{10} \left(\frac{K^2}{\sigma_n^2} \right). \tag{6.38}$$

In addition, we select the robot parameters to fit the TOMR used in [47] which describes a real robot. These corresponding parameters are shown in table 6.1.

In Figs 6.2 and 6.3 we observe the performance of the CMDA when the MCP (i.e., optimum path), the LP (i.e., linear path) and the CP (i.e., circular path) are used. We arbitrarily select a sampling interval $\Delta = 0.05\lambda$, which according to simulation results in [55] will be sufficient to obtain the maximum channel power from each path under noiseless conditions. First, we have to mention that the MCP and the LP are the same for $L'_p \in \{0.2\lambda, 0.4\lambda, 0.6\lambda\}$. For higher values of L'_p we note that the MCP outperforms the LP both in terms of channel power obtained and in terms of mechanical energy consumed. The former (channel power) is due to the fact that the MCP is optimized so that the wireless channel at the path points $(\mathbf{d}_1, \mathbf{d}_2, \cdots, \mathbf{d}_N)$ have minimum correlation between them, see (6.10). This in turn makes the wireless channel at the sampling points $(\mathbf{p}(t_s(1)), \mathbf{p}(t_s(2)), \cdots, \mathbf{p}(t_s(M)))$ have almost minimum correlation among them and thus the channel power obtained is high while in the case of the LP the correlation among the wireless channel sampling points is higher and thus the channel power obtained is lower. Now, it can be seen that the LP is the path that maximises the average distance between its end point and $\mathbf{q}_{opt}$. In consequence when the MCP is used the MR has to travel a smaller distance during the positioning phase and thus uses less mechanical energy than the case in which the LP is used.

Now, comparing the MCP with the CP under noiseless conditions we observe from Figs 6.2 and 6.3 that the MCP produces a much higher channel power and it also uses less mechanical energy for L'_p approximately between 1.0λ and slightly higher than 1.7λ. This 'strange' behaviour may be explained due to the fact that the shape of the MCP can significantly change depending on L_p and so this also implies that we cannot extrapolate the results of Figs 6.2 and 6.3 to higher values of L'_p.

Note that for the rest of the simulations we will not plot mechanical energy again. This is because under the conditions that we will consider in the simulations below, Fig. 6.3 remains virtually unchanged for each path.

Then in Fig. 6.4 we observe the channel power for $SNR = 10\text{dB}$, which represents a significantly noisy example. We observe the behaviour of all three paths for two

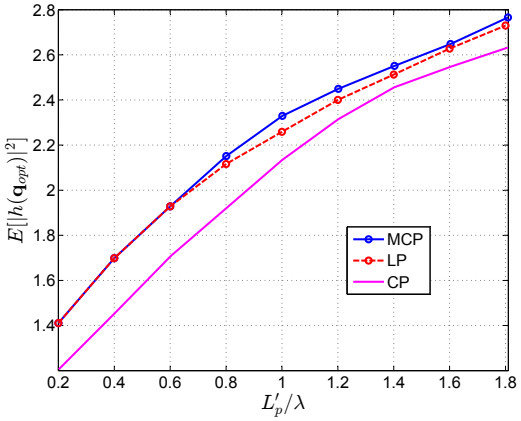

Figure 6.2: $\mathbb{E}[|h(\mathbf{q}_{opt})|^2]$ for different continuous paths and lengths under noiseless conditions and $\Delta = 0.05\lambda$.

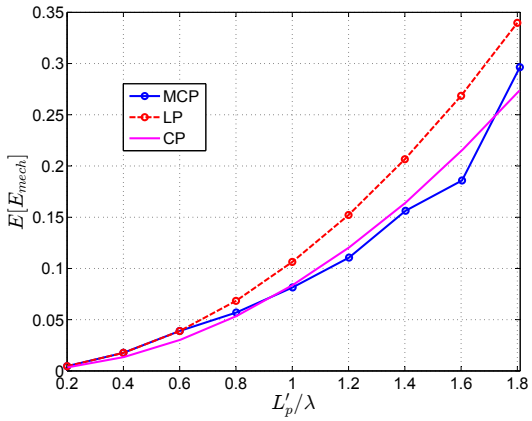

Figure 6.3: Mechanical energy consumption for different continuous paths and lengths under noiseless conditions and $\Delta = 0.05\lambda$.

different values of the parameter d (see (6.34)) which determines the number of sampling points used for each estimation of the channel gains along the path. In the first case we select $d = 0.3828\lambda$ and in the second case we select $d = 0.3\lambda$. Thus in the first case to estimate the channel at the sampling point $\mathbf{p}(t_s(k))$ the MR takes all the sampling points that are closer than the minimum distance at which the correlation is zero (i.e., 0.3828λ) while in the second case the MR takes the sampling points with channels that have a correlation higher than ≈ 0.3 in that area. This reduces slightly the amount of computation needed for the estimation of the channel gains and as we can observe in Fig. 6.4 this reduction in sampling points for the estimation process has an almost negligible effect on the channel power obtained.

From Fig. 6.5 we observe that for the noisy cases if we decrease the sampling rate by increasing the number of sampling points we can obtain better channel gain estimates and thus the performance of the CMDA approaches (to a certain extent)

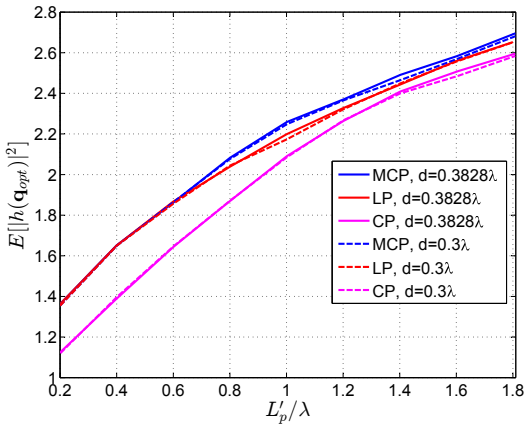

Figure 6.4: $\mathbb{E}[|h(\mathbf{q}_{opt})|^2]$ for different continuous paths, lengths and values of d with $SNR = 10\text{dB}$ and $\Delta = 0.05\lambda$.

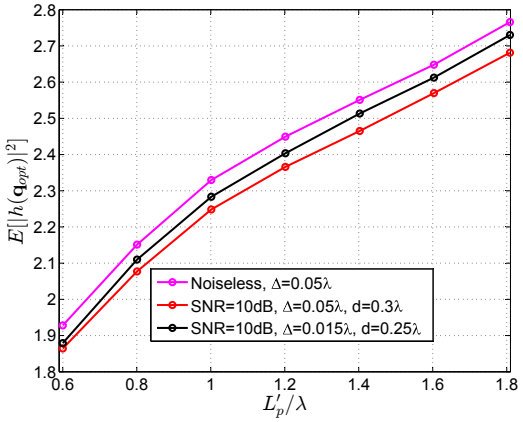

Figure 6.5: $\mathbb{E}[|h(\mathbf{q}_{opt})|^2]$ for the MCP under different conditions.

its performance in the noiseless case. Note that this occurs even when decreasing d. This is because what is important for the channel gain estimation is to have a larger number of samples but at the same time the samples must present high correlation with the channel to be estimated, so that their contribution to the estimation is significant. The first part implies that we should choose small values of Δ and the second part implies that we can choose small values of d to use only the samples with high correlation and discard the rest.

Now, the CMDA can be more efficient than an MDA based on discrete stopping points. This is because when the MR follows the continuous path it does not have to stop and restart, moving multiple times as it does, when it executes an MDA based on discrete stopping points. As a consequence, when the MR executes the CMDA it uses less energy in motion. In addition, in general when the MR executes the CMDA it collects more samples per unit distance travelled than when it executes the MDA

Table 6.2: MDMTA simulation results.

Number of stopping points	3	4	5
$\mathbb{E}[E_{mech}]$	0.0549	0.1458	0.2753
$\mathbb{E}[\lvert h(\mathbf{q}^2_{opt})\rvert]$	1.8301	2.0675	2.2501

based on stopping points and so the maximum channel gain obtained can be higher given that the MR travels the same length in both cases.

To illustrate this, we present in Table 6.2 the MDMTA with the optimum geometries used in the simulations section of chapter 2 and with its parameters selected to maximise the channel power that it delivers. In addition we run the simulations of the MDMTA with the same wavelength that we are using in this section (i.e., $\lambda = 14.02$cm), the same MR and the same execution time of 3 seconds in order to make a meaningful comparison with the CMDA. From Figs. 6.3-6.4 and Table 6.2 we note that given an amount of mechanical energy used the CMDA can obtain a higher channel power than the MDMTA or alternatively the CMDA uses less mechanical energy in obtaining certain channel power. Also, note that in this comparison the results of the MDMTA were obtained in a noiseless (best case) scenario while the results of the CMDA were calculated in a very noisy scenario. Therefore the CMDA is indeed much more efficient (in terms of mechanical energy) than the MDMTA in obtaining a high channel gain.

On the other hand, the MDAs that use stopping points are more robust to noise since they can take as many samples per stopping point as needed to satisfy a certain channel estimation error in order to ensure that the degradation in the performance of the MDA does not surpass a predefined level. But, in the case of the CMDA the MR only takes one sample per point and therefore it is more sensitive to noise. Therefore the MDAs based on discrete stopping points should be preferred when the SNR is significantly low due to its higher robustness against noise. But when the SNR is not significantly low CMDAs are preferred due to their their better performance in obtaining high channel gains while using lower mechanical energy.

6.4 Conclusions

We have solved the problem of how to optimise the shape of continuous paths for mobility diversity algorithms, given a specified path length. Our minimum correlation path (MCP) maximises the channel power obtainable through the CMDA given a fixed path length. This has been corroborated in the simulation section. And when compared to the linear path the MCP showed itself to be more efficient in terms of both channel power obtained and energy used in motion. We also showed that the MCP takes the form of a linear path for the case of very small-lengths. In addition we showed that the CMDA using the MCP can be more efficient than MDAs using discrete stopping points.

Chapter 7

Conclusion and Future work

7.1 Conclusion

In this thesis we have examined the design and performance of MDAs. At the time of beginning the research that is presented in this thesis the amount of work dealing with mobility diversity available in the literature was significantly scarce and the amount of knowledge regarding this technique was minimal. It was clearly understood and demonstrated experimentally that mobility diversity works. It was also understood that the points that the MR explores must be selected to obtain independent channels. Nevertheless there were no published results about how to optimise the position of those points and their physical distribution was also selected arbitrarily. Therefore, there was not a clear understanding of how to optimise the location of the points and so the main objective of this thesis was to provide an answer to this particular problem.

We began our research by considering simultaneously the channel gain obtained by the MDA and the amount of mechanical energy used during its execution. We developed and optimised different MDAs. In addition, we also provided different solutions regarding how to optimise the location of the points explored by the MR during the MDA.

Specifically, in the first part of this thesis which is composed of chapters 2-4 we considered the case of MDAs with a discrete search space. In chapter 2 we developed the MDMTA, which is a general MDA designed for discrete search spaces. We also developed two different methods to optimise the predetermined geometry of the stopping points for any number of them. These methods generate geometries that can provide high channel gain while requiring low amounts of mechanical energy during the MDA execution. Then in chapter 3 we developed path planners to adaptively optimise the location of each stopping point during the MDA execution. In that chapter we also showed that controlled channel correlation (introduced through the use of the path planners) can improve the performance of MDAs. This is an interesting result since for classical diversity techniques channel correlation degrades

their performance and thus in those techniques the designers try to avoid channel correlation. Finally in chapter 4 we concluded the treatment of MDAs with a discrete search space by extending the theory that we developed in the previous chapters for the case of multiple-link MDAs. Then in the second part of this thesis (chapters 5 and 6) we examined the case of MDAs with a continuous search space. In chapter 5 we customised a continuous search space MDA to improve the performance of an RF energy harvesting technique. The continuous search space of that chapter consisted of a straight line whose length we optimised. In chapter 6 we developed the CMDA which is a general MDA for continuous search spaces and we also solved the problem of how to optimise the actual shape of the continuous search space.

According to the results obtained we can say that in the context of MDAs with discrete search spaces when the shadowing term is known we should use the path planners with memory presented in chapter 3 to maximise the performance of the MDAs rather than using the predetermined geometries developed in chapter 2. But if the shadowing term is unknown then we can not implement the path planners of chapter 3 and so we should use the optimum geometries of chapter 2. Now, when comparing MDAs with discrete search spaces and MDAs with continuous search spaces we can say that the ones with discrete search spaces are more robust against noise than the ones with continuous search spaces. Nevertheless, the MDAs with continuous search spaces use less mechanical energy. Therefore MDAs with continuous search spaces should be preferred over MDAs with discrete search spaces when the SNR is high. But when the SNR is low we should prefer MDAs with discrete search spaces.

MDAs are a relatively new class of diversity whose main advantage is the fact that they can compensate small-scale fading without needing extra hardware as in multi-antenna diversity techniques. The cost of MDAs for compensating the small-scale fading and obtaining a good channel gain without needing extra hardware comes from the consumption of mechanical energy. Since the techniques developed in this thesis allow the MDA to provide high channel gains while requiring little mechanical energy then our results help reduce the (energy) cost of executing MDAs. This reduction in the energy needed to execute MDAs and the theory that we developed for such algorithms could help to initiate further research into their design and utilisation in the context of robotics communications.

7.2 Future Work

Although we have produced some interesting theoretical results for MDAs in general, there are still several questions which remain unanswered and should be addressed in future research. For example, all the work presented in this thesis has been done assuming Rayleigh fading. So a natural next step for this research should be to study MDAs under more general fading models like Nakagami and considerate also different spatial correlation functions for different scenarios.

Figure 7.1: Software defined radio which will be used to perform experimental research on MDAs.

Figure 7.2: Differential drive robot which will be used to perform experimental research on MDAs.

Another aspect that we should study is the applicability of MDAs for aerial robots. In that case the robot can move in a three dimensional space and so we should consider a fading channel model which is valid in a three dimensional space. In addition aerial MRs always consume mechanical energy as long as they are in the air so the statement of the problem would be different to the problem considered in this thesis in which the wheeled MR does not consume any mechanical energy if it does not move.

Also, multiple-link MDAs require more development in order to access their impact on wireless robotic networks. We can also extend this research to study the benefits of using MDAs for systems with two antennas. Then we could observe if those systems with just two antennas and moving extremely short distances (smaller that the ones considered in this thesis) could provide even more benefits than diversity techniques with a large number of antennas or MDAs with large search spaces.

Finally, the most important point for extending this research is the realisation of practical experiments to further validate and corroborate all the theory we have just developed as well as to develop MDAs which can operate robustly under real scenarios. We have already initiated such an approach with the software defined radio in Fig.7.1 and the MR in Fig. 7.2.

Appendix A

Algorithms

A.1 Hill climbing search

The hill climbing search [32] is an heuristic optimization algorithm to find an local maximum. Let us first consider the function $f(x_1, x_2, \cdots, x_N)$ and $x_j \in \mathbb{R}$ for all j.

If we want find a local maximum of $f(x_1, x_2, \cdots, x_N)$ using hill climbing search we have first to discretize the domain so that the new domain for x_j is $\{k\epsilon\}_{-\infty}^{+\infty}$ where ϵ is a small positive number selected by the user. Then we select an initial test point denoted by $x_1(0), x_2(0), \cdots, x_N(0)$. We can see the pseudocode in Algorithm 5.

Algorithm 5 Hill climbing search $(x_1(0), x_2(0), \cdots, x_N(0))$

while 1 **do**
  CurrentPoint $\leftarrow [x_1(0), x_2(0), \cdots, x_N(0)]^T$
  $J_{current} \leftarrow$ Eval (CurrentPoint, f) {Evaluate the function f at CurrentPoint.}
  $\mathcal{N} \leftarrow$ Neighbours (CurrentPoint) {Generates all the neighbours of CurrentPoint.}
  $\mathcal{J} \leftarrow$ Eval $(\mathcal{N}, f)$ {Evaluate the function f at all the points in $\mathcal{N}$.}
  if $J_{current} < \max\{\mathcal{J}\}$ **then**
    CurrentNext $\leftarrow$ ArgMaxEval $(\mathcal{N}, f)$ {Finds the point in $\mathcal{N}$ that produces the highest value of the function f.}
  else
    Terminate Algorithm
  end if
end while

A.2 Simulated annealing

The simulatead annealing algorithm [32] is an heuristic optimization algorithm used to find global minimum and avoid local minima. This optimization algorithm initially

behaves like a random search algorithm and smoothly changes its behaviour a to a close version of the hill climbing search algorithm. We can see the pseudocode in Algorithm 6.

Algorithm 6 Simulated annealing $([x_1(0), x_2(0), \cdots, x_N(0)]^T, Iterations, Temp_{max})$

CurrentPoint $\leftarrow [x_1(0), x_2(0), \cdots, x_N(0)]^T$
BestPoint $\leftarrow$ CurrentPoint
$J_{current} \leftarrow$ Eval (CurrentPoint, f)
$J_{best} \leftarrow J_{current}$
for $it = 1$ to $Iterations$ **do**
  NeighbourPoint $\leftarrow$ RandomNeighbour (CurrentPoint) {Generate randomly a point close to CurrentPoint.}
  $J_{neighbour} \leftarrow$ Eval (NeighbourPoint, f)
  $Temp_{current} \leftarrow$ UpdateTemperature $(Temp_{max}, it)$ {Updates the temperature variable. The UpdateTemperature function must be a decreasing function of it.}
  if $J_{current} > J_{neighbour}$ **then**
    CurrentPoint $\leftarrow$ NeighbourPoint
    if $J_{best} > J_{neighbour}$ **then**
      $J_{best} \leftarrow J_{neighbour}$
      BestPoint $\leftarrow$ NeighbourPoint
    end if
  else
    $r \leftarrow$ Random() {Generates a random number uniformly distributed between 0 and 1.}
    if $\exp\left(\frac{J_{current} - J_{neighbour}}{Temp_{current}}\right) > r$ **then**
      CurrentPoint $\leftarrow$ NeighbourPoint {With a probability p (which is a decreasing function it) we allow CurrentPoint to take worse positions. This step helps to avoid local minima.}
    end if
  end if
end for

Bibliography

[1] Cruz, Patricio J., and Rafael Fierro. "Towards optical wireless communications between micro unmanned aerial and ground systems", IEEE International Conference on Unmanned Aircraft Systems (ICUAS), 2015

[2] J. H. Jung, S. Park and S. Kim,"Multi-Robot Path Finding with Wireless Multihop Communications", IEEE Communications Magazine, vol. 48, iss. 7, 2010, pp. 126-132.

[3] A. Gonzalez-Ruiz and Y. Mostofi,"Cooperative Robotic Structure Mapping Using Wireless Measurements – A Comparison of Random and Coordinated Sampling Patterns", IEEE Sensors Journal, vol. 13, no. 7, July 2013, pp. 2571-2580.

[4] M. Malmirchegini and Y. Mostofi, "On the Spatial Predictability of Communication Channels", IEEE Transactions on wireless communications, vol. 11, no. 3, March 2012, pp. 964-978.

[5] J. Fink, A. Ribeiro and V. Kumar, "Robust Control for Mobility and Wireless Communication in Cyber-Physical Systems With Application to Robot Teams", Proceedings of the IEEE, vol. 100, no 1, January 2012, pp. 164-178.

[6] Kantaros, Yiannis, and Michael M. Zavlanos, "Distributed communication-aware coverage control by mobile sensor networks", Automatica 63 (2016) pp. 209-220.

[7] Zavlanos, Michael M., Alejandro Ribeiro, and George J. Pappas, "Network integrity in mobile robotic networks", IEEE Transactions on Automatic Control, vol. 58 no.1, 2013, pp. 3-18.

[8] J. Fink, Jonathan, Alejandro Ribeiro, and V. Kumar, "Robust control of mobility and communications in autonomous robot teams", IEEE Acces vol. 1, 2013, pp. 290-309.

[9] J. Fink, A. Ribeiro, and V. Kumar, "Robust Cyber-Physical Control of Mobility and Communication in Autonomous Robot Teams", Proceedings of the IEEE, vol. 100, iss. 1, pp. 164-178, 2012.

[10] J. Le Ny, A. Ribeiro and G. J. Pappas, "Adaptive Communication-Constrained Deployment of Unmanned Vehicle Systems", IEEE Journal on Selected Areas in Communications, Vol. 30 (5), June 2012.

[11] F. Meyer et al., "Distributed Estimation with Information-Seeking Control in Agent Networks", IEEE Journal on Selected Areas in Communications, vol. 33, no. 11, 2015, pp. 2439-2456.

[12] M. K. Simon, M. Alouini, *Digital Communication over Fading Channels*, John Wiley & Sons, In., 2005.

[13] D. Puccinelli and M. Haenggi, "Spatial Diversity Benefits by Means of Induced Fading", 3rd IEEE International Conference on Sensor and Ad Hoc Communications and Networks (SECON '06), Reston, VA, USA, September 2006., pp. 128-137.

[14] D. Puccinelli, M. Brennan and M. Haenggi, "Reactive Sink Mobility in Wireless Sensor Networks", Proc. of the 1st international MobiSys workshop on Mobile opportunistic networking 2007.

[15] M. Lindhe, K. H. Johansson abd A. Bicchi, "An experimental study of exploiting multipath fading for robot communications", Proc. Robotics Science and Systems, Atlanta, GA (June 2007).

[16] J. M. Smith, M. P. Olivieri, A. Lackpour and N. Hinnerschitz, "RF-mobility gain: concept, measurement campaign, and explotation", IEEE Wireless Communications, vol. 16, no. 1, February 2009, pp. 38-44.

[17] A. Ghaffarkhah and Y. Mostofi, "Path planning for networked robotic surveillance", IEEE Transactions on Signal Procesing, vol. 60, no. 7, July 2012.

[18] Vieira MAM, Taylor ME, Tandon P, et al. "Mitigating multipath fading in a mobile mesh network", Ad Hoc Networks vol. 11, no. 4, June 2013, pp. 1510-1521.

[19] Y. Yuan and Y. Mostofi, "Co-Optimization of Communication and Motion Planning of a Robotic Operation under Resource Constraints and in Fading Environments", IEEE Transactions on wireless communications vol. 12, no. 4, April 2013, pp. 1562-1572.

[20] M. Lindhe and K. H. Johansson,"Communication-Aware Trajectory Tracking", Proc. IEEE International Conference on Robotics and Automation, Pasadena, CA, USA, May 2008.

[21] M. Lindhe and K. H. Johansson, "Using robot mobility to exploit multipath fading", IEEE Wireless Communications, vol. 16, no. 1, February 2009.

[22] M. Lindhe and K. H. Johansson,"Adaptive Exploitation of Multipath Fading for Mobile Sensors", Proc. IEEE International Conference on Robotics and Automation (ICRA), Achorage Convention District, May 2010.

[23] M. Lindhe and K. H. Johansson,"Exploiting multipath fading with a mobile robot", The International Journal of Robotics Research February 1, 2015 34: 173-200.

[24] S. G. Tzafestas, *Introduction to Mobile Robot Control*, Elsevier, 2014.

[25] R. Siegwart., I.R. Nourbakhsh and D. Scaramuzza, *Introduction to autonomous mobile robots*, MIT Press, 2011.

[26] H. Kim, B.K. Kim ,"Minimum-energy trajectory planning and control on a straight line with rotation for three-wheeled omni-directional mobile robots", Proceedings of the IEEE/RSJ International Conference on Intelligent Robots and Systems (IROS), 2012, pp 3119 - 3124.

[27] A. Goldsmith, *Wireless Communications*, Cambridge University Press, 2005.

[28] W.C. Jakes, *Microwave Mobile Communications*, Wiley. IEEE Press, 2011.

[29] M. Malmirchegini and Y. Mostofi, "On the Spatial Predictability of Commucation Channels", IEEE Transactions on Wireless Communications, vol. 11, no. 3, March 2012.

[30] D. Bonilla Licea, D. McLernon, M. Ghogho and S. A. Raza Zaidi, "An Energy Saving Robot Mobility Diversity Algorithm for Wireless Communications", Proc. of the 21st European Signal Processing Conference (EUSIPCO), 2013.

[31] P. J. Bevelacqua and C. A. Balanis, "Optimizing Antenna Array Geometry for Interference Suppression", IEEE Transactions On Antennas And Propagation, vol. 55, no. 3, March 2007.

[32] S. Russell, P. Norving, *Artificial Intellingence: A Modern Approach*, Prentice Hall, 2003.

[33] A. Algans, K. I. Pedersen and P. E. Mgensen, "Experimental Analysis of the Joint Statistical Properties of Azimuth Spread, Delay Spread, and Shadow Fading", IEEE Journal on Selected Areads in Communications, vol. 20, no. 3, April 2002.

[34] B. Korte and J. Vygen, *Combinatorial optimization: Theory and algorithms*, 4th Edition, Springer, 2008.

[35] D. E. Kirk, *Optimal control theory: An introduction*. Dover Publications, Inc., 2004.

[36] A. H. Nuttall, "Some integrals involving the Q-function" Naval Underwater Systems Center (NUSC) technical report, April 1972.

[37] D. Bonilla Licea, D. McLernon and M. Ghogho, "Optimal trajectory design for a DTOA based multi-robot angle of arrival estimation system for rescue operations", Proc. IEEE International Conference on Acoustics, Speech and Signal Processing (ICASSP), 2014.

[38] M. Piñuela, P. D. Mitcheson and S. Lucyszyn, "Ambient RF Energy Harvesting in Urban and Semi-Urban Environments", IEEE Transactions on Microwave Theory and Techniques, vol. 61, no. 7, july 2013, pp. 2715-2726.

[39] X. Lu, P. Wang, D. Niyato, D. I. Kim and Z. Han, "Wireless Networks With RF Energy Harvesting: A Contemporary Survey", IEEE Communication Surveys & Tutorials, vol. 17, no. 2, 2015, pp. 757-789.

[40] H.Y. Yongguo Mei, Yung-Hsiang Lu and L.C.S.G. "A case study of mobile robots energy consumption and conservation techniques", Proc. of 12th International Conference on Advanced Robotics, ICAR'05", 2005.

[41] G. Caprari and R. Siegwart, "Mobile micro-robots ready to use: Alice", Proc. of IEEE/RSJ International Conference on Intelligent Robots and Systems, 2005. (IROS 2005).

[42] A. H. Coarasa, P. Nintanavongsa, S. Sanyal and K.R. Chowdhurry, "Impact of mobile transmitter sources on radio frequency wireless energy harvesting", Proc. of 2013 International Conference on Computing, Networking and Communications, Green Computing, Networking and Communications Symposium", 2013.

[43] J. O. McSpadden, L. F. and K. Chang,"Design and Experimentss of a High-Conversion-Efficiency 5.8-GHz Rectenna", IEEE transactions on microwave theory and techniques", vol. 46, no. 12, 1998, pp. 2053-2060.

[44] G. Caprari and T. Estier and R. Siegwart "Fascination of down scaling- Alice the sugar cube robot", Journal of Micromechatronics, vol. 1, no. 3, 2002, pp. 177-189.

[45] X. Zhou, R. Zhang and C. K. Ho "Wireless Information and Power Transfer: Architecture Design and Rate-Energy Tradeoff", IEEE Transactions on Communications, vol. 61, no. 11, November 2013, pp. 4754-4767.

[46] G. Dudek and M. Jenkin, *Computational principles of mobile robotics*, Cambridge University Press, 2000.

[47] C. H. Kim and B. K. Kim "Minimum-Energy Rotational Trajectory Planning for Differential-Driven Wheeled Mobile Robots", Proc. of the 13th International Conference on Advanced Robotics (ICAR), 2007.

[48] R. Weber, *Introduction to Microwave Circuits: Radio Frequency and Design Applications*, Wiley-IEEE Press, 2001.

[49] A. Kansal, J. Hsu, S. Zahedi and M. B. Srivastava, "Power Management in Energy Harvesting Sensor", ACM Transactions on Embedded Computing Systems (TECS) - Special Section LCTES'05, vol. 6, no. 4, September 2007.

[50] Frank L. Lewis and Vassilis L. Syrmos, *Optimal control, second edition*, Wiley-Interscience Publication, 1995.

[51] N. Blaustein and Y. Ben Shimol, "Prediction of frequency dependence of path loss and link-budget design for various terrestrial communication links", IEEE Transactions on Antennas and propagation, vol. 52 no. 10, 2004, pp. 2719-2729.

[52] A. R. Moghimi, Hsin-Mu Tsai and Cem U. Saraydar, "Characterizing Intra-Car Wireless Channels", IEEE Transactions on Vehicular Technology, vol. 58, no. 9, 2009, pp. 5299-5309.

[53] Daniel Bonilla Licea, Mounir Ghogho, Des McLernon and Syed Ali Raza Zaidi, "Mobility Diversity-Assisted Wireless Communication for Mobile Robots", IEEE Transactions on Robotics, vol. 32, no. 1, 2016, pp. 214-229.

[54] B. Siciliano, L. Sciavicco, L. Villani and G. Oriolo, *Robotics Modelling, Planning and Control*, Springer, 2010.

[55] Daniel Bonilla Licea, Syed Ali Raza Zaidi, Des McLernon and Mounir Ghogho, "Improving Radio Energy Harvesting in Robots using Mobility Diversity", IEEE Transactions on Signal Processing, vol. 64, no. 8, 2016, pp. 2065-2077.

[56] Y. Yan and Y. Mostofi, "Robotic Router Formation in Realistic Communication Environments", IEEE Transactions on Robotics, vol. 28, no. 4, August 2012.